NON-COMMUTATIVE QUANTUM MECHANICS IN 3-DIMENSIONAL FUZZY SPACE AND ITS APPLICATIONS

by

Hendrikus Wilhelm GROENEWALD

Dissertation presented for the degree of Doctor of Philosophy in the Faculty of Science at Stellenbosch University

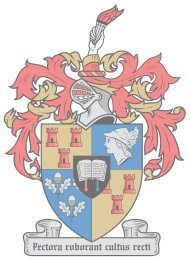

UNIVERSITEIT
iYUNIVESITHI
STELLENBOSCH
UNIVERSITY

Faculty of Science
Department of Physics

Promoter : Prof. Frederik G. Scholtz

Co-promoter : Dr. Johannes N. Kriel

March 2018

DECLARATION

By submitting this dissertation electronically, I declare that the entirety of the work contained therein is my own, original work, that I am the authorship owner thereof (unless to the extent explicitly otherwise stated) and that I have not previously in its entirety or in part submitted it for obtaining any qualification.

Date: March 2018

ABSTRACT

As the structure of space-time at very short length scales comparable to the Planck length remains a contentious issue, this study aims to determine whether non-commutative space-time would prove to be an appropriate candidate for space-time at short length scales. Also, it aims to test whether it would be possible to observe non-commutative effects on macroscopic scales. By providing a formulation for quantum mechanics where fuzzy commutation relations for spatial coordinates are assumed, this study was able to make notable progress toward this goal. Exact solutions to the non-commutative free particle and spherical well problems were achieved and effects exclusive to non-commutative systems were observed, in particular an upper bound on the kinetic energy of a particle and a finite number of bound states in the spherical well problem. Significant deviations from the normal behaviour of commutative systems were also observed in the study of scattering states of the fuzzy well where states with high incident energies experience the spherical well as a repulsive potential. Finally, thermodynamic studies of non-interacting fermions confined in fuzzy space provided drastically different results for high energy, high particle density and low temperature systems in comparison to standard results. These results include an incompressibility limit for the fermion gas, as well as an apparent duality between high density and low density systems.

OPSOMMING

Aangesien die struktuur van ruimtetyd op baie kort lengteskale, vergelykbaar met die Planck-lengte, steeds 'n omstrede saak bly, beoog hierdie studie om vas te stel of nie-kommutatiewe ruimtetyd 'n gepaste kandidaat vir ruimte-tyd op kort lengte skale sal wees. Dit beoog ook om te toets of dit moontlik is om nie-kommutatiewe effekte op makroskopiese skale waar te neem. Deur 'n formulering vir kwantummeganika te verskaf waar "fuzzy" kommutasieverbande vir ruimtelike koördinate aanvaar word, kon hierdie studie merkbare vordering maak in die rigting van hierdie doelwit. Eksakte oplossings vir die nie-kommutatiewe vrye deeltjies en sferiese put probleme is verkry en effekte eksklusief tot nie-kommutatiewe stelsels is waargeneem, veral 'n bogrens op die kinetiese energie van 'n deeltjie en 'n eindige aantal gebonde toestande in die sferiese put probleem. Beduidende afwykings van die normale gedrag van kommutatiewe stelsels is ook waargeneem in die studie oor verstrooiingstoestande van die "fuzzy"-put waar toestande met hoë invalenergieë die sferiese put as 'n afstotende potensiaal ervaar. Ten slotte het termodinamiese studies van nie-wisselwerkende fermione inbeperk in "fuzzy"-ruimte drasties verskillende resultate vir hoë energie, hoë deeltjie digtheid en lae temperatuur stelsels gelewer in vergelyking met standaard resultate. Hierdie resultate sluit in 'n onsaampersbaarheidslimiet vir die fermiongas, sowel as 'n duidelike dualiteit tussen hoë- en laedigtheidstelsels.

"O, the depth of the riches of the wisdom and knowledge of God!
How unsearchable His judgments, and untraceable His ways!"
- Romans 11:33

ACKNOWLEDGEMENTS

I would like to make some effort in thanking institutions, companies and individuals who helped me achieve this milestone. From financial support, to small contributions, all help was greatly appreciated. I extend my thanks to

- My supervisors Prof. F. G. Scholtz and Dr. J. N. Kriel for their guidance, patience and endless source of knowledge.
- The National Institute for Theoretical Physics (NIThePP) and also to Stellenbosch University for their financial support during my studies.
- VASTech for their financial support and to my colleagues and management there for their constant encouragement.
- My family for their never-ending encouragement and support, as well as my close friends who helped me through the personal turmoils that accompany any PhD project.

CONTENTS

CHAPTER 1

INTRODUCTION

A problem that we face in our current understanding of modern physics is the lack of a complete description for the structure of space-time at very short length scales on the order of the Planck length. There have been attempts in the past to propose non-commutative space-time as a viable description at the shortest length scales by Snyder [1], but it was not until the recent works of Doplicher *et al.* [2] that non-commutative space-time regained attention with strong arguments that support non-commutative space-time as a candidate description at short length scales. Later on non-commutative coordinates also emerged in the low energy limit of certain string theories [3].

These works inspired additional research and work within quantum mechanics [4, 5, 6, 7] and quantum field theories [8, 9] gained some attention. Unfortunately, since energies required to probe Planck length scales only existed in the very start of the universe, it is impossible to obtain empirical data that would enable realistic studies at these length scales. However, it is often thought that non-commutative effects might become observable at the high energies, temperatures and densities often in very large astrophysical objects such as black holes, neutron stars and even white dwarfs. These physical objects may serve as indirect sources of data that may be used in the search for non-commutative effects. Indeed, a study done on dense fermion gases in two-dimensional non-commutative space [10] exhibits notable differences in its thermodynamic behaviour at high energies and low temperatures when compared to conventional studies. This gives some promise that non-commutative effects might in certain instances become observable with current technologies.

One drawback however is that most of the studies done in non-commutative quantum mechanics and thermodynamics are limited to two dimensions, which cannot be extended to a non-commutative description for real world objects. Initial attempts to extend the two-dimensional formulation to three dimensions resulted in problematic breaking of rotational invariance when the simplest non-commutative commutation relations were taken [11]. A breakthrough came in a study conducted by Gáliková and Prešnajder [12] who were able to preserve rotational invariance by assuming fuzzy commutation relations. This selection of commutation relations and the formulation of quantum mechanics built thereon enabled them to find exact solutions to the

time-independent Schrödinger equation with a Coulomb potential.

Having access to a good basis for non-commutative space in three dimensions may serve as the perfect starting point in the pursuit of finding non-commutative effects in real world systems. Unfortunately, a full formulation of the quantum mechanics for free particles, as well as particles confined to a piece-wise constant potential well, was still lacking. Key results in these studies, in particular the energy spectrum and density of states, are required before an attempt could be made to study the thermodynamics of fermions confined in three-dimensional non-commutative space.

This then serves as the motivation behind this dissertation: In the hopes of finding significantly different thermodynamic behaviour for fermion gases in three-dimensional non-commutative space, we aim to establish both the necessary quantum mechanical and thermodynamic formulations that are needed to study the possibility of observing qualitative non-commutative effects in real systems. If this study proves successful, it will provide an important milestone in the search for non-commutative effects and will provide a good platform for future research in the same field.

The outline for this dissertation will therefore be as follows:

- We shall first briefly review similar work done in two-dimensional quantum mechanics and the approach followed there that will serve as a basis for our approach in three dimensions. Thereafter, we shall outline the formulation of quantum mechanics in three-dimensional fuzzy space and detail the solutions to the free particle and spherical well problems. Throughout the chapter we will obtain the necessary key results such as the respective energy spectra and the density of states that would be needed in the following chapters.

- The following section will take a slight detour as we will then focus on the study of particle scattering in the presence of a spherical fuzzy well. Even though this deviates slightly from the main goal behind this dissertation of studying thermodynamics of fermions in fuzzy space, it will be seen that the formulation and study of scattering in fuzzy space follows naturally from the previous results and provides noteworthy results. Some of these results will also highlight stark differences between scattering in non-commutative space and the analogous commutative system.

- Thereafter we will use the key results from previous chapters and formulate the thermody-

namic system of fermions confined in fuzzy space. After the formulation is done and the means of obtaining the central thermodynamic quantities is achieved, we will proceed to do qualitative and numerical studies on these quantities. We will then do a comparison of the thermodynamics observed in the non-commutative system and the analogous commutative system.

- Lastly we will conclude our work with a summary of the work done and the results it has produced. We will also then provide an outlook for future research that may follow from the studies conducted in this dissertation.

CHAPTER 2

NON-COMMUTATIVE QUANTUM MECHANICS IN TWO DIMENSIONS

As the construction of space-time with discretization at very small length scales can be approached using several different methods, we will discuss a few of these methods throughout this chapter that relate to our construction of a non-commutative system in 3-dimensional space. Since non-commutativity can only be realised in spaces of at least two dimensions, the simplest case to investigate the effect of non-commutativity in quantum mechanics would be 2-dimensional space. However, non-commutative quantum mechanics in 2-dimensions has already been investigated in some detail [5, 6, 7] and only an overview of the underlying theory will be covered in this chapter. This will be critical and supportive to the development of the non-commutative quantum theory in 3-dimensional space.

This chapter, therefore, serves as a brief literature review of [5, 6, 7] on the formulation of non-commutative quantum mechanics in 2-dimensional space. The chapters following this one develop the notion of non-commutative quantum mechanics in 3-dimensional space along the same lines. Special emphasis is placed on the preservation of rotational symmetry, which requires a deviation from the most naive constant commutation relations to those of the fuzzy sphere. All results presented in subsequent chapters are new and have been published [13, 16, 17].

2.1 Formulation of the configuration and quantum Hilbert spaces

In this section we review the basic formulation of non-commutative quantum mechanics in two dimensions as represented in [5, 6].

A simple way to introduce non-commutativity in two dimensions is through the commutation relations given by

$$[\hat{x}_1, \hat{x}_2] = i\theta. \tag{2.1}$$

Here θ is a real variable quantifying the extent of non-commutativity and $\hat{x}_1, \hat{x}_2$ are the two coordinate operators. The first step in constructing the non-commutative quantum theory for this coordinate algebra is to introduce a concrete realization of the coordinate algebra as operators on some Hilbert space $\mathcal{H}_c$, which we will refer to as the configuration space. From the coordinate

algebra in (2.1) it is natural to construct a pair of boson creation- and annihilation operators given by

$$b = \frac{1}{\sqrt{2\theta}}(\hat{x}_1 + i\hat{x}_2), \qquad b^\dagger = \frac{1}{\sqrt{2\theta}}(\hat{x}_1 - i\hat{x}_2). \tag{2.2}$$

A natural choice for $\mathcal{H}_c$ is therefore the boson Fock space spanned by

$$\mathcal{H}_c = \text{span}\{|n\rangle\}_{n=0}^{\infty} \tag{2.3}$$

where $|n\rangle = \frac{1}{\sqrt{n!}}(b^\dagger)^n |0\rangle$ and $b|0\rangle = 0$. Given the radial operator

$$\hat{r} = \hat{x}_1^2 + \hat{x}_2^2 = \theta(2b^\dagger b + 1_c), \tag{2.4}$$

where $1_c = \sum_{n=0}^{\infty} |n\rangle\langle n|$ is the identity operator on the configuration space, one notes that $\mathcal{H}_c$ corresponds to a "polar" choice of coordinates in which the radius is quantized.

Having defined the configuration space, we now proceed to construct the non-commutative quantum Hilbert space. Keeping in mind that for the commutative case the quantum Hilbert space is the set of all square-integrable functions of the coordinates, the natural generalization to the non-commutative case is the algebra of Hilbert-Schmidt operators generated by the coordinate operators, i.e.

$$\mathcal{H}_q = \left\{ \psi(\hat{x}_1, \hat{x}_2) \ : \ \text{Tr}_c \left(\psi(\hat{x}_1, \hat{x}_2)^\dagger \psi(\hat{x}_1, \hat{x}_2) \right) < \infty \right\}. \tag{2.5}$$

Here we used the subscript q in order to distinguish the quantum Hilbert space from the configuration space. As per notation used in [6], we also distinguish between the states of the configuration space, denoted by $|\cdot\rangle$, and the states of the quantum space, denoted by $|\cdot)$. Additionally, we also, from this point onward, distinguish between the states of these Hilbert spaces by referring to states in the configuration space simply as states, while we refer to states in the quantum Hilbert space as wavefunctions.

The inner product in the quantum space is defined by

$$(\psi\,|\,\phi) = (\psi\,,\,\phi) = \text{Tr}_c(\psi^\dagger \phi), \tag{2.6}$$

where $|\psi) = \psi(\hat{x}_1, \hat{x}_2)$ and $|\phi) = \phi(\hat{x}_1, \hat{x}_2)$ are both arbitrary wavefunctions represented as states of the quantum space.

The final step in setting up the quantum system is to construct a representation on the quantum

Hilbert space of the non-commutative Heisenberg algebra:

$$\begin{aligned}\left[\hat{x}_{1,q}\,,\,\hat{x}_{2,q}\right] &= i\theta,\\ \left[\hat{x}_{j,q}\,,\,\hat{p}_{k,q}\right] &= i\hbar\,\delta_{jk},\\ \left[\hat{p}_{1,q}\,,\,\hat{p}_{2,q}\right] &= 0.\end{aligned} \tag{2.7}$$

The representation is realised by defining the action of the operators in (2.7) on an arbitrary wavefunction as

$$\begin{aligned}\hat{x}_{j,q}\,\psi(\hat{x}_1,\hat{x}_2) &= \hat{x}_j\,\psi(\hat{x}_1,\hat{x}_2),\\ \hat{p}_{j,q}\,\psi(\hat{x}_1,\hat{x}_2) &= \varepsilon_{jk}\frac{\hbar}{\theta}\left[\hat{x}_k\,,\,\psi(\hat{x}_1,\hat{x}_2)\right],\end{aligned} \tag{2.8}$$

where ε_{jk} is anti-symmetric. For reasons that will become apparent later it is also convenient to define complex momenta through

$$\begin{aligned}p_q &= \hat{p}_{1,q} + i\hat{p}_{2,q} = -i\hbar\sqrt{\frac{2}{\theta}}\,[b\,,\,\psi(\hat{x}_1,\hat{x}_2)] \qquad \text{and}\\ \overline{p}_q &= \hat{p}_{1,q} - i\hat{p}_{2,q} = i\hbar\sqrt{\frac{2}{\theta}}\left[b^\dagger,\psi(\hat{x}_1\,,\,\hat{x}_2)\right],\end{aligned} \tag{2.9}$$

where it should also be noted that $p_q^2 = \overline{p}_q p_q = p_q\overline{p}_q$.

Finally, we write down the non-commutative equivalent of the non-relativistic time-independent Schrödinger equation. It is given by

$$\left[\frac{p_q^2}{2\mu} + V_q(\hat{x}_1,\hat{x}_2)\right]\psi(\hat{x}_1,\hat{x}_2) = E\,\psi(\hat{x}_1,\hat{x}_2) \tag{2.10}$$

where μ is the particle mass, $V_q(\hat{x}_1,\hat{x}_2)$ an arbitrary potential and E the energy.

From here on the program is as in the commutative case, i.e. to find the solutions for the Schrödinger equation for both free particles and particles in the presence of a varying potential. For the purposes of the studies in this dissertation, we only investigate the free particle and that of a piecewise constant potential, which we will later use to describe confined particles. However, as coordinates no longer commute, it is necessary to revisit the notions of positions and position measurement. We, therefore, briefly summarize these notions as described in [5].

Firstly, we introduce the normalized coherent states defined by

$$|z\rangle = e^{-\overline{z}z/2}e^{zb^\dagger}\,|0\rangle\,, \tag{2.11}$$

where $|z\rangle$ are minimal uncertainty states that provide an overcomplete basis of the configuration space and $z = \frac{1}{\sqrt{2\theta}}(x_1 + ix_2)$. One may use the coherent states to construct corresponding states in the quantum Hilbert space through

$$|z) = |z\rangle \langle z| . \tag{2.12}$$

The position representation of a wavefunction is then introduced through the inner product

$$(z\,|\,\psi) = \mathrm{Tr}_c\left(|z\rangle \langle z|\,\psi(\hat{x}_1, \hat{x}_2)\right) = \langle z|\,\psi(\hat{x}_1, \hat{x}_2)\,|z\rangle . \tag{2.13}$$

2.2 The spherical well in two dimensions

With the quantum Hilbert space and position representation in place, we are now able to identify the necessary components of the non-commutative Schrödinger equation with a piecewise constant potential, also known as the non-commutative spherical well.

In the following, we would like to solve for a particle moving in a potential with a constant value of V_1 inside a disk with of radius R and V_2 outside the disc. It is therefore necessary that we define two projection operators P and Q that would project the states in the configuration space into the appropriate regions. These two projection operators are easily found to be

$$P = \sum_{n=0}^{M} |n\rangle \langle n| \qquad \text{and} \qquad Q = \sum_{n=M+1}^{\infty} |n\rangle \langle n| , \tag{2.14}$$

where the positive integer M determines the radius through $R^2 = \theta(2M+1)$ by use of (2.4). From this construction it holds that $P^2 = P$, $Q^2 = Q$, $P\,Q = Q\,P = 0$ and $P + Q = 1_c$. Furthermore, we construct the projection operator counter-parts that act on the quantum Hilbert space simply as

$$P_q\psi(\hat{x}_1, \hat{x}_2) = P\,\psi(\hat{x}_1, \hat{x}_2) \qquad \text{and} \qquad Q_q\psi(\hat{x}_1, \hat{x}_2) = Q\,\psi(\hat{x}_1, \hat{x}_2). \tag{2.15}$$

We are now able to define the piecewise potential as

$$V_q = V_1 P_q + V_2 Q_q, \tag{2.16}$$

which results in the final form of the spherical well problem given by

$$\left[\frac{p_q^2}{2\mu} + V_1 P_q + V_2 Q_q\right] \psi(\hat{x}_1, \hat{x}_2) = E\,\psi(\hat{x}_1, \hat{x}_2). \tag{2.17}$$

In the commutative case this problem is solved by considering two independent Schrödinger equations, each having a constant potential of V_1 and V_2 respectively, while keeping the energy (eigenvalue) the same for both. The solutions to these two equations, which we will denote as ψ_1 and ψ_2, will also serve as the solutions to the original piecewise potential where ψ_1 corresponds to the region with a potential V_1 and ψ_2 corresponds to the region with potential V_2. These two solutions, however, need to have their function values, as well as derivatives, match up at the boundary between the two regions. The matching conditions are essential in computing the bound states and scattering coefficients in the scattering states.

Following the same philosophy as the commutative case, we provide an analogous approach in the non-commutative case. We start with the two constant potential equations:

$$\begin{aligned}\left[\frac{p_q^2}{2\mu} + V_1\right] \psi_1(\hat{x}_1, \hat{x}_2) &= E\,\psi_1(\hat{x}_1, \hat{x}_2),\\ \left[\frac{p_q^2}{2\mu} + V_2\right] \psi_2(\hat{x}_1, \hat{x}_2) &= E\,\psi_2(\hat{x}_1, \hat{x}_2).\end{aligned} \tag{2.18}$$

Since the final solution to the piecewise potential will be of the form $\psi(\hat{x}_1, \hat{x}_2) = P_q\psi_1(\hat{x}_1, \hat{x}_2) + Q_q\psi_2(\hat{x}_1, \hat{x}_2)$, we ultimately need to find solutions to the following set of equations following from (2.18):

$$\begin{aligned}P_q\left[\frac{p_q^2}{2\mu} + V_1\right] \psi_1(\hat{x}_1, \hat{x}_2) &= E\,P_q\psi_1(\hat{x}_1, \hat{x}_2),\\ Q_q\left[\frac{p_q^2}{2\mu} + V_2\right] \psi_2(\hat{x}_1, \hat{x}_2) &= E\,Q_q\psi_2(\hat{x}_1, \hat{x}_2),\end{aligned} \tag{2.19}$$

where we applied P_q to the left of the first equation, and Q_q to the left of the second. From this we try to construct a solution to (2.17) of the form $\psi(\hat{x}_1, \hat{x}_2) = P_q\psi_1(\hat{x}_1, \hat{x}_2) + Q_q\psi_2(\hat{x}_1, \hat{x}_2)$. We substitute this form into (2.17) and by using (2.19) and the fact that $\left[p_q^2\,,\,Q_q\right] = -\left[p_q^2\,,\,P_q\right]$, we arrive at the following condition that needs to be satisfied:

$$\Omega_q\psi_1(\hat{x}_1, \hat{x}_2) = \Omega_q\psi_2(\hat{x}_1, \hat{x}_2), \tag{2.20}$$

where $\Omega_q = \left[p_q^2\,,\,P_q\right]$. By doing some further calculations, and by taking the inner-product first

with $|n\rangle$ and then $|l\rangle$, we find that the key conditions to be satisfied in (2.20) are given by the two equations

$$\begin{aligned} \langle M+1|\,\psi_1(\hat{x}_1,\hat{x}_2)\,|l+1\rangle &= \langle M+1|\,\psi_2(\hat{x}_1,\hat{x}_2)\,|l+1\rangle\,, \qquad \forall l \geq 0, \\ \langle M|\,\psi_1(\hat{x}_1,\hat{x}_2)\,|l-1\rangle &= \langle M|\,\psi_2(\hat{x}_1,\hat{x}_2)\,|l-1\rangle\,, \qquad \forall l > 0. \end{aligned} \tag{2.21}$$

The only remaining task, therefore, is to solve the two constant potential problems for $\psi_1(\hat{x}_1,\hat{x}_2)$ and $\psi_2(\hat{x}_1,\hat{x}_2)$, whereafter we can apply the matching conditions in (2.21).

The constant potential problem where $V_q(\hat{x}_1,\hat{x}_2)$ in (2.10) is set to a constant V, can be simplified to the form of

$$\left(p_q^2 + k^2\hbar^2\right)\psi(\hat{x}_1,\hat{x}_2) = 0, \tag{2.22}$$

where $k^2 = 2\mu(V-E)/\hbar^2$. Here k^2 can both be positive or negative depending on whether bound- or scattering states are considered. The most general form in which the wavefunction $\psi(\hat{x}_1,\hat{x}_2)$ can be expressed, is given by

$$\psi(\hat{x}_1,\hat{x}_2) = \sum_{k=0}^{\infty}\sum_{l=0}^{\infty} c_{k,l}(b^\dagger)^k b^l \equiv \sum_{m=-\infty}^{\infty}\psi_m, \tag{2.23}$$

where

$$\begin{aligned} \psi_m &= \sum_{k=0}^{\infty} c_{k,k+m}(b^\dagger)^k b^{k+m}, \qquad m \geq 0, \\ \psi_m &= \sum_{k=0}^{\infty} c_{k+|m|,k}(b^\dagger)^{k+|m|} b^k, \qquad m < 0, \end{aligned} \tag{2.24}$$

and

$$\begin{aligned} [b^\dagger b\,,\,\psi_m] &= -m\,\psi_m, \qquad \forall m, \\ [b^\dagger b\,,\,p_q^2\psi_m] &= -m\,p_q^2\psi_m, \qquad \forall m. \end{aligned} \tag{2.25}$$

From (2.25) it is evident that p_q^2, as well as constant potential terms, will not mix wavefunctions with different values of m. We may, therefore, without the loss of generality only consider solutions of the form ψ_m, where we restrict our attention to a single value of m. Additionally, it is easily verified that $(p_q^2\psi_m)^\dagger = p_q^2\psi_m^\dagger$ and therefore both ψ_m and $\psi_m^\dagger$ are solutions to (2.22). This enables us to easily construct two linear independent Hermitian solutions through $\psi_m + \psi_m^\dagger$ and $i\left(\psi_m - \psi_m^\dagger\right)$. Given this fact, we are free to choose the solution ψ_m to be Hermitian with a useful consequence being that $\psi_m^\dagger = \psi_{-m}$. Since we only need to find the matrix elements that would satisfy the matching conditions in (2.21), we will only consider the $m \geq 0$ case as

the $m < 0$ is simply related to the positive case. Furthermore, the only non-vanishing matrix elements are given by $\langle n|\,\psi_m\,|n+m\rangle$ for $n \geq 0$. Therefore, we will take the matrix elements of (2.22) between $|n\rangle$ and $|n+m\rangle$. The end result of the Schrödinger equation taken between $|n\rangle$ and $|n+m\rangle$ is expressed through the recursion relation given by

$$\begin{aligned}(2n+m+1+z)\,\langle n|\,\psi_m\,|n+m\rangle &= \sqrt{n(n+m)}\,\langle n-1|\,\psi_m\,|n+m-1\rangle \\ &\quad + \sqrt{(n+1)(n+m+1)}\,\langle n+1|\,\psi_m\,|n+m+1\rangle\,,\end{aligned} \tag{2.26}$$

where $z = \frac{1}{2}\theta k^2$. This recursion relation has two linear independent solutions given by

$$\begin{aligned}\langle n|\,\psi_m\,|n+m\rangle &= c_1(m,z)\sqrt{\frac{(n+m)!}{n!\,m!}}\;M(-n,m+1,-z), \quad \text{and} \\ \langle n|\,\psi_m\,|n+m\rangle &= c_2(m,z)\sqrt{\frac{n!(n+m)!}{m!}}\;U(n+1,1-m,z), \quad \forall m,n \geq 0.\end{aligned} \tag{2.27}$$

Here $c_1(m,z)$ and $c_2(m,z)$ are, at this point, arbitrary functions of m and z, while $M(a,b,z)$ and $U(a,b,z)$ are the two solutions of the confluent hypergeometric differential equation. We now find that the most general solution for (2.26), therefore, is given by

$$\begin{aligned}\langle n|\,\psi_m\,|n+m\rangle &= c_1(m,z)\sqrt{\frac{n!\,m!}{(n+m)!}}\;L_n^m(-z) \\ &\quad + c_2(m,z)\sqrt{\frac{n!(n+m)!}{m!}}\;U(n+1,1-m,z), \quad \forall m,n \geq 0,\end{aligned} \tag{2.28}$$

where the $L_n^m(z)$ is a Laguerre polynomial and is associated to the Kummer's function $M(a,b,z)$ with a negative integer value for a. Similarly, for the $m < 0$ case it can be shown that the corresponding matrix element is given by

$$\begin{aligned}\langle n-m|\,\psi_m\,|n\rangle &= c_1^*(|m|,z)\sqrt{\frac{n!\,|m|!}{(n+|m|)!}}\;L_n^{|m|}(-z) \\ &\quad + c_2^*(|m|,z)\sqrt{\frac{n!(n+|m|)!}{|m|!}}\;U(n+1,1-|m|,z), \quad \forall m<0, n \geq 0.\end{aligned} \tag{2.29}$$

It remains now to determine the functions $c_1(m,z)$ and $c_2(m,z)$. In the works of [6], these functions were determined by ensuring that (2.28) and (2.29) have the correct commutative limits. Achieving this, they noted that $\hat{r}^2\,|n\rangle = \theta(2n+1)\,|n\rangle \equiv r^2\,|n\rangle$. The commutative limit was then taken by keeping m and r fixed, while taking $\theta \to 0$ and $n \to \infty$. Furthermore, we replace $\theta = r^2/2n$ in the definition for z so that we have the form $z = r^2k^2/4n$.

First considering the case of scattering states, i.e. $E > V$, we find for $m \geq 0$ and large n that (2.28) obtains the form of

$$\begin{aligned}\langle n|\,\psi_m\,|n+m\rangle = c_1\left(m, \frac{-\kappa^2 r^2}{4n}\right)\sqrt{m!}\,n^{-m/2}\,L_n^m\left(\frac{\kappa^2 r^2}{4n}\right) \\ + c_2\left(m, \frac{-\kappa^2 r^2}{4n}\right)\sqrt{\frac{2\pi}{m!}}e^{-n}n^{n+\frac{m}{2}+\frac{1}{2}}\,U\left(n+1\,,\,1-m\,,\,\frac{-\kappa^2 r^2}{4n}\right),\end{aligned} \tag{2.30}$$

where $\kappa^2 = -k^2$ and $\kappa > 0$. To achieve the correct commutative limit, it is necessary that $c_1(m,z)$ and $c_2(m,z)$ should take on the forms of $c_1(m,z) = c_1(m)\,z^{m/2}$ and $c_2(m,z) = c_2(m)\,z^{-m/2}$. The final scattering solution in the commutative limit is then given by

$$\lim_{n\to\infty}\langle n|\,\psi_m\,|n+m\rangle = c_1(m)(-1)^{m/2}J_m(\kappa r) + \frac{c_2(m)\pi(\pm i)^{m+1}}{\sqrt{m!}}\left(J_m(\kappa r) \pm iY_m(\kappa r)\right), \tag{2.31}$$

where J_m and Y_m are the Bessel functions of the first- and second kind, respectively, and $c_1(m)$ and $c_2(m)$ are normalization factors with their forms undetermined at this point. As Y_m is singular near the origin, it is automatically excluded from being considered a solution inside the disk ($n \leq M$). It necessitates that $c_2(m)$ be zero for $n \leq M$ for all values of m, whereas outside the disk ($n > M$) we have that both factors are accepted.

Now, considering bound states where $E < V$ and, therefore, $k^2 > 0$, we find in the large n limit and $m \geq 0$ that (2.28) simplifies to

$$\lim_{n\to\infty}\langle n|\,\psi_m\,|n+m\rangle = c_1(m)(-1)^{m/2}\,I_m(kr) + \frac{2c_2(m)}{\sqrt{m!}}\,K_m(kr), \tag{2.32}$$

where I_m and K_m are the modified Bessel functions of the first- and second kind respectively. In this case we have that I_m grows exponentially outside the disk ($n > M$) and, therefore, can not be used as part of the solution for bound states. This leads to $c_1(m) = 0$ for all values of m. Once again, the solutions for $m < 0$ for the bound- and scattering states can easily be related to these.

As we now have the necessary forms of solutions to bound- and scattering states for the well problem, we are now able to complete the matching conditions set in (2.21). For simplicity we will assume that the potential inside the disk will be $V_1 = 0$, while outside the disk we simply have $V_2 = V$. Later we will take the limit where $V \to \infty$. For the $m \geq 0$ case we have that the relevant form for the matrix elements for the wavefunction inside the well ($\psi_1(\hat{x}_1, \hat{x}_2)$) is given

by

$$\langle n|\,\psi_{\text{in},m}(\hat{x}_1,\hat{x}_2)\,|n+m\rangle = c_1(m)\,z_{\text{in}}^{m/2}\sqrt{\frac{n!m!}{(n+m)!}}\,L_n^m(-z_{\text{in}}),\quad \forall m,\,n\geq 0, \tag{2.33}$$

with $z_{\text{in}} = -\frac{\mu E\theta}{\hbar^2} \equiv -\frac{\theta k_{\text{in}}^2}{2}$. Outside of the disk we only consider bound states as we will be taking the $V\to\infty$ limit. Therefore, we have the matrix elements given by

$$\langle n|\,\psi_{\text{out},m}(\hat{x}_1,\hat{x}_2)\,|n+m\rangle = c_2(m)\,z_{\text{out}}^{-m/2}\sqrt{\frac{n!(n+m)!}{m!}}\,U(n+1,1-m,z_{\text{out}}),\quad \forall m,\,n\geq 0, \tag{2.34}$$

where $z_{\text{out}} = \frac{\mu(V-E)\theta}{\hbar^2} \equiv \frac{\theta k_{\text{out}}^2}{2}$. We now have the final components necessary to compute the matching conditions given in (2.21). The final form of these matching conditions are given by

$$\begin{aligned}
&\langle M+1|\,\psi_{in,m}(\hat{x}_1,\hat{x}_2)\,|M+m+1\rangle = \langle M+1|\,\psi_{out,m}(\hat{x}_1,\hat{x}_2)\,|M+m+1\rangle\,,\\
&\langle M|\,\psi_{in,m}(\hat{x}_1,\hat{x}_2)\,|M+m\rangle = \langle M|\,\psi_{out,m}(\hat{x}_1,\hat{x}_2)\,|M+m\rangle\,,\qquad \forall m\geq 0.
\end{aligned} \tag{2.35}$$

From (2.35) we see that the function values should match at the well border. Furthermore, subtracting the second equation from the first results in

$$\begin{aligned}
&\langle M+1|\,\psi_{in,m}(\hat{x}_1,\hat{x}_2)\,|M+m+1\rangle - \langle M|\,\psi_{in,m}(\hat{x}_1,\hat{x}_2)\,|M+m\rangle\\
&= \langle M+1|\,\psi_{out,m}(\hat{x}_1,\hat{x}_2)\,|M+m+1\rangle - \langle M|\,\psi_{out,m}(\hat{x}_1,\hat{x}_2)\,|M+m\rangle\,,\qquad \forall m\geq 0.
\end{aligned} \tag{2.36}$$

In (2.36) we see that both sides of the equation contain the equivalent of the first derivatives at the well border for both the wavefunctions inside- and outside the well and, therefore, requires that the derivatives of the two functions match up as well. The matching conditions in (2.35) and (2.36) are the direct non-commutative equivalents of the commutative case where the wavefunction values and first derivatives match up on the well border.

Consequently, when substituting the final forms of (2.33) and (2.34) into (2.35), we find the following matching equations

$$\begin{aligned}
&c_1(m)z_{\text{in}}^{m/2}\sqrt{\frac{(M+1)!\,m!}{(M+m+1)!}}\,L_{M+1}^m(-z_{\text{in}})\\
&\qquad = c_2(m)z_{\text{out}}^{-m/2}\sqrt{\frac{(M+1)!(M+m+1)!}{m!}}\,U(M+2,1-m,z_{\text{out}}),
\end{aligned} \tag{2.37}$$

and

$$c_1(m)z_{\text{in}}^{m/2}\sqrt{\frac{M!\,m!}{(M+m)!}}\,L_M^m(-z_{\text{in}}) = c_2(m)z_{\text{out}}^{-m/2}\sqrt{\frac{M!(M+m)!}{m!}}\,U(M+1,1-m,z_{\text{out}}). \quad (2.38)$$

By dividing equations (2.37) and (2.38), we find that the currently unknown constants $c_1(m)$ and $c_2(m)$ no longer feature and we have a final expression that can be used to calculate the permitted bound state energies of a system for all values of $m \geq 0$. This expression for bound state energies is given by

$$\sqrt{\frac{M+1}{M+m+1}}\,\frac{L_{M+1}^m(-z_{\text{in}})}{L_M^m(-z_{\text{in}})} = \sqrt{(M+1)(M+m+1)}\,\frac{U(M+2,1-m,z_{\text{out}})}{U(M+1,1-m,z_{\text{out}})}, \quad \forall m \geq 0. \quad (2.39)$$

One finds that the above reduces, in the commutative limit where we have a well radius of R, to the expected commutative result given by

$$\frac{k_{\text{in}}J_m'(k_{\text{in}}R)}{J_m(k_{\text{in}}R)} = \frac{k_{\text{out}}K_m'(k_{\text{out}}R)}{K_m(k_{\text{out}}R)}. \quad (2.40)$$

Although the exact expressions for $c_1(m)$ and $c_2(m)$ remain unknown, we are still able to determine the ratio $c_1(m)/c_2(m)$ by substituting the energies calculated in (2.39) into either (2.37) and (2.38).

Since we are ultimately interested in the energy solutions for the infinite well, in the limit $V \to \infty$ we solve for the energies in (2.39) for this limit. Since, in the case of the infinite well, the wavefunction has to vanish everywhere outside the well, we find that the energies are obtained from the condition:

$$L_{M+1}^m\left(\frac{\theta k^2}{2}\right) = 0, \qquad \forall m \geq 0, \quad (2.41)$$

with $k^2 = \frac{2\mu E}{\hbar^2}$. Furthermore, it is clearly seen that there exist $M+1$ bound states for each sector in the postive angular momentum range.

For the case of negative momenta ($-m$ with $m > 0$) we follow a similar method. The bound state energies for negative momenta are now found through the expression given by

$$\sqrt{\frac{M-m+1}{M+1}}\,\frac{L_{M-m+1}^m(-z_{\text{in}})}{L_{M-m}^m(-z_{\text{in}})} = \sqrt{(M+1)(M-m+1)}\,\frac{U(M-m+2,\,1-m,\,z_{\text{out}})}{U(M-m+1,\,1-m,\,z_{\text{out}})}, \quad (2.42)$$

for all $0 < m \leq M$. This reduces, in the limit where $V \to \infty$, to

$$L^m_{M-m+1}\left(\frac{\theta k^2}{2}\right) = 0, \qquad 0 < m \leq M. \tag{2.43}$$

This time we see that there are $M - m + 1$ bound states for each negative angular momentum sector where $0 < m < M$. This naturally sets the upper- and lower bounds on the number of bounds states to $1 \leq M - m + 1 \leq M$.

Calculating the bound state energies in (2.41) and (2.43) is done by finding the zeros of each Laguerre polynomial.

CHAPTER 3

NON-COMMUTATIVE QUANTUM MECHANICS IN THREE DIMENSIONS

As mentioned previously, the work contained here is original and is, in part, inspired by the approach followed in Chapter 2. Here we detail the basic formalism of 3-dimensional fuzzy space which follows closely the approach used in [12]. This recollection of the formalism is detailed in Sections 3.1 and 3.2. From Section 3.3 onward we have the original work produced during this PhD project, where a section of the results was published in [13].

We investigate the behaviour of various free particle solutions and find interesting results for the allowed energies for free particles in fuzzy space. Thereafter we show how a potential well is constructed in fuzzy space and then apply this to the infinite well problem. Results from the finite well are used in the next chapter on scattering states of the finite fuzzy well, whereas the results of the infinite well are used in a later chapter to study the thermodynamics of a Fermi gas in fuzzy space.

3.1 The classical configuration space

Three-dimensional fuzzy space is described by the set of coordinate operators $\hat{X}_i$ that obey the $SU(2)$ commutation relations

$$[\hat{X}_i, \hat{X}_j] = 2i\theta\varepsilon_{ijk}\hat{X}_k, \tag{3.1}$$

for $i = 1, 2, 3$ and with θ the real, non-commutative length scale.

As in the previous chapter, the first step in setting up the quantum system is to find a concrete realization of the coordinate algebra (3.1). Introducing two pairs of creation- and annihilation operators $(\hat{a}_\alpha, \hat{a}_\alpha^\dagger)$ for $\alpha = 1, 2$, we are able to express the coordinate operators $\hat{X}_i$ as

$$\hat{X}_i = \theta\hat{a}^\dagger\sigma^{(i)}\hat{a} \equiv \theta\sigma^{(i)}_{\alpha\beta}\hat{a}^\dagger_\alpha\hat{a}_\beta, \tag{3.2}$$

with $\sigma^{(i)}$ the Pauli matrices. The creation and annihilation operators obey the standard commutation relations

$$[\hat{a}_\alpha, \hat{a}^\dagger_\beta] = \delta_{\alpha\beta}, \qquad [\hat{a}_\alpha, \hat{a}_\beta] = [\hat{a}^\dagger_\alpha, \hat{a}^\dagger_\beta] = 0. \tag{3.3}$$

The following explicit computation shows that the operators in (3.2) indeed satisfy the algebra (3.1):

$$\begin{aligned}
[\hat{X}_i, \hat{X}_j] &= \left[\theta\sigma^{(i)}_{\alpha\beta}\hat{a}^\dagger_\alpha\hat{a}_\beta\,,\ \theta\sigma^{(j)}_{\mu\nu}\hat{a}^\dagger_\mu\hat{a}_\nu\right] \\
&= \theta^2\sigma^{(i)}_{\alpha\beta}\sigma^{(j)}_{\mu\nu}\left(\hat{a}^\dagger_\alpha\hat{a}_\beta\hat{a}^\dagger_\mu\hat{a}_\nu - \hat{a}^\dagger_\mu\hat{a}_\nu\hat{a}^\dagger_\alpha\hat{a}_\beta\right) \\
&= \theta^2\sigma^{(i)}_{\alpha\beta}\sigma^{(j)}_{\mu\nu}\left(\hat{a}^\dagger_\alpha\left(\hat{a}^\dagger_\mu\hat{a}_\beta + \delta_{\mu\beta}\right)\hat{a}_\nu - \hat{a}^\dagger_\mu\left(\hat{a}^\dagger_\alpha\hat{a}_\nu + \delta_{\nu\alpha}\right)\hat{a}_\beta\right) \\
&= \theta^2\left(\hat{a}^\dagger_\alpha\sigma^{(i)}_{\alpha\beta}\sigma^{(j)}_{\beta\nu}\hat{a}_\nu - \hat{a}^\dagger_\mu\sigma^{(j)}_{\mu\alpha}\sigma^{(i)}_{\alpha\beta}\hat{a}_\beta\right) \\
&= \theta^2\,\hat{a}^\dagger\left[\sigma^{(i)}\,,\,\sigma^{(j)}\right]\hat{a} \\
&= 2i\theta^2\varepsilon_{ijk}\hat{a}^\dagger\sigma^{(k)}\hat{a} \\
&= 2i\theta\varepsilon_{ijk}\hat{X}_k,
\end{aligned} \tag{3.4}$$

where we used the notation in (3.2) to rewrite the operators in their respective matrix- and vector forms. This is the well-known Schwinger realization of $SU(2)$. The creation- and annihilation operators act on the classical configuration space $\mathcal{H}_c$, which we identify with the underlying Fock space, spanned by

$$\mathcal{H}_c = \text{span}\left\{|n_1, n_2\rangle = \frac{(\hat{a}^\dagger_1)^{n_1}(\hat{a}^\dagger_2)^{n_2}}{\sqrt{n_1!n_2!}}\,|0,0\rangle\right\}. \tag{3.5}$$

We also note that for the counting operator $\hat{N} = \hat{a}^\dagger_\alpha\hat{a}_\alpha$

$$\hat{N}\,|n_1, n_2\rangle = (n_1 + n_2)\,|n_1, n_2\rangle = n\,|n_1, n_2\rangle\,, \tag{3.6}$$

with $n = n_1 + n_2$, which is consistent with the action of the creation- and annihilation operators on $\mathcal{H}_c$:

$$\begin{aligned}
\hat{a}^\dagger_\alpha\,|n_1, n_2\rangle &= \sqrt{n_\alpha + 1}\,|n_1 + \delta_{\alpha,1}\,,\ n_2 + \delta_{\alpha,2}\rangle\,, \\
\hat{a}_\alpha\,|n_1, n_2\rangle &= \sqrt{n_\alpha}\,|n_1 - \delta_{\alpha,1}\,,\ n_2 - \delta_{\alpha,2}\rangle\,,
\end{aligned} \tag{3.7}$$

for $\alpha = 1, 2$ and where $\hat{a}_1\,|0, n_2\rangle = \hat{a}_2\,|n_1, 0\rangle = 0$. Furthermore, the Casimir operator, which naturally commutes with every $\hat{X}_i$, is given by

$$\hat{X}^2 = \hat{X}_i\hat{X}_i = \theta^2\hat{N}(\hat{N} + 2), \tag{3.8}$$

where the calculation is shown in Section A.1. Using

$$\hat{r} = \theta(\hat{N} + 1) \tag{3.9}$$

as a measure of radial distance, the 3-dimensional fuzzy space described by the set of coordinate operators (3.2) can, therefore, be thought of as having an "onion" structure consisting of a collection of concentric fuzzy spheres whose radii are determined by the counting operator $\hat{N}$. Note that for this interpretation it is essential that each $SU(2)$ irrep occurs exactly once, as should be clear from (3.8). Furthermore, the coordinate operators $\hat{X}_i$ and $\hat{r}$ obey the relations

$$\left[\hat{X}_i\,,\,\hat{r}\right] = 0, \qquad \hat{r}^2 - \hat{X}^2 = \theta^2. \tag{3.10}$$

3.2 The quantum Hilbert space

As before, the natural identification of the quantum Hilbert space $\mathcal{H}_q$ is the algebra of Hilbert-Schmidt operators generated by the coordinate operators (3.2). Since the coordinates commute with the Casimir operator, so must the elements of the algebra. We find that $\mathcal{H}_q$ is described by:

$$\mathcal{H}_q = \left\{ \hat{\psi} = \sum_{m_i,n_i=0}^{\infty} C_{n_1,n_2}^{m_1,m_2} (\hat{a}_1^\dagger)^{m_1} (\hat{a}_2^\dagger)^{m_2} \hat{a}_1^{n_1} \hat{a}_2^{n_2} \;:\; m_1 + m_2 = n_1 + n_2 \text{ and } \mathrm{Tr}_c(\hat{\psi}^\dagger\, \hat{r}\, \hat{\psi}) < \infty \right\}. \tag{3.11}$$

From (3.11) it is clear that $\mathcal{H}_q$ is a Hilbert space spanned by functions which possess a finite weighted Hilbert-Schmidt norm

$$\|\hat{\psi}\|^2 = 4\pi\theta^3\, \mathrm{Tr}_c \left(\hat{\psi}^\dagger\, (\hat{N} + 1)\, \hat{\psi}\right) = 4\pi\theta^2\, \mathrm{Tr}_c(\hat{\psi}^\dagger\, \hat{r}\, \hat{\psi}). \tag{3.12}$$

The choice of the rotationally invariant weight $w(\hat{r}) = 4\pi\theta^2\hat{r}$ arises directly from the requirement that a ball, with radius R, should possess a standard volume in 3-dimensional fuzzy space in the large R limit. By using $\mathcal{F}_n = \{|n_1, n_2\rangle \mid n_1 + n_2 = n\}$ as the notation for the underlying Fock space, we find that the projector $\hat{P}_n$ on the subspace $\mathcal{F}_0 \bigoplus \ldots \bigoplus \mathcal{F}_n$, corresponds to the characteristic functions of a ball with radius $R = \theta(\hat{N} + 1)$. Therefore, we find that the volume of the ball is given by

$$V_R = 4\pi\theta^3 \mathrm{Tr}_c \left((\hat{N} + 1)\hat{P}_n\right) = 4\pi\theta^3 \sum_{k=0}^{n} (k+1)^2 = \frac{4\pi}{3} R^3 \left[1 + \mathcal{O}\left(\frac{\theta}{R}\right)\right], \tag{3.13}$$

confirming that the weight $w(\hat{r})$ has the desired property.

From the results above, we define the inner product between two elements of $\mathcal{H}_q$ as

$$\left(\hat{\psi}\,\middle|\,\hat{\phi}\right) = 4\pi\theta^2\,\mathrm{Tr}_c(\hat{\psi}^\dagger\,\hat{r}\,\hat{\phi}). \tag{3.14}$$

It is important to note that we distiguish between elements of $\mathcal{H}_c$ and $\mathcal{H}_q$ by reserving the notation of $|\cdot\rangle$ for elements of $\mathcal{H}_c$ and $|\cdot)$ for elements of $\mathcal{H}_q$.

The angular momentum operators are given by

$$\hat{L}_i\hat{\psi} = \frac{\hbar}{2\theta}[\hat{X}_i, \hat{\psi}], \tag{3.15}$$

and obey the usual commutation relations

$$[\hat{L}_i, \hat{L}_j] = i\hbar\varepsilon_{ijk}\hat{L}_k. \tag{3.16}$$

The simultaneous eigenstates of $\hat{L}_3$ and $\hat{L}^2$ are given by

$$\hat{\psi}_{jm} = \theta^j \sum_{(jm)} \frac{(\hat{a}_1^\dagger)^{m_1}(\hat{a}_2^\dagger)^{m_2}}{m_1!\,m_2!} :R(\hat{N}): \frac{(\hat{a}_1)^{n_1}(-\hat{a}_2)^{n_2}}{n_1!\,n_2!}, \tag{3.17}$$

for $j = 0, 1, 2, \ldots$ and $m = -j, \ldots, +j$. The summation indices assume non-negative integers satisfying $m_1 + m_2 = n_1 + n_2 = j$ and $m_1 - m_2 - n_1 + n_2 = 2m$. Here we see that the radial dependence is entirely captured in $:R(\hat{N}):$ and the angular dependence captured in the creation- and annihilation filled factors. We can, therefore, refer to $\hat{\psi}_{jm}$ as the wavefunction of a particle with angular momentum j and $\hat{L}_3$ projection m.

In order to continue, it is necessary at this stage to outline properties of the radial operator and eigenstates.

Firstly, as we note that we have a normal ordering of the radial function $R(\hat{N})$ in the wavefunction above, we inspect the behaviour of the normal ordering of a function of the counting operator $\hat{N}$. Assuming a Taylor expansion, it is sufficient to study the normal ordering of powers of $\hat{N}$:

$$:\hat{N}^k: |n_1, n_2\rangle = \frac{\hat{N}!}{(\hat{N}-k)!}\,|n_1, n_2\rangle\,. \tag{3.18}$$

This is easily proved via induction and is shown in Section A.2. Using (3.18) we also find the

following:

$$\begin{aligned}\left(:\hat{N}^{k+1}: \,-\hat{N}:\hat{N}^{k}:\right)|n_1,n_2\rangle &= \Big(n(n-1)(n-2)\dots(n-k+1)(n-k)\\ &\qquad -n^2(n-1)(n-2)\dots(n-k+1)\Big)|n_1,n_2\rangle\\ &= (n-k-n)\left(n(n-1)\dots(n-k+1)\right)|n_1,n_2\rangle\\ &= -k:\hat{N}^{k}:|n_1,n_2\rangle\end{aligned}$$

$$\Rightarrow \hat{N}:\hat{N}^{k}: = :\hat{N}^{k+1}: \,+k:\hat{N}^{k}:. \tag{3.19}$$

When viewing the wavefunction, we find the radial dependence of the wavefunction is contained in the normal ordered form of the function $R(\hat{N}) = \Sigma_{k=0}^{\infty} c_k \hat{N}^k$ given by

$$\bar{R}(\hat{N}) \equiv :R(\hat{N}): = \sum_{k=1}^{\infty} c_k :\hat{N}^k: = \sum_{k=2}^{\infty} c_k \frac{\hat{N}!}{(\hat{N}-k)!}. \tag{3.20}$$

From (3.19) and (3.20) it can easily be seen that

$$\begin{aligned}\hat{N}:R(\hat{N}): \,&= \sum_{k=0}^{\infty} c_k\, \hat{N}:\hat{N}^k:\\ &= \sum_{k=0}^{\infty} c_k \left(:\hat{N}^{k+1}: \,+k:\hat{N}^k:\right)\\ &= :\hat{N}\,R(\hat{N}): \,+\, :\hat{N}\,R'(\hat{N}):,\end{aligned} \tag{3.21}$$

where we use the following notation

$$R(\hat{N}) = \sum_{k=0}^{\infty} c_k \hat{N}^k, \quad R'(\hat{N}) = \sum_{k=0}^{\infty} k\, c_k \hat{N}^{k-1}, \quad R''(\hat{N}) = \sum_{k=0}^{\infty} k(k-1)\, c_k \hat{N}^{k-2}. \tag{3.22}$$

Next we wish to find the operators corresponding to differentiation of a wavefunction, and in particular we are interested in the second order derivate with respect to the radial coordinate. We start off by investigating the following double commutator

$$\left[\hat{a}_\alpha^\dagger, [\hat{a}_\alpha, \hat{\psi}_{jm}]\right] = \theta^j \left[\hat{a}_\alpha^\dagger\,, \left[\hat{a}_\alpha^\dagger\,, \sum_{(jm)} \frac{(\hat{a}_1^\dagger)^{m_1}(\hat{a}_2^\dagger)^{m_2}}{m_1!\,m_2!} :R(\hat{N}): \frac{(\hat{a}_1)^{n_1}(-\hat{a}_2)^{n_2}}{n_1!\,n_2!}\right]\right], \tag{3.23}$$

as a double commutator is well-known to be an analog of the second order differential operator. Following the calculation outlined in Section A.5 we find that (3.23) equates to

$$[\hat{a}_\alpha^\dagger,[\hat{a}_\alpha,\hat{\psi}_{jm}]] = -\theta^j \sum_{(jm)} \frac{(\hat{a}_1^\dagger)^{m_1}(\hat{a}_2^\dagger)^{m_2}}{m_1!\,m_2!} :[\hat{N}\,R''(\hat{N}) + 2(j+1)\,R'(\hat{N})]: \frac{(\hat{a}_1)^{n_1}(-\hat{a}_2)^{n_2}}{n_1!\,n_2!}. \tag{3.24}$$

Given the results above, we have that a suitable radial Laplacian on the quantum Hilbert space is given by [12]

$$\Delta_\theta \hat{\psi}_{jm} \equiv -\frac{1}{\theta\hat{r}}\left[\hat{a}_\alpha^\dagger,[\hat{a}_\alpha,\hat{\psi}_{jm}]\right]. \tag{3.25}$$

Here we find that the factor of $\hat{r}^{-1}$ is needed in order for Δ_θ to be Hermitian with respect to the inner product (3.14) and θ^{-1} is necessary to preserve the dimensions.

Another useful result, as outlined in Section A.6, is that

$$\hat{r}\,\hat{\psi}_{jm} = \theta^{j+1} \sum_{(jm)} \frac{(\hat{a}_1^\dagger)^{m_1}(\hat{a}_2^\dagger)^{m_2}}{m_1!\,m_2!} :[(\hat{N}+j+1)\,R(\hat{N}) + \hat{N}\,R'(\hat{N})]: \frac{(\hat{a}_1)^{n_1}(-\hat{a}_2)^{n_2}}{n_1!\,n_2!}. \tag{3.26}$$

3.3 Free particle in fuzzy space

The Hamiltonian for a non-commutative free particle is given by

$$H_0 = -\frac{\hbar^2}{2m}\Delta_\theta, \tag{3.27}$$

and, correspondingly, the non-commutative time-independent Schrödinger equation for a free particle reads:

$$H_0\hat{\psi} = -\frac{\hbar^2}{2m}\Delta_\theta\hat{\psi} = \frac{\hbar^2}{2m\theta\hat{r}}[\hat{a}_\alpha^\dagger,[\hat{a}_\alpha,\hat{\psi}]] = E\hat{\psi}. \tag{3.28}$$

For the eigenstates provided in (3.17) this reduces to

$$[\hat{a}_\alpha^\dagger,[\hat{a}_\alpha,\hat{\psi}_{jm}]] = \theta k^2 \hat{r}\,\hat{\psi}_{jm}, \tag{3.29}$$

where $k = \frac{\sqrt{2mE}}{\hbar}$. Substituting (3.23) and (3.26) into (3.29), one finds the governing expression

$$:\Big(\hat{N}\,R''(\hat{N}) + [2(j+1) + \kappa^2\hat{N}]\,R'(\hat{N}) + \kappa^2[\hat{N}+j+1]\,R(\hat{N})\Big): = 0, \tag{3.30}$$

where $\kappa = \theta k$. Since the coefficients c_k, as defined in (3.20), for the radial function remains unknown at this point, we are left to find the exact solutions to $\bar{R}(\hat{N}) \equiv \bar{R}(n)$ for which (3.30)

can be satisfied. Where we have decided to simplify notation by replacing $\hat{N}$ with n, without the loss of generality, where referring to n simply refers to the value of operator $\hat{N}$ on a given state.

As will soon become apparent, each term within (3.30) can be written as a function of $\bar{R}(n)$. By rewriting all the terms in (3.30) into functions of $\bar{R}(n)$ we hope to find a general expression that we can solve exactly using standard techniques.

We start off with the simplest non-trivial term. This is given by

$$\begin{aligned} :\hat{N}\,R(\hat{N}): &= \sum_{k=0}^{\infty} c_k \;:\hat{N}^{k+1}: = \sum_{k=0}^{\infty} c_k \,\frac{n!}{(n-(k+1))!} \\ &= \sum_{k=0}^{\infty} c_k \,\frac{n!}{((n-1)-k)!} \\ &= \sum_{k=0}^{\infty} n\,c_k \,\frac{(n-1)!}{((n-1)-k)!} \\ &= n\,\bar{R}(n-1), \end{aligned} \tag{3.31}$$

and thereby we have identified a method to map non-trivial normal ordered products of $\hat{N}$ and $R(\hat{N})$ to $\bar{R}(n)$. The next non-trivial term identified is

$$\begin{aligned} :R'(\hat{N}): &= \sum_{k=0}^{\infty} k\,c_k \;:\hat{N}^{k-1}: = \sum_{k=0}^{\infty} k\,c_k \,\frac{n!}{(n-(k-1))!} \\ &= \sum_{k=0}^{\infty} k\,c_k \,\frac{n!}{(n-k+1)!} = \sum_{k=0}^{\infty} c_k \,\frac{n!}{(n-k)!}\,\frac{k}{(n-k+1)} \\ &= \sum_{k=0}^{\infty} c_k \,\frac{n!}{(n-k)!}\,\frac{k(n+1)}{(n+1)^2-k(n+1)} \\ &= \sum_{k=0}^{\infty} c_k \,\frac{n!}{(n-k)!}\left(\frac{k(n+1)}{(n+1)^2-k(n+1)} + \frac{(n+1)^2-(n+1)^2}{(n+1)^2-k(n+1)}\right) \\ &= \sum_{k=0}^{\infty} c_k \,\frac{n!}{(n-k)!}\left(\frac{(n+1)}{(n+1)-k} - 1\right) \\ &= \sum_{k=0}^{\infty} c_k \left(\frac{(n+1)!}{((n+1)-k)!} - \frac{n!}{(n-k)!}\right) \\ &= \bar{R}(n+1) - \bar{R}(n) \equiv \bar{R}'(n), \end{aligned} \tag{3.32}$$

where we see that we have defined the discrete analogue of the derivative which we note as $\bar{R}'(n)$.

By using the same method in (3.31) we can also easily show

$$:\hat{N}\,R'(\hat{N}):=n\,\bar{R}'(n-1)=n\left(\bar{R}(n)-\bar{R}(n-1)\right). \tag{3.33}$$

Similarly, using the method in (3.32), we find

$$:R''(\hat{N}):=\bar{R}''(n)=\bar{R}'(n+1)-\bar{R}'(n)=\bar{R}(n+2)-2\bar{R}(n+1)+\bar{R}(n), \tag{3.34}$$

from which it follows that

$$:\hat{N}R''(\hat{N}):=n\,\bar{R}''(n-1)=n\left(\bar{R}'(n+1)-\bar{R}'(n)\right)=n\left(\bar{R}(n+1)-2\bar{R}(n)+\bar{R}(n-1)\right). \tag{3.35}$$

Given the results from (3.31) to (3.35) and by substitution into (3.30) we find the final radial equation to be solved is

$$(n+2j+2)\,\bar{R}(n+1)+(\kappa^2-2)(n+j+1)\,\bar{R}(n)+n\,\bar{R}(n-1)=0, \qquad n\geq 0. \tag{3.36}$$

We, therefore, find that the final form of the non-commutative radial Schrödinger equation (3.30) reduces to a recursion equation in $\bar{R}(n)$ that can, in theory, be solved exactly. However, in practice, finding solutions to recursion equations is a daunting task and we will need to find alternative methods to find solutions that satisfy the recursion equation.

One of these alternative methods is to view the expression within the normal ordering in (3.30) as a differential equation for $\bar{R}(N)$ and solve it accordingly. The solutions to this differential equation can then be normal ordered as functions of $\hat{N}$ and the results thereof should also then satisfy the recursion equation. This alternative method is an easier route to finding the final solutions to the non-commutative radial Schrödinger equation.

3.3.1 Solving the radial Schrödinger equation as a differential equation

When viewing the expression within the normal ordering of (3.30) as a differential equation in $\hat{N}$, the differential equation reads

$$\hat{N}R''(\hat{N})+[2(j+1)+\kappa^2\hat{N}]\,R'(\hat{N})+\kappa^2[\hat{N}+j+1]\,R(\hat{N})=0. \tag{3.37}$$

Using standard techniques, it is found that the solution to this differential equation is a linear combination of

$$R_J(\hat{N}) = \hat{N}^{-(j+\frac{1}{2})} e^{-\frac{\kappa^2 \hat{N}}{2}} J_{j+\frac{1}{2}}\left(\frac{\kappa}{2}\hat{N}\sqrt{4-\kappa^2}\right) \tag{3.38}$$

and

$$R_Y(\hat{N}) = \hat{N}^{-(j+\frac{1}{2})} e^{-\frac{\kappa^2 \hat{N}}{2}} Y_{j+\frac{1}{2}}\left(\frac{\kappa}{2}\hat{N}\sqrt{4-\kappa^2}\right), \tag{3.39}$$

where $J_\nu(x)$ and $Y_\nu(x)$ are the Bessel functions of the first and second kind respectively. The latter are often referred to as Neumann functions and the former simply as Bessel functions. Normal ordering these two functions would require that we find the Taylor expansions for both the Bessel- and Neumann functions. The Taylor expansions are given by eqs. (9.1.2) and (9.1.10) in [14]:

$$J_\nu(x) = (\frac{1}{2}x)^\nu \sum_{k=0}^{\infty} \frac{(-\frac{1}{4}x^2)^k}{k!\,\Gamma(\nu+k+1)} \tag{3.40}$$

and

$$\begin{aligned} Y_\nu(x) &= J_\nu(x)\cot(\nu\pi) - J_{-\nu}(x)\operatorname{cosec}(\nu\pi) \\ &= \cot(\nu\pi)(\frac{1}{2}x)^\nu \sum_{k=0}^{\infty} \frac{(-\frac{1}{4}x^2)^k}{k!\,\Gamma(\nu+k+1)} - \operatorname{cosec}(\nu\pi)(\frac{1}{2}x)^{-\nu} \sum_{k=0}^{\infty} \frac{(-\frac{1}{4}x^2)^k}{k!\,\Gamma(-\nu+k+1)}, \end{aligned} \tag{3.41}$$

for all non-integer ν. Since, in our case, $\nu = j + \frac{1}{2}$ and therefore would always be a half-integer number, we see that the cotangent term in the Taylor expansion for the Neumann function will always be 0.

We now find the normal ordered expressions for the solutions given in (3.38) and (3.39). Normal ordering the Bessel factor (3.38) by use of the Taylor expansion given by (3.40) results in

$$\bar{R}_J(n) = \frac{2^{-(2j+1)}\left(1-\frac{\kappa^2}{2}\right)^n \left(-\kappa\sqrt{4-\kappa^2}\right)^{j+\frac{1}{2}}}{\Gamma(j+\frac{3}{2})} {}_2F_1(-\frac{n}{2}\,, -\frac{(n-1)}{2}\,;\, j+\frac{3}{2}\,;\, 1-\frac{4}{(\kappa^2-2)^2}), \tag{3.42}$$

where ${}_2F_1$ is a hypergeometric function. Normal ordering the Neumann part (3.39) with use of (3.41) results in

$$\bar{R}_Y(n) = (-1)^{j+1} 2^{-n} (2-\kappa^2)^{n+2j+1} \left(\kappa\sqrt{4-\kappa^2}\right)^{-(j+\frac{1}{2})} \frac{\Gamma(n+1)}{\Gamma(n+2j+2)\,\Gamma(-j+\frac{1}{2})} \tag{3.43}$$

$$\times\ {}_2F_1(-\frac{(n+2j+1)}{2}\,, -\frac{(n+2j)}{2}\,;\, -j+\frac{1}{2}\,;\, 1-\frac{4}{(\kappa^2-2)^2}). \tag{3.44}$$

The computations of the normal ordered solutions are outlined in A.7.

With a simple check we see that both these solutions are solutions of the recursion equation in (3.36). However, we find that $\bar{R}_Y(n)$ is singular for $n < 0$ and, therefore, cannot satisfy the recursion equation given in (3.36) for $n = 0$. Therefore, as expected, the normal ordered Neumann function can only be used for solutions that do not include the origin in its domain.

We therefore conclude that the free particle radial solutions to (3.30) should take the form of

$$\begin{aligned} &\Psi(n) = C\ \bar{R}_J(n), \qquad n \geq 0, \\ &\qquad \text{and} \\ &\Psi(n) = A\ \bar{R}_J(n) + B\ \bar{R}_Y(n), \qquad n \geq 1, \end{aligned} \tag{3.45}$$

where A, B and C are normalization constants.

3.3.2 Square-integrability of the free particle solutions in different energy sectors

A prerequisite for the free particle radial solutions to be acceptable solutions is that they must be square integrable in the sense of (3.11). As will become apparent in what follows, we see that the square-integrability of the radial solutions is highly dependent on the energy sector in which the solutions are calculated.

Reflecting on the final forms of the radial solutions in (3.42) and (3.44), we easily identify three global energy sectors in which the behaviour of the solutions differ. Keeping in mind that the normal ordered Neumann function does not satisfy the radial Schrödinger equation at the origin, these energy sectors, and the associated behaviour of the solutions, are as follow:

(i) $0 < \kappa < 2$

The first energy sector is that of a positive energy, however, with the energy bounded from above by $E < \frac{2\hbar^2}{\theta^2 m}$. In this energy sector we find that both the normal ordered Bessel- and Neumann functions are finite and real over the entire radial domain. Furthermore, we see that both solutions tend to 0 fast enough in the limit $n \to \infty$ such that the solutions are square-integrable. In the limits where $E \to 0$ and $E \to \frac{2\hbar^2}{\theta^2 m}$, we see that the radial wavefunctions take on the trivial solution of $\Psi(n) = 0$.

(ii) $\kappa > 2$

In this energy sector, where we have particle energies exceeding $\frac{2\hbar^2}{\theta^2 m}$, we find that the

solutions gain a complex phase. Furthermore, we also find that the norm of both solutions diverge as $n \to \infty$. These are, therefore, not admissable solutions of the free particle Schrödinger equation.

(iii) $\kappa = i\,\varepsilon,\ 0 < \varepsilon$

This sector corresponds to solutions of non-zero potentials, where the particle energy is less than the potential depth. In this energy sector we see that, again, both the normal ordered Bessel- and Neumann functions are complex valued and have their norms diverge as $n \to \infty$. However, there exists a unique combination of the two solutions to which the resulting combination tends to 0 as $n \to \infty$ and restores square-integrability over the domain $n \in [1, \infty)$. This unique combination is given by

$$\bar{R}_H(n) = \bar{R}_J(n) + i\bar{R}_Y(n). \tag{3.46}$$

As expected, $\bar{R}_H(n)$ is the normal ordered equivalent to the Hankel function of the first kind. The expression for $\bar{R}_H(n)$ is given by

$$\begin{aligned}\bar{R}_H(n) = &\frac{2(-1)^{j+1}\left(i\varepsilon\sqrt{4+\varepsilon^2}\right)^{j+\frac{1}{2}}\left(4+\varepsilon^2\right)^{-(2+2j+n)}\,\Gamma(1+n)}{\sqrt{\pi}\,\Gamma(2+j+n)} \\ &\times\ {}_2F_1\left(j+n+\frac{3}{2}\,,\,2+2j+n\,;\,3+2j+2n\,;\,\frac{4}{4+\varepsilon^2}\right).\end{aligned} \tag{3.47}$$

Due to the implicit dependence of the Hankel function on the Neumann function, we also find that the normal ordered Hankel function of the first kind does not satisfy the radial Schrödinger equation at the origin.

The different behaviours of the wavefunctions in each of the energy sectors are illustrated in Figure 3.1.

By probing the behaviours of the solutions in different energy sectors, we have now discovered the very interesting fact that there is a global cutoff in kinetic energy for a free particle. Since for $\kappa > 2$ there are no permissible square-integrable solutions and we find that the radial wavefunction for a free particle reduces to the trivial form of $\Psi(n) = 0$ and, therefore, no free particle state exists with a kinetic energy larger than $\frac{2\hbar^2}{\theta^2 m}$.

Since the wavelength for a particle is expressed as $\lambda = 2\pi/k = 2\pi\theta/\kappa$ and it is required that $\kappa \leq 2$, we find that the wavelength for a non-commutative particle is bound by $\lambda > \pi\theta$. Thus,

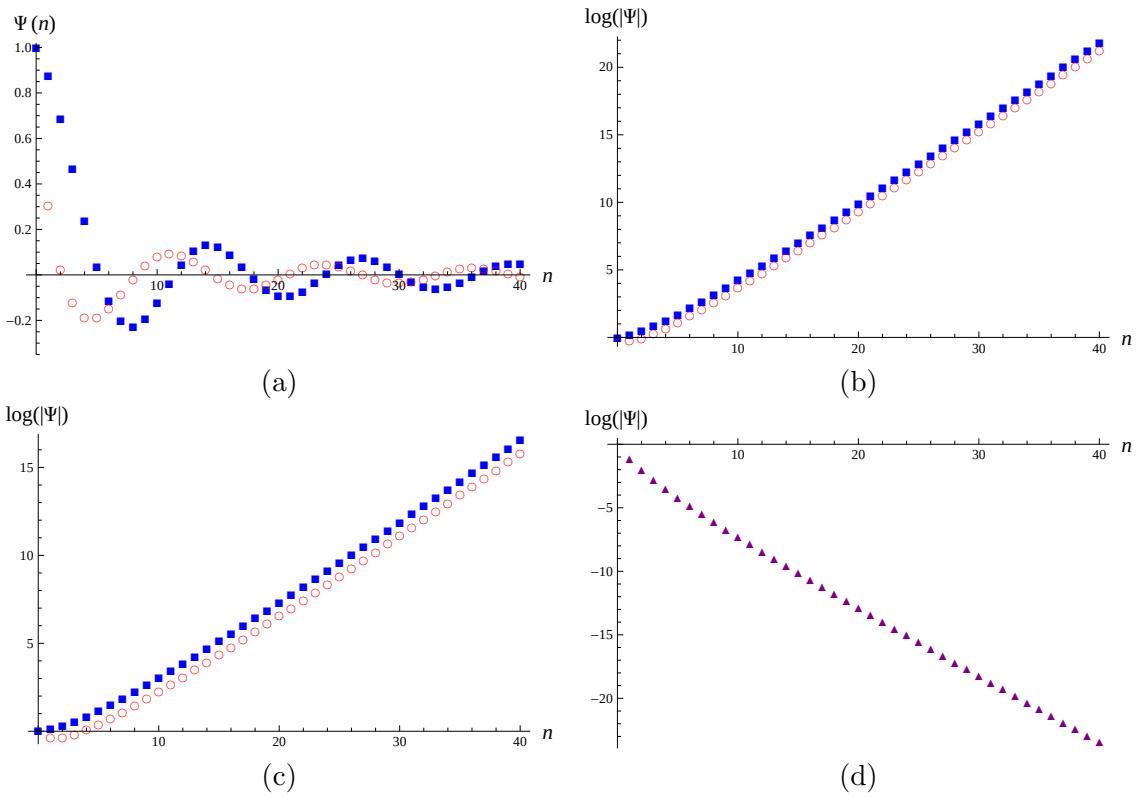

Figure 3.1: Illustrations for the different wavefunctions within different energy sectors. In subfigures (a) to (c) we have the normal ordered Bessel function marked with blue squares and the normal ordered Neumann function is marked with red circles. In subfigure (d) we only have the normal ordered Hankel function in purple triangles. The parameters used in the subfigures are as follows: (a) $\kappa = 0.5$, $j = 0$; (b) $\kappa = 2.1$, $j = 0$; (c) and (d) $\kappa = i\,0.5$, $j = 0$. All wavefunctions were scaled to exhibit the defining features.

a particle in our non-commutative system is unable to obtain a wavelength that probes length scales smaller than θ.

3.4 The non-commutative three-dimensional spherical well (Fuzzy well)

In order to construct a system with a potential well, we first need to define projection operators which seperates different sectors of the counting operator $\hat{N}$. For a single value of N, we could project onto all states with a total boson number N with

$$\hat{P}_N = \sum_{n=0}^{N} |n,\, N-n\rangle \langle n,\, N-n| \,. \tag{3.48}$$

One now defines, for a potential well problem, two projection operators which projects all configuration space states either inside or outside of the well of integer radius M. These projection operators are given by

$$P = \sum_{r=0}^{M} \hat{P}_r, \qquad Q = \sum_{r=M+1}^{\infty} \hat{P}_r, \tag{3.49}$$

from which it is clear that P projects onto all states within the well with radius M, and Q onto all states outside the well. Given these projection operators, the time-independent Schrödinger equation describing a 3-dimensional non-commutative spherical well would read

$$H\hat{\psi}_{jm} = -\frac{\hbar^2}{2m}\Delta_\theta \hat{\psi}_{jm} + (V_1 P + V_2 Q)\hat{\psi}_{jm} = E\hat{\psi}_{jm} \tag{3.50}$$

Considering the wavefunction $\hat{\psi}_{jm}$ as given in (3.17), the actions of the projection operators thereon are given by

$$P\,\hat{\psi}_{jm} = \theta^j \sum_{(jm)} \frac{(\hat{a}_1^\dagger)^{m_1}(\hat{a}_2^\dagger)^{m_2}}{m_1!\,m_2!}\,\Theta(M - n' - j)\,{:}R(\hat{N}){:}\,\frac{(\hat{a}_1)^{n_1}(-\hat{a}_2)^{n_2}}{n_1!\,n_2!} \tag{3.51}$$

and

$$Q\,\hat{\psi}_{jm} = \theta^j \sum_{(jm)} \frac{(\hat{a}_1^\dagger)^{m_1}(\hat{a}_2^\dagger)^{m_2}}{m_1!\,m_2!}\,\Theta\left(-[M + 1 - n' - j]\right)\,{:}R(\hat{N}){:}\,\frac{(\hat{a}_1)^{n_1}(-\hat{a}_2)^{n_2}}{n_1!\,n_2!}, \tag{3.52}$$

where $\Theta(\cdot)$ is the Heaviside step function, and n' inside the Heaviside step function is the total boson count as seen by $\hat{N}$ within the normal ordered radial function.

Substituting the results for the two projections from (3.51) and (3.52) into the Hamiltonian in (3.50), we find two radial equations identical to the form of (3.36):

$$(n + 2j + 2)\,\bar{R}(n + 1) + ({\kappa_i}^2 - 2)(n + j + 1)\,\bar{R}(n) + n\,\bar{R}(n - 1) = 0, \tag{3.53}$$

where

$$\kappa_i = \begin{cases} \kappa_1 = \frac{\theta\sqrt{2m(E-V_1)}}{\hbar}, & \text{if } 0 \leq n \leq M - j \\ \\ \kappa_2 = \frac{\theta\sqrt{2m(E-V_2)}}{\hbar}, & \text{if } n > M - j \end{cases}. \tag{3.54}$$

We see here that the quantity $(M - j)$ acts as an effective well radius which, for the purpose of simplifying notation, we will substitute with $\mathcal{M} = M - j$. To further simplify notation, we

relabel $\kappa_1 \to \kappa_{in}$ and $\kappa_2 \to \kappa_{out}$ as they represent the energy values of solutions inside and outside the well, respectively. Lastly we will assume that the potential inside the well assumes the value $V_1 = 0$ and outside the well $V_2 = V$, with V being a positive real number.

It is important to note at this stage that the angular momentum within the well is bound by $j \in [0, M]$, at which stage the well will effectively disappear for any particle with an angular momentum $j \geq M + 1$ and the well problem is reduced to only a single radial equation to be solved, effectively reducing it to a free particle.

We are now also able to identify solutions to the different regions of the spherical well:

- Inside the well, where $n \leq \mathcal{M}$, the only requirement is that the radial equation be solvable from the origin. Therefore, the only allowed solution will be the normal ordered Bessel function, since the normal ordered Neumann- and Hankel functions are excluded as valid solutions at the origin.
- Outside the well, where $n \geq \mathcal{M} + 1$, we find that any linear combination of the normal ordered Bessel- and Neumann functions is allowed for $V < E$, while only the normal ordered Hankel function is allowed for $V > E$.

As a reminder, the normal ordered Bessel-, Neumann- and Hankel functions are respectively given by eqs. (3.42), (3.44) and (3.47).

The next step is to find an expression for the matching conditions at the well-edge. This is necessary when calculating bound state energies, as well as scattering coefficients for the solutions. To find these matching conditions we first consider two radial solutions for the recursion equation (3.36). The solution inside the well, with $0 \leq n \leq \mathcal{M}$, reads:

$$(n + 2j + 2)\,\Psi_{in}(n + 1) + (\kappa_{in}^2 - 2)(n + j + 1)\,\Psi_{in}(n) + n\,\Psi_{in}(n - 1) = 0. \tag{3.55}$$

Outside the well, with $n > \mathcal{M}$, we have:

$$(n + 2j + 2)\,\Psi_{out}(n + 1) + (\kappa_{out}^2 - 2)(n + j + 1)\,\Psi_{out}(n) + n\,\Psi_{out}(n - 1) = 0. \tag{3.56}$$

Here $\Psi_{in}(n)$ and $\Psi_{out}(n)$ respectively refer to the radial wavefunctions inside and outside the well.

Firstly we notice that when $n = \mathcal{M}$, (3.55) determines the value of $\Psi_{in}(\mathcal{M}+1)$. However, $\mathcal{M}+1$

falls outside the well where the radial solution is determined by Ψ_{out}, from which we can conclude that at $n = \mathcal{M} + 1$, in order for the Schrödinger equation to be satisfied, we must require that

$$\Psi_{in}(\mathcal{M}+1) = \alpha\, \Psi_{out}(\mathcal{M}+1), \tag{3.57}$$

where α is a normalisation constant. This is our first matching condition. A similar argument applied to (3.56) shows that

$$\Psi_{in}(\mathcal{M}) = \alpha\, \Psi_{out}(\mathcal{M}). \tag{3.58}$$

Dividing (3.57) by (3.58) gives us our final matching condition:

$$\frac{\Psi_{in}(\mathcal{M}+1)}{\Psi_{in}(\mathcal{M})} = \frac{\Psi_{out}(\mathcal{M}+1)}{\Psi_{out}(\mathcal{M})}\ . \tag{3.59}$$

We note that both eqs. (3.57) and (3.58) require that both wavefunctions are equal at the well-edge, while (3.59) requires that the slope for both wavefunctions should be equal at the edge. These matching conditions agree with the standard matching conditions one would find in the commutative case.

We use matching conditions in (3.57), (3.58) and (3.59) in order to find the energy solutions of the system, as well as the scattering coefficients. The latter will be covered in the next chapter.

3.5 The infinite well

Based on the results in the previous section, we can now discuss the case of the infinite spherical well, i.e. we attempt to find the appropriate solutions in the limit where $V \to \infty$.

We start off by investigating the solution outside of the well. In the case of the commutative infinite well we have that all solutions should die out as soon as they enter the well-border and, therefore, a solution of $\psi(r) = 0$ with $r \geq R$ is the only permitted solution for a well of radius R. We expect to see the same behaviour in the non-commutative case.

Given that the solution outside the well has the form of the normal ordered Haskel function, we investigate the ratio on the right-hand side of eq. (3.59). Recalling that $\kappa = i\varepsilon \sim i\sqrt{V-E},\ 0 < \varepsilon$, we find that the limit of $V \to \infty$ implies $\varepsilon \to \infty$ in (3.47). We therefore do an expansion of

$\frac{\Psi_{out}(\mathcal{M}+1)}{\Psi_{out}(\mathcal{M})}$ around $\varepsilon \to \infty$ with the result being

$$\lim_{\varepsilon\to\infty} \frac{\Psi_{out}(\mathcal{M}+1)}{\Psi_{out}(\mathcal{M})} = \lim_{\varepsilon\to\infty} \frac{\bar{R}_H(M-j+1)}{\bar{R}_H(M-j)} = \lim_{\varepsilon\to\infty} \frac{\mathcal{M}+1}{(\mathcal{M}+j+2)\,\varepsilon^2} + \mathcal{O}(\frac{1}{\varepsilon^4}) + \dots \,. \quad (3.60)$$

In the limit $V, \varepsilon \to \infty$, equation (3.60) clearly vanishes, from which we conclude that $\Psi_{out}(\mathcal{M}+1)$ should also vanish. Even more, by applying the same technique, we can extend (3.60) to show that the ratio of $\frac{\Psi_{out}(n+1)}{\Psi_{out}(n)}$ will always vanish for any $n \geq \mathcal{M}$ and, therefore, the solution outside the well will always vanish, agreeing with the expected result.

3.5.1 Finding energy solutions for the infinite well

In the limit when $V, \varepsilon \to \infty$, we have that $\Psi_{in}(\mathcal{M}+1) \to 0$ through the use of eqs. (3.60) and (3.57). This implies that in order for us to find the energy solutions to the infinite well, we need to find the zeros of normal ordered Bessel function given in (3.42) at $n = \mathcal{M}+1$. However, finding the zeros of a hypergeometric function is not an easy task and we would prefer to have the normal ordered Bessel function in a form better suited to the task at hand.

By using eq. (15.3.21) in [14], we can rewrite the hypergeometric function $\Psi_{in}(n)$, which is simply the normal order Bessel function (3.42), into the form of

$$\Psi_{in}(n) \propto \frac{1}{\Gamma(j+\frac{3}{2})}\, {}_2F_1(-n\,,\, n+2j+2\,;\, j+\frac{3}{2}\,;\, \frac{\kappa^2}{4}), \quad (3.61)$$

where we assumed that $\kappa_{in} = \kappa$ and we have kept only the gamma function normalising pre-factors. Furthermore, we can use eq.(15.4.6) in [14] to rewrite (3.61) as a Jacobi polynomial:

$$\Psi_{in}(n) \propto \frac{\Gamma(n+1)}{\Gamma(n+j+\frac{3}{2})}\, P_n^{(j+\frac{1}{2},j+\frac{1}{2})}(1-\frac{\kappa^2}{2}). \quad (3.62)$$

Finding the zeros for $\Psi_{in}(\mathcal{M}+1)$ therefore requires that we find the zeros of the Jacobi polynomial in (3.62) with $n = \mathcal{M}+1 = M-j+1$. The final quantization condition from which we may calculate the energy solutions is then given by

$$P_{M-j+1}^{(j+\frac{1}{2},j+\frac{1}{2})}(1-\theta^2 m_0 E/\hbar^2) = 0, \quad (3.63)$$

where we used the fact that $\kappa = \theta k = \theta\frac{\sqrt{2m_0 E}}{\hbar}$.

We may now use the properties of the Jacobi polynomial in (3.63) to elaborate on facts of the

energy spectrum for the infinite well. Firstly, it is known that the zeroes of the Jacobi polynomial $P_n^{(\alpha,\beta)}(x)$ is restricted to domain $x_0 \in (-1, 1)$. This, again confirms that our energy solutions are bound from below and above by $E \in (0\,, \frac{2\hbar^2}{\theta^2 m_0})$ which we have already seen in previous sections. Another property is that the Jacobi polynomial has exactly $M - j + 1$ unique zeroes, which implies that for a given value of the angular momentum j, there exists only a finite number of bound states. Since the angular momentum itself is bound by $j \leq M$, we find that the infinite spherical fuzzy well has a finite number of bound states in its entirety.

We can easily calculate the maximum number of single particle states for an infinite well of integer radius M. Given that the maximum number of energy solutions for a given j is $M - j + 1$, we find the total number of bound states to be

$$\begin{aligned} N^{(\max)} &= \sum_{j=0}^{M} \sum_{m=-j}^{+j} M - j + 1 \\ &= \frac{1}{6}(M+1)(M+2)(2M+3) \\ &= \frac{M^3}{3} + \mathcal{O}(M^2). \end{aligned} \tag{3.64}$$

We therefore see that the total number of bound states is proportional, up to leading order, to M^3. Since the Euclidean radius of the well is given by $R = \theta(M + 1)$, and therefore $M \sim \frac{R}{\theta}$, we see that the total number of bound states is proportional to the volume of the system and inversely proportional to θ^3. This suggests that each single particle bound state occupies a finite volume $V_0 \sim \theta^3$ and that the total number of bound states is, therefore, simply the volume of the well divided by V_0. This has important implications for the thermodynamics of Fermi gases as it suggests the existence of a maximum density.

As an illustration, we see in Figure 3.2 that not only is the total number of bound states affected by our choice of θ and R, but the actual energy levels also get lowered as the effects of non-commutativity become stronger. We also clearly see from the figure that as $\theta \to 0$, we find the energy levels tend to the expected commutative energy spectrum of the infinite well given by

$$E_n = \frac{n^2\pi^2\hbar^2}{2m_0 R} \quad n = 1, 2, 3, \ldots \quad . \tag{3.65}$$

As a final note, we find that the Jacobi polynomial with equal arguments $P_n^{(\alpha,\alpha)}(x)$ is symmetric around $x = 0$. Therefore, the solutions to (3.63) is arranged symmetrically around $E = \frac{\hbar^2}{\theta^2 m_0}$.

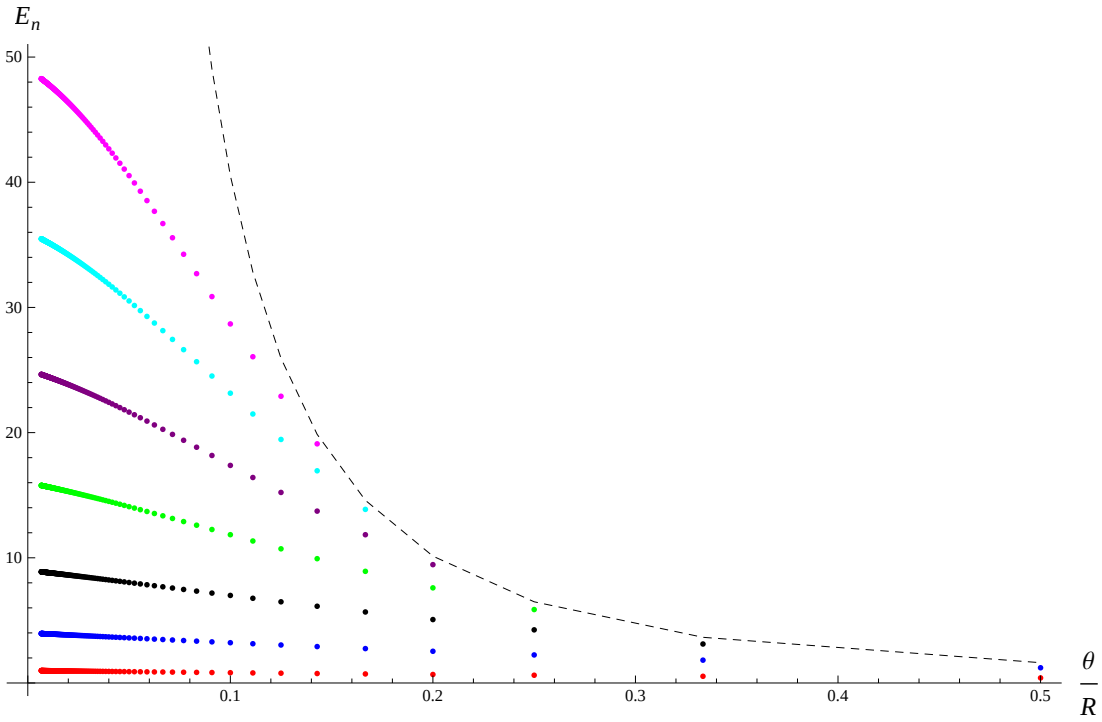

Figure 3.2: Normalized bound state energy values for as function of the non-commutative parameter θ. Each set of similarly colored points correspond to the same energy level as set out by the infinite well energy spectrum, where we only show the $j = 0$ energy levels. The dashed black line indicates the maximum allowed kinetic energy per particle for a given value of θ.

3.5.2 The commutative limit

In the commutative limit, i.e. in the limit that $\theta \to 0$, we want to see if the polynomial for which we should find the zeros would reduce to the expected spherical Bessel function as in the commutative infinite spherical well. For a fixed Euclidean well radius $R = \theta(M + 1)$, we find that if $\theta \to 0$ then we should have that $M \to \infty$ in such a way that R stays fixed. We now can investigate the zeros of (3.62) at $n = M - j + 1$ in the large M limit. Note that in the large M limit we have that $M - j + 1 \sim M$, and therefore $n \sim M$, and also that $\theta = \frac{R}{(M+1)} \sim \frac{R}{M}$. Another fact to note is that the pre-factor in (3.62) goes like $n^{-j-\frac{1}{2}}$. Thus, we can rewrite (3.62) in the large M limit as

$$\lim_{M\to\infty} \Psi_{in}(n) \propto \lim_{M\to\infty} \frac{1}{M^{j+\frac{1}{2}}} P_M^{(j+\frac{1}{2},j+\frac{1}{2})}(1 - \frac{k^2R^2}{2M^2}), \tag{3.66}$$

which we can use in conjunction with eq.(22.15.1) in [14] to obtain the commutative limit polynomial:

$$\lim_{M\to\infty} \Psi_{in}(n) \;\propto\; \left(\frac{2}{\kappa R}\right)^{l+\frac{1}{2}} J_{l+\frac{1}{2}}(\kappa R) \;=\; \frac{2^{l+1}}{\sqrt{\pi}}\frac{1}{(\kappa R)^l}\, j_l(\kappa R), \tag{3.67}$$

which is identical, up to a constant, to the radial solution of the commutative case. Note that we replaced our previous notation of the angular moment j with l in order to avoid confusion with the spherical Bessel function $j_l(x)$.

3.5.3 Additional properties of the bound state spectrum of the infinite well

We now discuss additional properties of the bound state spectrum of the infinite well which will be of particular use during the thermodynamic calculations in Chapter 5.

Upon using the symmetry relation $P_n^{(\alpha,\alpha)}(-x) = (-1)^n P_n^{(\alpha,\alpha)}(x)$ and the freedom to shift the energies by a constant, we see that we are able to rewrite the quantization condition in (3.63) as

$$P_{M-j+1}^{(j+\frac{1}{2},j+\frac{1}{2})}(\theta^2 m_0 E/\hbar^2) = P_{M-j+1}^{(j+\frac{1}{2},j+\frac{1}{2})}(\frac{E}{E_0}) = 0, \tag{3.68}$$

with $E_0 = \hbar^2/(\theta^2 m_0)$. Note that, due to shifting the energies, the bound state energies are now arranged symmetrically around $E = 0$. This form will be of particular mathematical use when we want to calculate the density of states in the large M limit.

In order to study the thermodynamics of particles trapped in our infinite spherical well, we require the density of states, which is related to the density of zeros of the Jacobi polynomial (3.68). There has been some work done on finding the density of zeroes of orthogonal polynomials [15] and specifically work done on Jacobi polynomials as well [22, 23]. We find in these works that the density of zeroes for (3.68), for $0 \ll j \ll M$, is given by

$$d_0(x, M, j) = \frac{M\sqrt{1 - x^2 - (\frac{j}{M})^2}}{(M-j)\pi\,(1-x^2)}, \tag{3.69}$$

where $x = E/E_0$. Since the total number of states for a given value of M and j is $(M - j)$ in the large M and j limit, we find then, by multiplying by $(M - j)$, the density of states for a fixed value of M, j and angular momentum projection m:

$$d(x, \lambda) = \frac{\sqrt{1 - x^2 - \lambda^2}}{\pi\,(1 - x^2)}, \tag{3.70}$$

where we have that $\lambda = j/M$ and, by definition, $d(x, \lambda) = 0$ for $|x| > \sqrt{1-\lambda^2}$.

We record one final result for later use. If the well contains spinless fermions then the maximum value of the z-component of the total angular momentum is denoted $\hbar L_3^{(\max)}$. This maximum is reached by filling all the single particle states with positive angular momentum projection m. A simple summations yields

$$\begin{aligned} L_3^{(\max)} &= \sum_{j=0}^{M} \sum_{m=0}^{+j} m(M-j+1) \\ &= \frac{1}{24} M(M+1)(M+2)(M+3) \\ &= \frac{M^4}{24} + \mathcal{O}(M^3). \end{aligned} \tag{3.71}$$

CHAPTER 4

SCATTERING STATES OF THE FINITE FUZZY WELL

In the previous chapter we established a quantum mechanical formulation for single particles in 3-dimensional non-commutative space, or fuzzy space. Explicit solutions for the time-independent Schrödinger equation were obtained for free particles and particles in the presence of a potential well. One particularly useful result in the potential well problem is that of the matching conditions for wavefunctions. These matching conditions, given by eq. (3.59), not only provide us with a means of obtaining the energy solutions for particles in a finite well, but also serves as the basis for finding scattering coefficients when investigating particle scattering in the presence of a finite fuzzy well.

However, before a complete formalism for particle scattering in fuzzy space can be established, it is necessary to obtain a consistent interpretation of position measurement, representation and probability currents in fuzzy space since the coordinates no longer commute. In [5] the notion of a positive operator valued measure (POVM) was introduced that provided a logical and consistent interpretation of position measurements in non-commutative space as strong position measurements were replaced by weak measurements. This approach was used to provide a clear interpretation of spatial probability densities and currents in fuzzy space, thereby enabling us to investigate particle scattering in the finite fuzzy well system. These formalisms and results were collected and published in [16] and will serve as the reference on which this chapter is built.

In this chapter we shall, therefore, outline how the position representation provided by POVMs is used to construct spatial probability densities and currents. Thereafter we give the formulation of particle scattering based on this approach with the accompanying results on particle scattering from a finite fuzzy well.

4.1 Position representation in fuzzy space

As mentioned in the introduction to this chapter, exact position measurements are, by definition, impossible in fuzzy space as the coordinates no longer commute. It is therefore necessary that we find a new interpretation to position measurements in fuzzy space as scattering theory is primarily dependent on probability densities and fluxes. In [5] the notion of positive operator

valued measures (POVMs) was used to give meaning to position measurement in a weak sense and we will briefly outline this approach in this section.

Recall that the configuration space $\mathcal{H}_c$ is the Fock space for the Schwinger realization of the $SU(2)$ coordinate algebra and is given by the equation (3.5). We may also relabel the basis states of $\mathcal{H}_c$ as

$$|j,m\rangle \equiv |n_1,n_2\rangle\,, \quad \text{with} \quad j=(n_1+n_2)/2=\frac{n}{2}, \quad m=(n_1-n_2)/2. \tag{4.1}$$

These relabeled states, $|j,m\rangle$, can be considered to represent a particle that is localized at radial distance of $r=\theta(n+1)=\theta(2j+1)$ from the origin, but delocalized in the two angular directions. It is now our goal to find the best localization for a particle with a given value of j. We do this by considering a unit vector[1] $\hat{u}=(\sin(\phi_1)\sin(\phi_2),\sin(\phi_1)\sin(\phi_2),\cos(\phi_1))$ and try to find a state for which the component of its position vector $\hat{\vec{X}}=(\hat{X}_1,\hat{X}_2,\hat{X}_3)$ along $\hat{u}$ is maximal. By achieving this, we are assured that we have found the best possible localization for the particle state $|j,m\rangle$ at the radial distance of $r=\theta(2j+1)$ around the point (ϕ_1,ϕ_2). These optimally localized states are described by

$$|n,z\rangle = \frac{1}{(1+zz^*)^{\frac{n}{2}}}\, e^{z\hat{X}_+}\, \left|j=\frac{n}{2},\ m=-\frac{n}{2}\right\rangle, \tag{4.2}$$

where $\hat{X}_+=\hat{X}_1+i\hat{X}_2$ and $z\in\mathbb{C}$. The states in (4.2) are noted to be the $SU(2)$ coherent states [20]. Furthermore, these states satisfy the relation $\hat{u}\cdot\hat{\vec{X}}\,|n,z\rangle=\theta n\,|n,z\rangle$, when z is related to the angular coordinates through $z=\cot(\phi_1/2)e^{-i\phi_2}$.

We are now able to obtain the identity operator on the configuration space $\mathcal{H}_c$ using these optimally localized states. This identity operator is given by

$$\hat{I}_c=\sum_{n=0}^{\infty}\int dz\,dz^*\mu_n(z,z^*)\,|n,z\rangle\,\langle n,z| \tag{4.3}$$

with

$$\mu_n(z,z^*)=\frac{1+n}{\pi(1+zz^*)^2}. \tag{4.4}$$

It is also possible to apply a similar construction on the quantum Hilbert space $\mathcal{H}_q$ by introducing

[1] Note that we kept the notation for θ as the non-commutative length parameter as to stay consistent between chapters. In order to accommodate notation for spherical coordinates we used ϕ_1 and ϕ_2 as the polar angle and azimuthal angle, respectively. This notation will be used throughout this chapter.

the states

$$|n,z,w) = \frac{|n,z\rangle\langle n,w|}{\sqrt{4\pi\theta^3(n+1)}}, \tag{4.5}$$

where the resulting identity operator on $\mathcal{H}_q$ is given by

$$\hat{I}_q = \sum_{n=0}^{\infty} \int dz\, dz^* \mu_n(z,z^*) \int dw\, dw^* \mu_n(w,w^*)\, |n,z,w)\, (n,z,w|\,. \tag{4.6}$$

By use of results in [21], we are able to rewrite eq. (4.6) into

$$\hat{I}_q = \sum_{n=0}^{\infty} \int dz\, dz^* \mu_n(z,z^*)\, |n,z,z) \star_n (n,z,z|\,, \tag{4.7}$$

where the star product $\star_n$ is defined by

$$\star_n = \int dw\, dw^* e^{\overleftarrow{\partial_z} w} \mu_n(z+w, z^*+w^*)\, |\langle n,z\,|\,n,z+w\rangle|^2\, e^{w^*\overrightarrow{\partial_{z^*}}}. \tag{4.8}$$

From the above it is clear that the operators given by

$$\hat{\pi}_{n,z} = |n,z,z) \star_n (n,z,z| \tag{4.9}$$

provide us with a positive operator valued measure.

If we now consider a particle described by the pure state density matrix $\rho = \left|\hat{\psi}\right)\left(\hat{\psi}\right|$, we find that the probability density at a radial distance of $r = \theta(n+1)$ and angular coordinates $z = z(\phi_1, \phi_2)$ is given by

$$P(n,z) = \mathrm{Tr}_q(\hat{\pi}_{n,z}\,\rho) = \left(\hat{\psi}\middle|\, n,z,z\right) \star_n \left(n,z,z\middle|\,\hat{\psi}\right). \tag{4.10}$$

We find, therefore, that the position representation of $\hat{\psi}$ is given by

$$\left(n,z,z\middle|\,\hat{\psi}\right) = \sqrt{4\pi\theta^3(n+1)}\,\left\langle n,z\middle|\,\hat{\psi}\,\middle|n,z\right\rangle. \tag{4.11}$$

Lastly, from [21] we have the identity

$$\left\langle n,z\middle|\,\hat{\psi}\,\hat{\phi}\,\middle|n,z\right\rangle = \left\langle n,z\middle|\,\hat{\psi}\,\middle|n,z\right\rangle \star_n \left\langle n,z\middle|\,\hat{\phi}\,\middle|n,z\right\rangle, \tag{4.12}$$

which enables us to rewrite the probability density in (4.10) into the useful form of

$$P(n,z) = 4\pi\theta^3(n+1)\left\langle n,z\right|\hat{\psi}^\dagger\,\hat{\psi}\left|n,z\right\rangle. \tag{4.13}$$

4.2 Probability currents

To compute probability currents in fuzzy space, it is necessary to consider the continuity equation for the probability density $P(n,z,t)$. In this case the time evolution is generated by the Hamiltonian

$$H_\theta = -\frac{\hbar^2}{2m}\Delta_\theta + V(\hat{r}). \tag{4.14}$$

It then follows from (4.4) and (4.13) that

$$\begin{aligned}\frac{d}{dt}\left[\mu_n(z,z^*)P(n,z,t)\right] &= \frac{4\theta^3}{i\hbar}\frac{(n+1)^2}{(1+z\,z^*)^2}\left\langle n,z\right|\hat{\psi}^\dagger H_\theta\hat{\psi} - (H_\theta\hat{\psi})^\dagger\hat{\psi}\left|n,z\right\rangle \\ &= \frac{2i\hbar\theta}{m}\frac{n+1}{(1+z\,z^*)^2}\left\langle n,z\right|\left[\hat{\psi}^\dagger\hat{a}_\alpha^\dagger\hat{\psi}\,,\,\hat{a}_\alpha\right] - \left[\hat{a}_\alpha^\dagger\,,\,\hat{\psi}^\dagger\hat{a}_\alpha\hat{\psi}\right]\left|n,z\right\rangle, \end{aligned}\tag{4.15}$$

where it is important to note that $V(\hat{r})$ disappeared as it commutes with $\hat{\psi}$, and the positive operator valued measure is automatically included as per our derivation of (4.13).

The next step will be to show that (4.15) can be expressed as a divergence in spherical coordinates where the radial axis is discretized. Considering the unnormalized coherent states defined by $|n,z\rangle_u \equiv (1+z\,z^*)^{n/2}\,|n,z\rangle$, we find the following useful identities

$$\begin{aligned}\hat{a}_1\,|n,z\rangle_u &= \sqrt{n}\,z\;|n-1,z\rangle_u\,,\\ \hat{a}_2\,|n,z\rangle_u &= \sqrt{n}\;|n-1,z\rangle_u\,,\\ \hat{a}_1^\dagger\,|n,z\rangle_u &= \sqrt{n+1}\,\partial_z\;|n+1,z\rangle_u\,,\\ \hat{a}_2^\dagger\,|n,z\rangle_u &= \sqrt{n+1}\;|n+1,z\rangle_u\,.\end{aligned}\tag{4.16}$$

These identities enable us to rewrite (4.15) in the form:

$$\begin{aligned}\frac{d}{dt}\left[\mu_n(z,z^*)P(n,z,t)\right] &= -\Big[\sin(\phi_1)\Delta_r[r(r+\theta)j_r(r,\phi_1,\phi_2)] \\ &\quad + r\frac{\partial}{\partial\phi_1}[\sin(\phi_1)j_{\phi_1}(r,\phi_1,\phi_2)] \\ &\quad + r\frac{\partial}{\partial\phi_2}j_{\phi_2}(r,\phi_1,\phi_2)\Big]. \end{aligned} \tag{4.17}$$

Here $r=\theta(n+1)$ and Δ_r is the discrete radial derivative acting as $\Delta_r f(r) \equiv \frac{f(r)-f(r-\theta)}{\theta}$. We see that (4.17) is indeed given as a total divergence which includes the Jacobian $J = r^2\sin(\phi_1)$ and we have, therefore, obtained an expression for the probability current where the spherical components are calculated to be

$$\begin{aligned} j_r(r,\phi_1,\phi_2) &= -\frac{\hbar}{m}\frac{\mathrm{Im}(M_1+M_2)}{n+1}, \\ j_{\phi_1}(r,\phi_1,\phi_2) &= \frac{\hbar}{m}\frac{\mathrm{Im}(M_1 - z\,z^*M_2)}{\sqrt{z\,z^*}\,(n+1)} \quad \text{and} \\ j_{\phi_2}(r,\phi_1,\phi_2) &= \frac{\hbar}{m}\frac{\mathrm{Re}(M_1 - z\,z^*M_2)}{\sqrt{z\,z^*}\,(n+1)}, \end{aligned} \tag{4.18}$$

where the angular coordinates are still contained in $z=\cot(\phi_1/2)e^{-i\phi_2}$ and the matrix elements M_α are given by

$$M_\alpha = \left\langle n+1,z\right| \hat{\psi}^\dagger\hat{a}_\alpha^\dagger\hat{\psi}\hat{a}_\alpha \left|n+1,z\right\rangle. \tag{4.19}$$

What is left is for us to calculate these matrix elements M_α for free particles and thereby obtain a complete description of probability currents in fuzzy space.

Currently our formulation for free particles in fuzzy space in Chapter 3 lacks a description for plane waves. We do, however, see that the Schrödinger equation for free particles (3.28) also permits plane waves as solutions and we may simply find a plane wave description that acts as a solution. The most natural way to define a plane wave then will be $\hat{\psi}_{\vec{k}} = e^{i\vec{k}\cdot\hat{\vec{X}}}$ which transforms under rotations as $e^{-i\phi\,\hat{u}\cdot\hat{\vec{L}}/\hbar}\hat{\psi}_{\vec{k}} = \hat{\psi}_{R\vec{k}}$ with $R\equiv R_\phi(\hat{u})$ being the rotation matrix.

Since the Schrödinger equation is rotationally invariant we are free to choose the momentum vector $\vec{k}$ for the plane waves to be orientated in the z direction. Therefore, the plane waves can

be written as

$$\hat{\psi}_{|\vec{k}|\hat{z}} = e^{i|\vec{k}|\hat{x}_3} = e^{i|\vec{k}|(\hat{a}_1^\dagger \hat{a}_1 - \hat{a}_2^\dagger \hat{a}_2)}. \tag{4.20}$$

Inserting (4.20) into (3.28) we find that

$$H_0\, \hat{\psi}_{|\vec{k}|\hat{z}} = \frac{2\hbar^2}{m\theta^2} \sin^2\left(\frac{|\vec{k}|\theta}{2}\right) \hat{\psi}_{|\vec{k}|\hat{z}}. \tag{4.21}$$

Since the energy is expressed as $E = \frac{\hbar^2\kappa^2}{2m\theta^2}$, we find that $\kappa = 2\sin\left(\frac{|\vec{k}|\theta}{2}\right)$ in the case of plane waves. We also find that the upper limit to the kinetic energy $E_{\max} = \frac{2\hbar^2}{m\theta^2}$, as found in the previous chapter, can be deduced from the fact that the momentum in (4.20) should be restricted to $|\vec{k}| \in [0, \frac{\pi}{\theta})$ in order for the states to be linearly independent.

Now that we have descriptions for both plane- and spherical waves in fuzzy space, we are able to determine their respective probability current densities through the use of (4.19). For the plane waves, by use of (4.20), we find the matrix elements to be

$$\begin{aligned} M_1 &= (n+1)\cos^2\left(\frac{\phi_1}{2}\right) e^{-i\theta|\vec{k}|} \quad \text{and} \\ M_2 &= (n+1)\sin^2\left(\frac{\phi_1}{2}\right) e^{+i\theta|\vec{k}|}. \end{aligned} \tag{4.22}$$

By using the results of (4.22) and substituting into (4.18) we find the probability current in Cartesian coordinates to be

$$j_z = \frac{\hbar \sin(|\vec{k}|\theta)}{m}. \tag{4.23}$$

Before calculating the matrix elements for spherical waves, we note that we are able to rewrite the standard spherical eigenstates in (3.17) as

$$\hat{\psi}_{jm} = \bar{R}(\hat{N} - j)\mathcal{Y}_{jm} \quad \text{with} \quad \mathcal{Y}_{jm} = \sum_{(jm)} \frac{(\hat{a}_1^\dagger)^{m_1}(\hat{a}_2^\dagger)^{m_2}}{m_1!\, m_2!} \frac{(\hat{a}_1)^{n_1}(-\hat{a}_2)^{n_2}}{n_1!\, n_2!}. \tag{4.24}$$

Here $\mathcal{Y}_{jm}$ is the non-commutative equivalent to the standard spherical harmonics $Y_{jm}(\phi_1, \phi_2)$ and the non-commutative parameter θ has been absorbed into the radial function $\bar{R}(\hat{N})$. Making the effect of $\mathcal{Y}_{jm}$ explicit in the position representation given by (4.11), we find through the help of

the identities in (4.16) that

$$\begin{aligned}\langle n,z|\,\mathcal{Y}_{jm}\,|n,z\rangle &= \frac{n!}{(n-j)!}\frac{1}{(1+z\,z^*)^j}\sum_{(jm)}\frac{(-1)^{n_2}(z^*)^{m_1}z^{n_1}}{n_1!n_2!m_1!m_2!}\\ &= \frac{n!}{(n-j)!}\frac{1}{j!(j+m)!}e^{im\phi_2}P_j^m(\cos(\phi_1)),\end{aligned} \tag{4.25}$$

which is indeed proportional to $Y_{jm}(\phi_1,\phi_2)$.

For the purpose of calculating the matrix elements, we take a superposition of all $m=0$ partial spherical waves from which we obtain the expression

$$\hat{\psi} = \sum_{j=0} a_j \bar{R}(n-j)(j!)^2\mathcal{Y}_{l0}, \tag{4.26}$$

where we the requirement of axial symmetry excludes all $m\neq 0$ partial spherical waves.

By using the property of the star product given in (4.12) we find the matrix elements at large radial distances to be

$$\begin{aligned}M_\alpha &= \sum_{j,j'} a_j^* a_{j'}\bar{R}_j^*(n+1-j)\bar{R}_{j'}(n-j')(j!)^2(j'!)^2\\ &\times \left\langle n+1,z\right|\mathcal{Y}_{j0}\left|n+1,z\right\rangle \star_{n+1}\left\langle n+1,z\right|\hat{a}_\alpha^\dagger\mathcal{Y}_{j'0}\hat{a}_\alpha\left|n+1,z\right\rangle.\end{aligned} \tag{4.27}$$

In order to resolve the contribution made from the star product, we first investigate its asymptotic behaviour. From [15] we find that the star product can be resolved as the $1/n$ expansion given by

$$\star_n = 1+\sum_{k=1}^{\infty}\frac{2^k}{n^k}\sum_{p,q=1}^{k}\overleftarrow{\partial}_z^{\,p}\Lambda_{p,q}^{(k)}(z,z^*)\,\overrightarrow{\partial}_{z^*}^{\,q}, \tag{4.28}$$

where $\Lambda_{p,q}^{(k)}(z,z^*)$ is a function of z and z^*, whereas $\overleftarrow{\partial}$ and $\overrightarrow{\partial}$ signifies taking the partial derivative to the left and right, respectively.

From eq. (4.28) we find that as the power of $1/n$ in each term grows, the maximum possible order of partial derivatives also increases. We can therefore, in the large-n limit, choose to neglect all the negative powers of n on the condition that the derivatives do not contribute any additional powers of n.

In the position representation for $\mathcal{Y}_{jm}$ we find that the powers for z and z^* are governed by the

values of j and j'. In order for the asymptotic approximation of $\star_n \approx 1$ to hold, it is necessary to be ensure that only a finite number of terms in the partial wave expansion of $\hat{\psi}$ in (4.26) are non-zero. This implies that there should be a maximum value for j beyond which $a_j = 0$. We have indeed already shown in Chapter 3 that, for the case of a finite potential well, we see a maximum allowed value for j after which the effects of the potential is ignored. Since we are developing a scattering theory for that particular case, we will now proceed with the assumption that we may approximate the star product in (4.27) to 1.

We are now able to determine the probability current for spherical waves. Again, by utilizing the identities provided in (4.16), we find that $M_1 = z\, z^* M_2$. From the general expressions for the probability current provided in (4.18), we find therefore only the radial current in the large-n limit to be non-zero and is given by

$$j_r(n, \phi_1, \phi_2) = \frac{\hbar}{m} \operatorname{Im}\left[\sum_{j,j'} n^{j+j'} a_j a^*_{j'} P_j(\phi_1) P_{j'}(\phi_1) \bar{R}_j(n-j+1)\, \bar{R}^*_{j'}(n-j')\right]. \tag{4.29}$$

4.3 Scattering theory

We are now in a position to investigate particle scattering by a finite range radial potential $V(\hat{r})$ in fuzzy space. From the time-independent description we are, therefore, seeking energy eigenstates of the form

$$\hat{\psi} = e^{i|\vec{k}|\hat{X}_3} + \hat{\psi}^{(+)}, \tag{4.30}$$

with $e^{i|\vec{k}|\hat{X}_3}$ being the incident plane wave and $\hat{\psi}^{(+)}$ the scattered wave. Outside of the range of the radial potential we should find that $\hat{\psi}^{(+)}$ reduces to a free particle solution with its probability current directed away from the origin.

For us to apply this requirement and find appropriate solutions for $\hat{\psi}^{(+)}$, we first need to consider the asymptotic behaviour of our free particle solutions in Chapter 3. Reminding ourselves of the non-commutative analogues to the two Bessel functions and Hankel function as given in eqs. (3.42), (3.44) and (3.47), we seek to find their asymptotic expressions in the large-n limit.

By utilizing identities 15.3.21 and 15.4.6 in [14] to rewrite the free particle solutions from hypergeometric functions into Jacobi polynomials, we are able to apply theorem 8.21.8 in [19] in the large-n limit to the polynomials to obtain

$$\bar{R}_J(n) \approx \frac{\sin[(n-j-1)|\vec{k}|\theta - j\pi/2]}{n^{j+1}} \quad \text{and} \quad \bar{R}_Y(n) \approx -\frac{\cos[(n-j-1)|\vec{k}|\theta - j\pi/2]}{n^{j+1}}. \tag{4.31}$$

From this we also find that the Hankel function results in an outgoing radial wave:

$$\bar{R}_H(n) = \bar{R}_J(n) + i\bar{R}_Y(n) \approx \frac{e^{i(n+j+1)|\vec{k}|\theta}}{(i\,n)^{j+1}}. \tag{4.32}$$

This suggests that $\hat{\psi}^{(+)}$ has the form

$$\hat{\psi}^{(+)} = \sum_j a_j (j!)^2 \hat{\psi}_{H,j0} = \sum_j a_j \bar{R}_H(\hat{n}-j)(j!)^2 \mathcal{Y}_{j0} \tag{4.33}$$

where axial symmetry has excluded terms with $m \neq 0$ from the final expression.

We can now derive the expression for the differential cross section from the probability currents of two components of $\hat{\psi}$. We may use the probability current for plane waves given by eq. (4.23). In the case of spherical waves, we may simply use the expression of the analogue Hankel function given in (4.32) and substitute it into (4.29). From these we are able to determine the differential cross section as

$$\frac{d\sigma}{d\Omega} = \frac{|j_r|r^2}{|j_z|} = \theta^2 \left| \sum_j a_j P_j(\cos(\phi_1)) e^{-ij\pi/2} \right|^2. \tag{4.34}$$

In order to determine the coefficients a_j it is required that we perform partial wave expansions for the general eigenstate $\hat{\psi}$ and that of the incoming plane wave. For the incoming plane wave we find the expansion to be the analogue to the commutative plane wave expansion of spherical harmonics and Bessel functions given by

$$e^{i|\vec{k}|\hat{X}_3} = \sum_j d_j \bar{R}_j(\hat{n}-j)(j!)^2 \mathcal{Y}_{j0}. \tag{4.35}$$

We determine the coefficients d_j in this case by considering the position representation of (4.35). By using the identities in (4.16) we arrive at the result

$$\left\langle n,z \right| e^{i|\vec{k}|\hat{X}_3} \left| n,z \right\rangle = \left[\cos(|\vec{k}|\theta) + i\cos(\phi_1)\sin(|\vec{k}|\theta) \right]^n. \tag{4.36}$$

Since we also know from (4.25) that $\langle n,z|\,\mathcal{Y}_{jm}\,|n,z\rangle \sim P_j(\cos(\phi_1))$, we may simply expand the polynomials $(z-x)^n$ as a series of Legendre polynomials $P_j(x)$. Using the orthogonality of the Legendre polynomials and identity 7.228 in [24], we find the coefficients for the plane wave expansion to be

$$d_j = i^j(2j+1)\csc(|\vec{k}|\theta). \tag{4.37}$$

As a final step in determining the scattering coefficients, we consider the full wave function $\hat{\psi}$ which should be an asymptotic solution of the free particle problem which we express by

$$\hat{\psi} = \sum_j (A_j \hat{\psi}_{J,j0} + B_j \hat{\psi}_{Y,j0}). \tag{4.38}$$

By setting this equal to the sum of the expansions for the plane- and scattered waves, we find the final expression for the scattering coefficients to be

$$a_j = \frac{d_j B_j}{iA_j - B_j} = i d_j e^{i\delta_j} \sin(\delta_j), \quad \text{where} \quad \tan(\delta_j) = -\frac{B_j}{A_j}. \tag{4.39}$$

From this we find that the final expression for the differential cross section is then given by

$$\frac{d\sigma}{d\Omega} = \frac{\theta^2}{\sin^2(|\vec{k}|\theta)} \left| \sum_j (2j+1) \sin(\delta_j) e^{i\delta_j} P_j(\cos(\phi_1)) \right|^2, \tag{4.40}$$

whereas the total cross section is

$$\sigma_{\text{tot}} = \sum_j \sigma_j = \frac{\theta^2}{\sin^2(|\vec{k}|\theta)} \sum_j 4\pi(2j+1) \sin^2(\delta_j). \tag{4.41}$$

From the last two results we see that the expressions closely resemble the differential- and total cross sections of the commutative case, except for the extra $\frac{\theta^2}{\sin^2(|\vec{k}|\theta)}$ factor. In the case of extremely low incident energies $|\vec{k}|\theta \ll 1$ we have that $\sin(|\vec{k}|\theta) \approx |\vec{k}|\theta$ and therefore (4.40) and (4.41) will reduce to the normal commutative results. More explicitly, we may rewrite the energy terms in (4.41) in terms of κ. Earlier we found that $\kappa = 2\sin(\frac{|\vec{k}|\theta}{2})$, which results in (4.41) being rewritten as

$$\sigma_{\text{tot}} = \sum_j \sigma_j = \frac{\theta^2}{\kappa^2(1 - \frac{\kappa^2}{4})} \sum_j 4\pi(2j+1) \sin^2(\delta_j), \tag{4.42}$$

where $\kappa = \theta k$ and $E = \frac{\hbar^2 \kappa^2}{2m\theta^2} = \frac{\hbar^2 k^2}{2m}$. In this form it is clearest to see that in the limit of $\theta \to 0$ we obtain the exact expression for the differential- and total cross sections of the commutative case, since the prefactor in (4.40) and (4.42) becomes

$$\lim_{\theta \to 0} \frac{\theta^2}{\kappa^2(1 - \frac{\kappa^2}{4})} = \lim_{\theta \to 0} \frac{1}{k^2(1 - \frac{\theta^2 k^2}{4})} = \frac{1}{k^2}. \tag{4.43}$$

4.4 Particle scattering from the finite fuzzy well

Since we are now in possession of a clear formalism of particle scattering in fuzzy space, we can investigate particle scattering by the finite spherical fuzzy well as developed in Chapter 3.

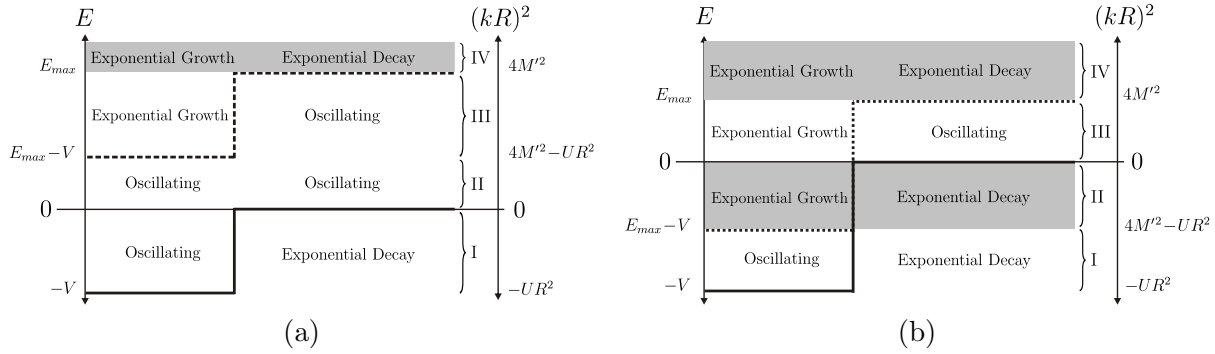

Figure 4.1: Taken from [16]. Illustrations of the various energy regions and the corresponding behaviour of the wavefunction. The gray regions do not support bound or scattering states. Here (a) corresponds to a shallow well where the potential depth is less than the maximum allowed free particle kinetic energy, whereas (b) corresponds to a deep well where the potential depth exceeds this maximum free particle kinetic energy. Additionally, we note that we define $M' \equiv M+1$ and $V = \frac{\hbar^2 U}{2m}$.

Before we proceed, it is interesting to note that there are different scattering situations, depending on the values for the incident particle energy and the potential well depth. Given the results for fuzzy well energy solutions obtained in Chapter 3, we have the following scattering scenarios for combinations of κ_{in} and κ_{out}:

- **For** $0 < \kappa_{in} < 2$ **and** $\kappa_{out} = i\epsilon,\ \epsilon \in \mathbb{R}^+$ we have "ordinary" bound states where the energy solutions for square integrable wave functions are obtained from the matching conditions. This scenario coincides with region I in both Figure 4.1a and 4.1b.

- **For** $0 < \kappa_{out} < \kappa_{in} < 2$ we have "ordinary" scattering states where the linear combinations of solutions are fixed through the matching conditions. This scenario coincides with region II only in Figure 4.1a.

- **For** $\kappa_{in} > 2$ **and** $0 < \kappa_{out} < 2$ we have an interesting effect, unique to the non-commutative system, where the inside of the well appears to act as an apparent repulsive potential for any outside scattering wave. Inside the well we see the absolute value of the wave functions is finite at the origin, and grows exponentially outward. This scenario is displayed within region III only in Figure 4.1a.

- Any other combination of κ_{in} and κ_{out} results in non square-integrable solutions when the

matching conditions as outlined in equations (3.57), (3.58) and (3.59) are solved. These scenarios are captured by the grey regions in both plots of Figure 4.1.

Given these scenarios, we first focus only on the "ordinary" scattering states and scattering states with an apparent repulsive potential.

4.5 Ordinary scattering, phase shifts and scattering cross-section

By using the term "ordinary scattering" we refer to the situation where the energy inside and outside the well are both within the bounds on the free-particle energies and the particle energy is larger than the potential height of the well. However, it is assumed that the energy is smaller than the maximum allowed energy. Scenarios with energies close to the maximum energy are discussed in greater detail in the next section.

We start off the investigation into particle scattering by finding complete solutions for the wave functions inside- and outside the well, ensuring that the two parts match accordingly at the well boundary.

As discussed in Chapter 3, the only allowed solutions for the wave function inside the well are that of the NC-Bessel function. Therefore we may write the radial wave function inside the well as

$$\Psi(n,j) = \Psi_{in}(n,j,\kappa_{in}) = C\,\bar{R}_J(n,j,\kappa_{in}) \quad \forall n \leq M-j, \tag{4.44}$$

with C being a normalization constant that will be obtained at a later stage through the matching conditions.

Outside the well we write the general solution for the radial wave function as

$$\Psi(n,j) = \Psi_{out}(n,j,\kappa_{out}) = A\,\bar{R}_J(n,j,\kappa_{out}) + B\,\bar{R}_Y(n,j,\kappa_{out}) \quad \forall n \geq M-j+1. \tag{4.45}$$

Here the constants A and B should also be determined through the matching conditions. To do this, it is easier to compute the ratio $\frac{B}{A}$ and then later fix A or B to a constant value that is most convenient for us. Naturally, we shall normalize the wave functions at the end so that the solutions will integrate to 1.

We determine the ratio $\frac{B}{A}$ through the matching condition provided by (3.59), and by using

(4.44) and (4.45) we can write it as

$$\frac{\bar{R}_J(M-j+1,\, j,\, \kappa_{in})}{\bar{R}_J(M-j,\, j,\, \kappa_{in})} = \frac{\bar{R}_J(M-j+1,\, j,\, \kappa_{out}) + \frac{B}{A}\,\bar{R}_Y(M-j+1,\, j,\, \kappa_{out})}{\bar{R}_J(M-j,\, j,\, \kappa_{out}) + \frac{B}{A}\,\bar{R}_Y(M-j,\, j,\, \kappa_{out})}. \tag{4.46}$$

Solving for $\frac{B}{A}$ results in

$$\frac{B}{A} = \frac{\bar{R}_{J,in}(M-j+1)\,\bar{R}_{J,out}(M-j) - \bar{R}_{J,in}(M-j)\,\bar{R}_{J,out}(M-j+1)}{\bar{R}_{J,in}(M-j)\,\bar{R}_{Y,out}(M-j+1) - \bar{R}_{J,in}(M-j+1)\,\bar{R}_{Y,out}(M-j)}, \tag{4.47}$$

where we used the following simplified notation for display purposes:

$$\begin{aligned} \bar{R}_{J,in}(n) &= \bar{R}_J(n, j, \kappa_{in}), \\ \bar{R}_{J,out}(n) &= \bar{R}_J(n, j, \kappa_{out}), \\ \bar{R}_{Y,in}(n) &= \bar{R}_Y(n, j, \kappa_{in}) \qquad \text{and} \\ \bar{R}_{Y,out}(n) &= \bar{R}_J(n, j, \kappa_{out}). \end{aligned} \tag{4.48}$$

For convenience we will choose A to be 1 and, therefore, B will assume the value in (4.47). Now, since we have values for A and B, we may use the first matching condition (3.57) to compute C:

$$C = \frac{\bar{R}_{J,out}(M-j+1) + B\,\bar{R}_{Y,out}(M-j+1)}{\bar{R}_{J,in}(M-j+1)}. \tag{4.49}$$

We now have complete expressions for the radial wave function inside and outside of the well during ordinary scattering. It now naturally follows that one would like to calculate the phase shifts that arise due to the presence of the potential.

Given that we are able to determine the phase shifts from $\tan(\delta_j) = -\frac{B}{A}$ as provided by (4.39) and the total cross section provided in (4.41), we would like to investigate what effect non-commutativity has on the phase-shifts and cross-sections when compared to the commutative case. For this it will be necessary to keep length scales fixed so that our comparisons between non-commutative and commutative results may be consistent.

The length scales that we will be keeping fixed across our comparisons will be

- The particle wavelength outside of the well.
- The particle wavelength inside the well.
- The radius of the well.

We will, therefore, only be changing the non-commutativity parameter θ and comparisons will be made between results with different θ values and the commutative case. We will also keep the energy outside of the well sufficiently low and fixed so that the particle wavelength outside the well is much larger than the radius of the well, i.e. $kR \ll 1$.

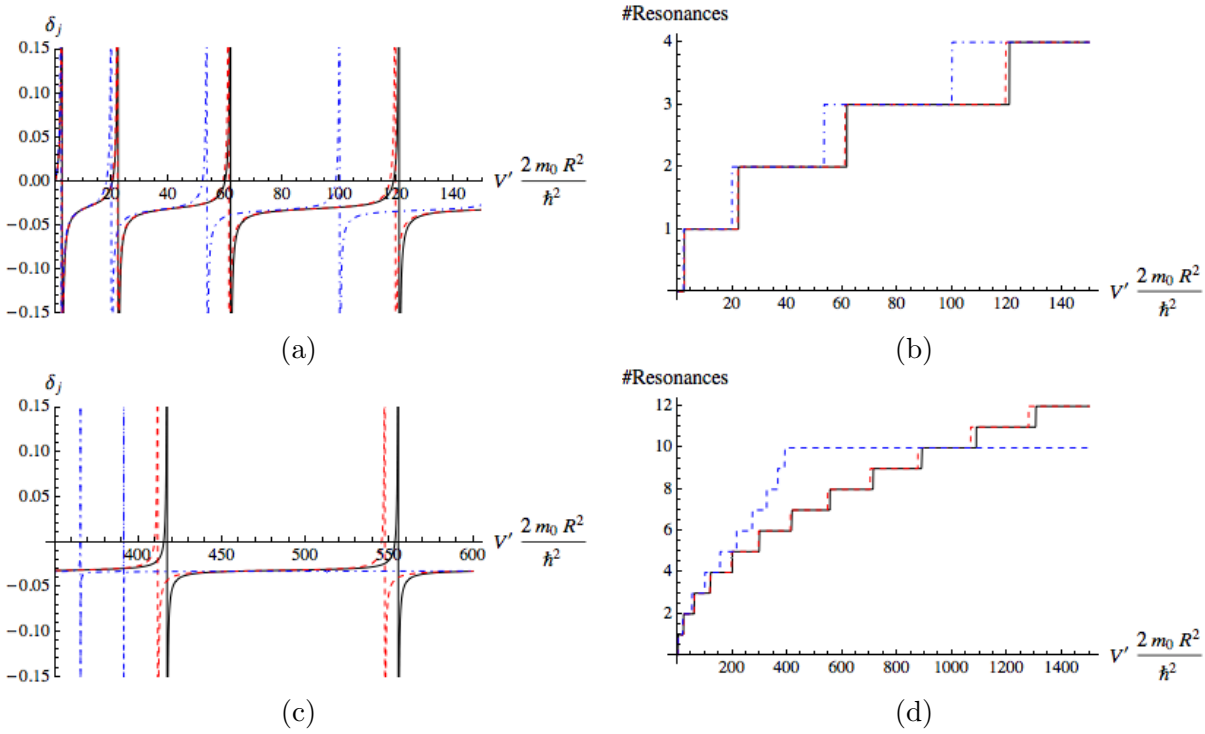

Figure 4.2: Illustrations of the scattering phase shifts and resonances as functions of potential height. For all plots we have $j = 0$, $k_{out}R = \sqrt{1/1000}$ and $k_{in}R = \sqrt{1/1000 + V'}$. The solid black line in each plot is the commutative result, while the dashed red line is the non-commutative result with $\theta = 0.01$ and the dot-dashed blue line is the non-commutative result with $\theta = 0.1$, keeping in mind that θ has units of length. In sub-figures (a) and (c) we limited the range to only display the region with defining features. In sub-figures (b) and (d) the y-axis displays the number of resonances encountered as we increase the value of V' from 0 upward.

From Figure 4.2 we find that with an increase in the effect of non-commutativity, i.e. increasing θ, resonance peaks are appearing at a faster rate. This suggests that bound states inside the well appear at a faster rate, when the potential height is increased, at larger values of the non-

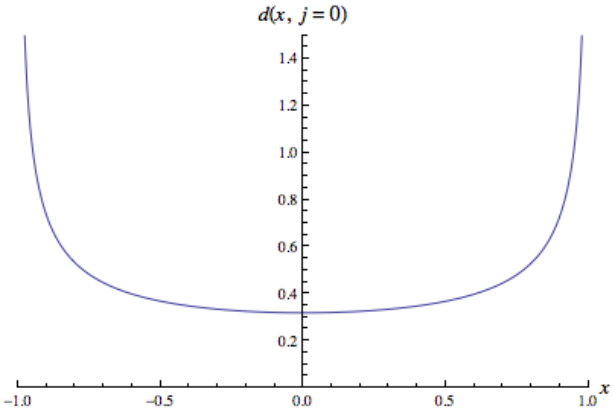

Figure 4.3: Illustration of the asymptotic density of zeroes for the Jacobi polynomial $P_n^{(\frac{1}{2},\frac{1}{2})}(x)$, where $j = 0$ and $n >> 1$.

commutativite parameter. This view is supported when we take a closer look at the density of states for commutative and non-commutative systems. As a reference, we will once again consider the infinite well problem for both the commutative and non-commutative cases. The $j = 0$ energy solutions for the commutative infinite spherical well are given by

$$E_n = \frac{n^2\pi^2\hbar^2}{2m_0R} \quad n = 1, 2, 3, \ldots, \tag{4.50}$$

while the $j = 0$ energy solutions for the infinite non-commutative fuzzy well are found by finding the zeros of the Jacobi polynomial

$$P_{M+1}^{(\frac{1}{2},\frac{1}{2})}(1 - m_0\theta^2 E/\hbar^2) = 0. \tag{4.51}$$

The commutative density of states clearly always decreases quadratically as the energy increases, however, in the non-commutative case we find that the density of states decreases at a similar tempo at first, but reaches a minimum and then increases again until the maximum possible kinetic energy is reached (as seen in Figure 4.3). This behaviour of the density of states in non-commutative systems correlates with the bound state resonances appearing at a faster rate as the strength of non-commutativity increases.

We also see another interesting effect from Figure 4.2: As the total number of resonance peaks is a measure of the number of bound states for a given potential height, we find that larger values of θ have fewer bound states inside the well as seen in sub-figures 4.2(c) and 4.2(d). This confirms that we only have a limited number of bound states for a given value of j.

For comparing the total scattering cross-section we opted to keep the potential height fixed and varied the energy, of which a few examples can be seen in Figure 4.4. Once again we notice the resonance peaks appear at lower energies in a system with a strong non-commutative parameter, relative to systems with a weaker non-commutative parameter and the commutative case. Furthermore, we see that when we increase the potential height to a value that is comparable to the maximum kinetic energy for a system with strong non-commutativity, the cross-section strictly decreases for that system as the energy is increased once the maximum kinetic energy inside the well has been reached. The weakly non-commutative case still exhibits regular cross-section behaviour compared to the commutative case, but with the resonance peaks moving to lower energies as we increase the energy.

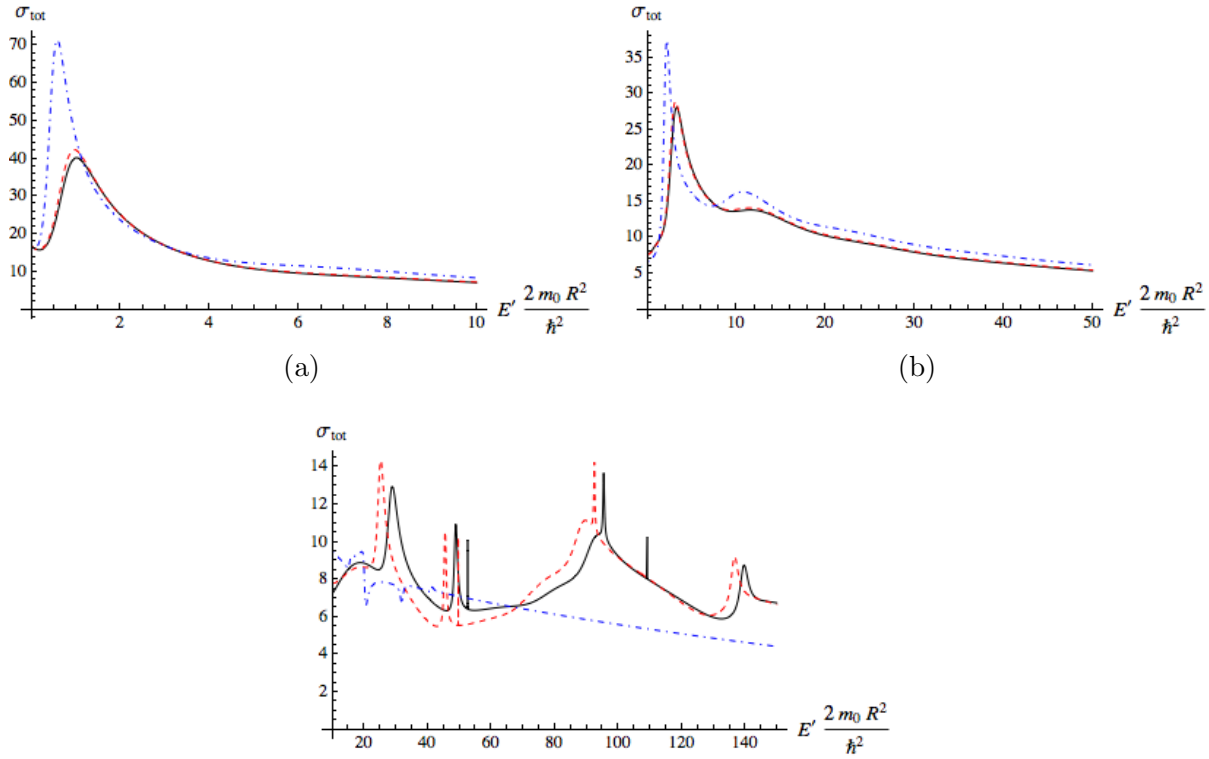

Figure 4.4: Illustrations of the total scattering cross-sections as a function of outside kinetic energy. For sub-figure (a) we have $V = 7.5\frac{\hbar^2}{2m_0R^2}$, for sub-figure (b) we have $V = 14.5\frac{\hbar^2}{2m_0R^2}$ and lastly for sub-figure (c) we have $V = 350\frac{\hbar^2}{2m_0R^2}$. The solid black line in each plot is the commutative result, while the dashed red line is the non-commutative result with $\theta = 0.01$ and the dot-dashed blue line is the non-commutative result with $\theta = 0.1$, keeping in mind that θ has units of length.

4.6 Scattering with an apparent repulsive potential

Now we explore regions where the kinetic energy outside the well may be very low, i.e. $kR \ll 1$ and $\theta k \ll 2$, but inside the well the kinetic energy is above the maximum allowed kinetic energy for a free particle. For this problem it would be more convenient to view our problem as having a potential well within the well-radius and 0 potential outside of the well:

$$V(n) = \begin{cases} V, & \text{if } 0 \leq n \leq M - j \\ \\ 0, & \text{if } n > M - j \end{cases} . \tag{4.52}$$

Since the wave function inside the well simply is the non-commutative Bessel function given in (3.42), we investigate the behaviour of the function at a kinetic energy larger than the maximum $\theta k = \kappa > 2$ inside the well. From (3.42) it follows that a κ value larger than 2 results in the function obtaining a complex phase and the normalisation factor of the function growing exponentially with n. This behaviour is consistent with the type of behaviour one would expect from negative energies, i.e. energies below a potential barrier. When we introduce negative energies into the NC-Bessel function, i.e. $\kappa = i\epsilon$ where $\epsilon \in \mathbb{R}^+$, we see the same behaviour albeit with a different complex phase. This suggests that we may think of a potential well that is deeper than the maximum allowed kinetic energy as an apparent positive or repulsive potential.

When we look at Figure 4.5 we see that, for a potential well with a depth greater than the maximum allowed kinetic energy, the phase shift values tend to those of a repulsive potential as we increase the potential depth. Upon further inspection, we find in the limit of an infinitely deep potential, $V \to -\infty$, that (4.47) takes the value

$$-\frac{B}{A} = \frac{\bar{R}_{J,out}(M-j)}{\bar{R}_{Y,out}(M-j)}, \tag{4.53}$$

which governs the asymptotic value for the phase shift through (4.39). This same ratio is also reached when we take the limit of an infinitely positive potential $V \to +\infty$. This confirms again that we may view a very deep potential as a repulsive potential. Furthermore, the results in (4.53) also agree with the results we find from the commutative hard sphere scattering where the ratio for hard sphere scattering is given by

$$-\frac{B_l}{A_l} = \frac{j_l(kR)}{\eta_l(kR)}, \tag{4.54}$$

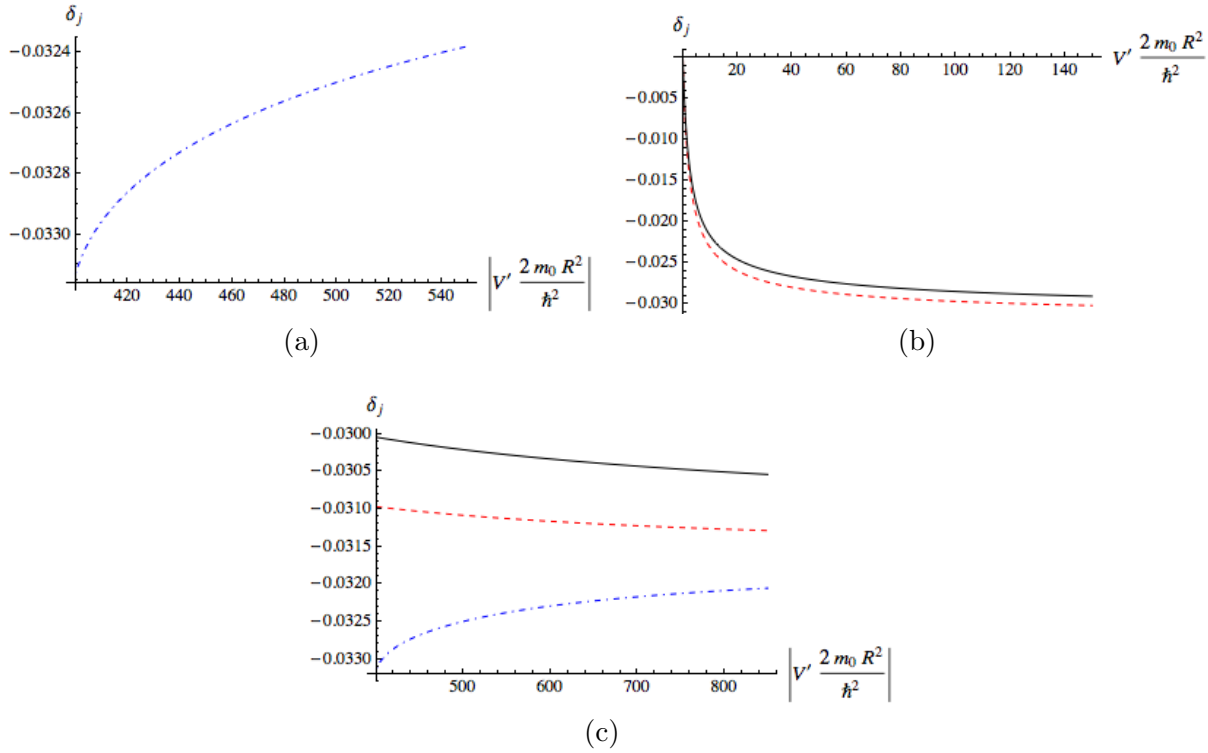

Figure 4.5: The phase shifts for potentials deeper than the maximum kinetic energy and positive repulsive potentials. For all three sub-figures we have the outside scattering energy as $kR = \sqrt{1/1000}$. In sub-figure (a) we have a non-commutative negative potential with the potential depth greater than that of the maximum kinetic energy for $\theta = 0.1$. In sub-figure (b) we have a positive or repulsive potential and display both the commutative (black line) and non-commutative (dashed red line) phase with $\theta = 0.1$. In sub-figure (c) we display all three the phase shift trends on the same plot with the absolute value of the potential on the x-axis.

where $j_l(x)$ and $\eta_l(x)$ are the spherical Bessel functions of the first- and second kind, respectively.

CHAPTER 5

THERMODYNAMICS OF A CONFINED FERMION GAS IN FUZZY SPACE

In the Chapter 3 we were successful in obtaining the energy spectrum of a particle confined by both a finite- and infinite well potential. These results, in particular the energy spectrum for the infinite well, now enables us to investigate the statistical properties of a gas of non-interacting particles confined in three dimensional non-commutative space, also referred to as fuzzy space.

This chapter will aim to investigate the statistical properties of a gas of fermionic particles confined in non-commutative space and whether its properties deviate from the same gas within traditional commutative space. Indeed, we will see throughout this chapter that the non-commutative nature of our system does cause deviations from the standard behaviour expected from gases in commutative spaces. We see these deviations arise in both low- and high density gases. Furthermore, we also find the novel result of a duality in the statistical behaviour between the low- and high density gases in fuzzy space.

The methodology and a selection of results within in this chapter inspired the content of one of our own published articles [17]. Even though the similarities between this chapter and the article are clear, some calculations were approached differently and, in some cases, different scenarios were considered. We will discuss and briefly review these differences and results at the end of this chapter.

5.1 The thermodynamic q-potential

We now turn to the thermodynamics of a non-interacting gas of spinless fermions which are confined to an infinite spherical well with radius $R = \theta(M+1)$ in non-commutative space. We will treat this system in the grand canonical ensemble and fix the average value of $\hbar L_3^{(\mathrm{tot})}$, the z-component of the total angular momentum. By fixing $L_3^{(\mathrm{tot})}$ we aim to study both rotating and non-rotating gases. The grand canonical potential reads

$$q\left(M,\beta,\mu,\omega\right) = \sum_{j=0}^{M}\sum_{m=-j}^{+j}\sum_{n}\log\left[1+e^{-\beta(E_{n,j}-\mu-\hbar\omega m)}\right]. \tag{5.1}$$

where $E_{n,j} = E_0 x_{n,j}$ with $E_0 = \frac{\hbar^2}{m_0\theta^2}$ the non-commutative energy scale. Here $\{x_{n,j}\}$ is the set of $M-j+1$ zeros of the Jacobi polynomial $P_{M-j+1}^{(j+1/2,j+1/2)}(x)$, as is required by the quantisation condition in (3.68). The ω parameter serves as a Lagrange multiplier for fixing $L_3^{(\mathrm{tot})}$ and we may take $\omega > 0$ without loss of generality. Switching to the dimensionless parameters for the inverse temperature $\tilde{\beta} = E_0\,\beta$, chemical potential $\tilde{\mu} = \mu/E_0$ and angular velocity $\tilde{\omega} = \hbar\omega/E_0$, we find the expression for the q-potential reads

$$q(M,\tilde{\beta},\tilde{\mu},\tilde{\omega}) = \sum_{j=0}^{M}\sum_{m=-j}^{+j}\sum_{n}\log\left[1+e^{-\tilde{\beta}(-x_{n,j}-\tilde{\mu}-m\tilde{\omega})}\right]. \tag{5.2}$$

In the thermodynamic (large M) limit the sums over j and m may be replaced by integrals over $\lambda = j/M$ and $\alpha = m/M$ while the n summation becomes $\int dx\, d(x,\lambda)$ with $d(x,\lambda)$ given in (3.70). This produces

$$q(M,\tilde{\beta},\tilde{\mu},w) = M^3\int_0^1 d\lambda\int_{-\lambda}^{+\lambda} d\alpha\int_{x_-(\lambda)}^{x_+(\lambda)} dx\, d(x,\lambda)\log\left[1+e^{-\tilde{\beta}(x-f(\alpha))}\right] \tag{5.3}$$

where $f(\alpha) = \tilde{\mu}+\alpha w$, $w = M\tilde{\omega}$ and $x_\pm(\lambda) = \pm\sqrt{1-\lambda^2}$. Here we see $f(\alpha)$ act as the effective chemical potential of the system. Equation (5.3) serves as the starting point for calculating the various thermodynamic quantities. The quantities are obtained from q using

$$N = \frac{1}{\tilde{\beta}}\frac{\partial q}{\partial\tilde{\mu}}, \qquad L_3^{(\mathrm{tot})} = \frac{M}{\tilde{\beta}}\frac{\partial q}{\partial w}, \qquad \frac{S}{k} = q - \tilde{\beta}\frac{\partial q}{\partial\tilde{\beta}} \quad \text{and} \quad \tilde{P} = \frac{q}{\tilde{\beta}\tilde{V}}. \tag{5.4}$$

Here S is the entropy, N the number of particles, $\tilde{P} = \frac{4\pi\theta^3}{E_0}P$ a dimensionless measure of the pressure with $\tilde{V} = \frac{M^3}{3} \approx \frac{V}{4\pi\theta^3}$ the dimensionless system volume. The latter is also (to leading order in M) the total number of single particle states available to the system, as calculated in (3.64), and thus represents the maximum number of spinless particles that can be accommodated by the system. It is therefore convenient to define

$$N_{\max} \equiv \tilde{V} = \frac{M^3}{3} \approx \frac{V}{4\pi\theta^3}. \tag{5.5}$$

Note that the physical meaning of $N_{\max}$ is the total number of cells with volume $V_0 \equiv 4\pi\theta^3$ that fit into the volume V. It is therefore also useful and sensible to define a maximum density, which is the density obtained when each cell is occupied by exactly one particle, i.e.

$$\rho_{\max} \equiv \frac{1}{V_0} = \frac{1}{4\pi\theta^3}. \tag{5.6}$$

In terms of $\rho_{\max}$ the dimensionful density reads

$$\rho = \frac{N}{V} = \rho_{\max}\tilde{\rho}, \tag{5.7}$$

where $\tilde{\rho} = \frac{N}{\tilde{V}}$ is the dimensionless density.

We introduce one further notion that will turn out to be useful later. Suppose we fix the number of particles in the system to be N. Then there is a minimum volume that can accommodate this number of particles given by

$$N \approx \tilde{V}_{\min} = \frac{M_{\min}^3}{3} = \frac{V_{\min}}{4\pi\theta^3}. \tag{5.8}$$

Here $M_{\min}$ is the smallest integer larger than or equal to $(3N)^{1/3}$, so that the equality between N and $\tilde{V}_{\min}$ holds to $\mathcal{O}(\frac{1}{M_{\min}})$. In further applications where N and $M_{\min}$ are assumed to be large, this correction will be ignored.

In some cases it is convenient to work in terms of the fugacity $z = e^{\tilde{\beta}\tilde{\mu}} = e^{\beta\mu}$. In terms of this the q-potential of (5.3) can be expressed as

$$q(M, \tilde{\beta}, z, w) = M^3 \int_0^1 d\lambda \int_{-\lambda}^{+\lambda} d\alpha \int_{x_-(\lambda)}^{x_+(\lambda)} dx\, d(x,\lambda) \log\left[1 + z\, e^{-\tilde{\beta}(x-\alpha w)}\right], \tag{5.9}$$

where $z \ll 1$ corresponds to the low density limit and $z \gg 1$ corresponds to the high density limit. The corresponding thermodynamic quantities are then given by

$$N = z\frac{\partial q}{\partial z}, \qquad L_3^{(\text{tot})} = \frac{M}{\tilde{\beta}}\frac{\partial q}{\partial w}, \qquad \frac{S}{k} = q - N\log z - \tilde{\beta}\frac{\partial q}{\partial \tilde{\beta}}, \quad \text{and} \quad \tilde{P} = \frac{q}{\tilde{\beta}\tilde{V}}. \tag{5.10}$$

A final useful result is that of the total density of states. This is obtained by integrating out λ in (3.70):

$$d(x) = \int_0^{\sqrt{1-x^2}} d\lambda\, 2\lambda\, d(x,\lambda) = \frac{2\sqrt{1-x^2}}{3\pi}. \tag{5.11}$$

5.1.1 The high/low density duality

Using the symmetry of the density of states under $x \to -x$ one can trivially rewrite (5.9) as

$$q(M, \tilde{\beta}, z, w) = \frac{M^3}{3}\log z + q(M, \tilde{\beta}, z^{-1}, w). \tag{5.12}$$

This demonstrates a remarkable duality between the high and low density q-potentials, i.e., we can express the high density q-potential ($z \gg 1$) in terms of the low density q-potential ($z \ll 1$). This duality, in turn, is a direct consequence of the infra-red/ultraviolet duality of the density of states.

5.1.2 The filling of single particle states

It will be useful to develop a qualitative understanding of how the $L_3^{(\text{tot})}$ constraint affects the filling of the single particle states. To this end, consider Figure 5.1 (a). The shaded region indicates the support of the function $d(x, \lambda)$, i.e. those values of $x = E/E_0$ and $\lambda = j/M$ for which the density of states are non-zero. We see that the $j = 0$ sector has the largest range of single particle energies, from $-E_0$ to $+E_0$, and that this range decreases as j is increased. Beyond $j_{max} = M$ there are no single particle states at any energy. It should be kept in mind that each point in the shaded region corresponds to $(2j + 1)$ states with different angular momentum projections.

Now consider the occupation of a state with energy $E = xE_0$, angular momentum $j = \lambda M$ and angular momentum projection $m = \alpha M$. Since we are taking a low temperature approach in our calculations we can, for the sake of simplicity, take $T = 0$ which sees the Fermi-Dirac distribution reduce to a step function

$$n_{FD}(x, \alpha) = \Theta(f(\alpha) - x), \tag{5.13}$$

with $f(\alpha) = \tilde{\mu} + \alpha w$ and $\alpha \in [-\lambda, \lambda]$. Clearly all states with energy values below the effective chemical potential $x < f(\alpha)$ will be occupied, while higher energy states are empty.

Since we aim to investigate two different systems, one with $L_3^{(\text{tot})} = 0$ and the other with $L_3^{(\text{tot})} > 0$, we will consider their processes of filling the particle states separately.

For the case where $L_3^{(\text{tot})} = 0$, and therefore $w = 0$, the Fermi-Dirac distribution is independent of α, and the occupation of a state is determined by its energy alone. It should be kept in mind that the energy states will fill up in such a way that $L_3^{(\text{tot})}$ will always be 0.

At positive $L_3^{(\text{tot})}$ and w we see that if $x < f(-\lambda)$ (or $x > f(\lambda)$) the state is occupied (or unoccupied) regardless of the value of α. However, for states with energies the range $x \in (f(-\lambda), f(\lambda))$ the occupation condition remains α-dependent. This is illustrated in Figure 5.1 (a) which shows how the two lines $x = f(\pm\lambda)$ divide the (λ, x) plane into three regions. The shading indicates the fraction of the $(2j + 1)$ states which are filled at each point. In region I all

the single particle states are filled. Conversely, in region III all single particle states are empty. Figure 5.1 (b) shows the contribution to $L_3^{(\mathrm{tot})}$ from the $2j+1$ states at each point. As expected, the only non-zero contribution to $L_3^{(\mathrm{tot})}$ is from region II where some, but not all, of the $(2j+1)$ momentum states within each energy state are filled.

With the above in mind, we now consider the behaviour of $\tilde{\mu}$ and w when the particle number N is increased while $L_3^{(\mathrm{tot})}$ remains fixed. Increasing N requires increasing $\tilde{\mu}$ which shifts the two lines in Figure 5.1 upwards. Doing so without adjusting w would lead to a decrease in the number of states in region II and eventually also a decrease in $L_3^{(\mathrm{tot})}$. To compensate for this we must increase w as this enlarges region II and increases the amount of particle states that may contribue to $L_3^{(\mathrm{tot})}$. Constraining $L_3^{(\mathrm{tot})}$ to a positive value therefore prohibits the complete filling of all the single particle states.

This implies the existence of a maximum possible critical density $\rho_c = N/N^{(\max)} < 1$, itself a function of $L_3^{(\mathrm{tot})}$, which is reached in the limit where both $\tilde{\mu}$ and w tend to infinity. This critical density serves as the maximum possible particle density for a given value of $L_3^{(\mathrm{tot})}$ at which we expect the pressure to diverge. Close to this critical density the support of $d(x,\lambda)$ will be divided into regions I and II by the nearly vertical $x = f(-\lambda)$ line. This is precisely the situation depicted in Figure 5.1 (c) and (d). As noted previously the contribution to $L_3^{(\mathrm{tot})}$ comes entirely from region II. At sufficiently high densities the $x = f(-\lambda)$ line must therefore intercept the λ axis somewhere between 0 and 1, which implies that $\tilde{\mu}/w < 1$.

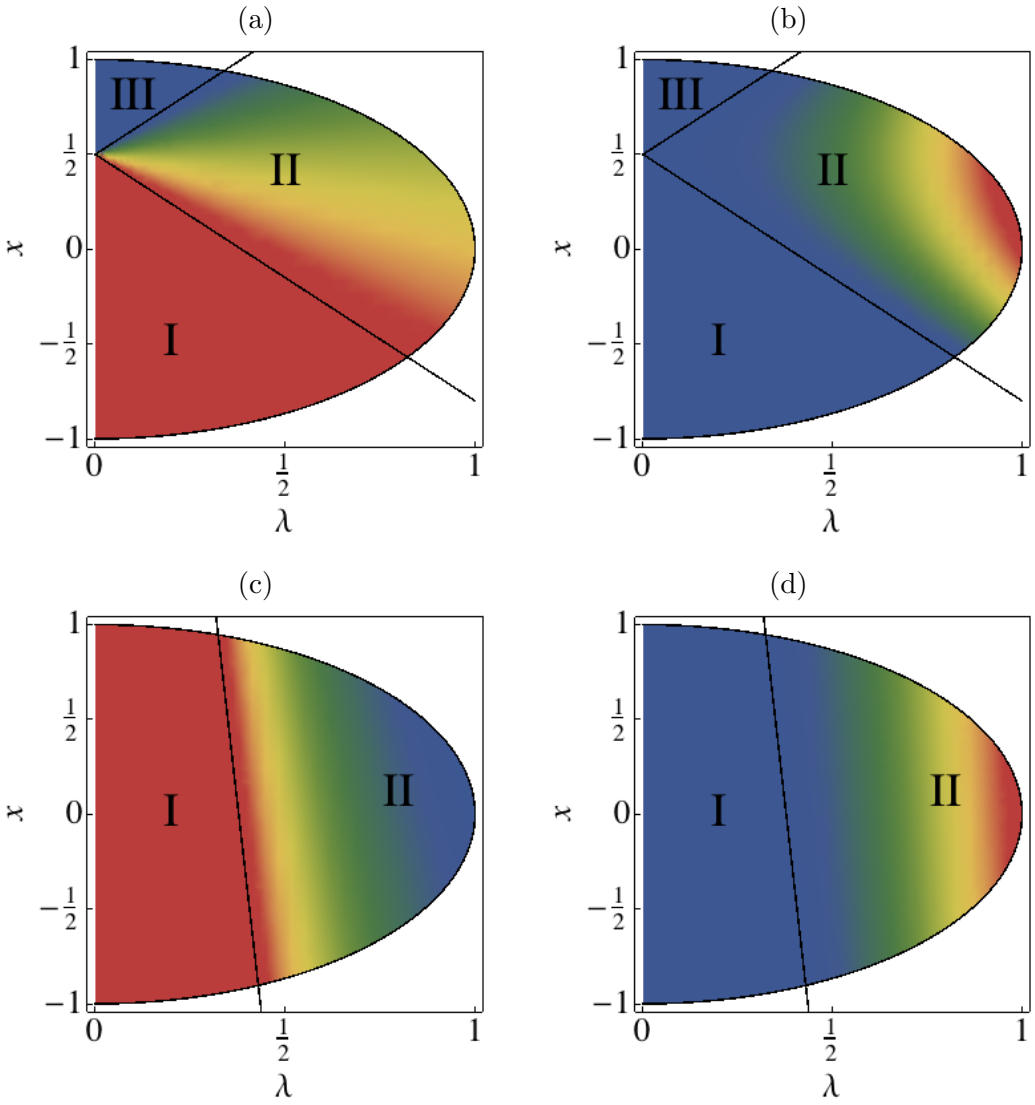

Figure 5.1: Illustration of the distributions of number of particles, (a) and (c), and angular momentum projection contribution, (b) and (d) per angular momentum sector in the energy vs single-particle angular momentum plane. In (a) and (c) the color range indicates state occupaction density with red (blue) indicating that all single particle states are occupied (unoccupied). In (b) and (d) the color range indicates the average single particle contribution to $L_3^{(\mathrm{tot})}$ with red (blue) indicating the maximum (minimum) possible contribution to $L_3^{(\mathrm{tot})}$. For (a) and (b) we have $\tilde{\mu} = 0.500$ and $w = 1.30$, while for (c) and (d) we have $\tilde{\mu} = 6.60$ and $w = 17.5$.

5.1.3 Calculation of the q-potential

Having discussed the general q-potential, as well as the process behind filling single particle states, we can now proceed to calculate the q-potential under certain conditions. As previously stated, in this dissertation we will focus on the two specific cases where we have $L_3^{(\text{tot})} = 0$ and $L_3^{(\text{tot})} > 0$, respectively. In the case of non-zero $L_3^{(\text{tot})}$, the q-potential could only be calculated at very high particle densities due to the technique used. However, for the case of $L_3^{(\text{tot})} = 0$, we obtained an expression that remains valid for all particle densities.

5.1.3.1 A high density, low temperature degenerate gas with $L_3^{(\text{tot})} > 0$

Here we consider a highly degenerate gas at low temperature with a positive, non-zero total angular momentum $L_3^{(\text{tot})}$. The technique used in this dissertation to compute the q-potential is quite involved and not immediately solvable for all the parameter values and combinations of $\tilde{\mu}$ and w. This has limited us to only consider the case where we have a large value for $\tilde{\mu}$ as well as a large value for w with the conditions that $\tilde{\mu} > 1$ and $w > \mu$. This corresponds to a low temperature degenerate gas near critical particle density. Furthermore, since a large amount of particle states contribute to the total angular momentum $L_3^{(\text{tot})}$, we will typically also see that the total angular momentum is comparable to the maximum allowed angular momentum expressed in (3.71). This implies that the angular momentum in this case will behave in a hyper-extensive manner.

Under these conditions the q-potential in (5.3) can be calculated using a systematic low temperature expansion. The details of this calculation appear in B.1. The result, up to order $\mathcal{O}(1/\tilde{\beta})$, is

$$q(M,\tilde{\beta},\tilde{\mu},w) = \frac{M^3}{12w^3}\left[\frac{\tilde{\beta}\left((\sqrt{1+w^2}-\tilde{\mu})^4+8w^3\tilde{\mu}\right)}{2}+\frac{\pi^2\left(\sqrt{1+w^2}-\tilde{\mu}\right)^2}{\tilde{\beta}}\right]. \tag{5.14}$$

5.1.3.2 Low temperature gas with $L_3^{(\text{tot})} = 0$

Here we set $w = 0$. The integral expression for the q-potential in (5.3) then simplifies to

$$q(M,\tilde{\beta},\tilde{\mu}) = M^3\int_{-1}^{1} dx\, d(x)\log\left[1+e^{-\tilde{\beta}(x-\tilde{\mu})}\right] \tag{5.15}$$

where $d(x)$ is given in (5.11). For $\tilde{\mu} \in (-1, 1)$ a Sommerfeld expansion in $1/\tilde{\beta}$ can be performed. To order $\mathcal{O}(1/\tilde{\beta})$ this yields

$$q(M, \tilde{\beta}, \tilde{\mu}) = \frac{M^3}{9\pi}\left[\tilde{\beta}\left(3\pi\tilde{\mu} + \sqrt{1-\tilde{\mu}^2}(2+\tilde{\mu}^2) - 3\tilde{\mu}\,\mathrm{ArcCos}(\tilde{\mu})\right) + \frac{\pi^2\sqrt{1-\tilde{\mu}^2}}{\tilde{\beta}}\right]. \tag{5.16}$$

When $\tilde{\mu} > 1$ the chemical potential no longer lies within the support of the total density of states, and so the Sommerfeld expansion is no longer valid. Instead, the appropriate low temperature expansion is

$$\log[1 + e^{-\tilde{\beta}(x-\tilde{\mu})}] \approx -\tilde{\beta}(x-\tilde{\mu}) + e^{\tilde{\beta}(x-\tilde{\mu})} + \mathcal{O}(e^{2\tilde{\beta}(x-\tilde{\mu})}). \tag{5.17}$$

Inserting this into (5.15) produces

$$q(M, \tilde{\beta}, \tilde{\mu}) = \frac{M^3}{3}\left[\tilde{\beta}\,\tilde{\mu} + \frac{2}{\tilde{\beta}}\,e^{-\tilde{\beta}\tilde{\mu}}\,I_{(1)}(\tilde{\beta})\right] \tag{5.18}$$

where $I_{(n)}(x)$ is the modified Bessel function of the first kind.

5.2 Calculating the central thermodynamic quantities

5.2.1 System with $L_3^{(\mathrm{tot})} > 0$

Utilizing the results of the previous section, we turn our attention to understanding the behaviour of the central thermodynamic quantities in the different parameter regimes. We first investigate the system with a large number of particles N and a total angular momentum projection $L_3^{(\mathrm{tot})}$ that is fixed to a positive value, with particular interest in the ways that these two paremeters affect the entropy S and dimensionless pressure $\tilde{P}$. Obtaining expressions for S and $\tilde{P}$ requires that we solve for $\tilde{\mu}$ and w as functions of N and $L_3^{(\mathrm{tot})}$. We can further simplify by introducing the particle density $\rho = N/N^{(\max)}$ and scaled total angular momentum projection $l = L_3^{(\mathrm{tot})}/L_3^{(\max)}$ so that we may have the solutions to $\tilde{\mu}$ and w as functions of thereof, where $N^{(\max)}$ and $L_3^{(\max)}$ are respectively given by (5.5) and (3.71) up to leading order in M.

Using (5.14) and (5.4) to solve $\tilde{\mu}$ and w as functions of the quantities described above, we find the solutions to $\tilde{\mu}$ and w up to order $\mathcal{O}(1/\tilde{\beta})$ are given by

$$\tilde{\mu} = \sqrt{1 + \frac{4}{C(\rho)}} - \frac{2(2-2\rho)^{1/3}}{\sqrt{C(\rho)}}, \qquad w = \frac{2}{\sqrt{C(\rho)}}, \tag{5.19}$$

where $C(\rho) = 8 - 6(2-2\rho)^{1/3} - l/(1-\rho)$. Investigating these solutions near the critical density

ρ_c yields

$$\tilde{\mu} \approx C_c(\rho_c)\frac{1-\rho_c}{\sqrt{2}(\rho_c-\rho)}\sqrt{\rho_c-\rho}, \qquad w \approx \frac{1}{C_c(\rho_c)\sqrt{2}\sqrt{\rho_c-\rho}}, \tag{5.20}$$

with $C_c(\rho_c) = \sqrt{(1-(2-2\rho_c)^{1/3})/(1-\rho_c)}$, where ρ_c can be calculated for a fixed l with

$$l = 2\left(4-3(2-2\rho_c)^{1/3}\right)(1-\rho_c). \tag{5.21}$$

Here we see that, as the particle density nears critical density, both $\tilde{\mu}$ and w tend to infinity with a ratio of

$$\lim_{\rho\to\rho_c}\frac{\tilde{\mu}(\rho,\rho_c)}{w(\rho,\rho_c)} = 1-(2-2\rho_c)^{1/3}, \tag{5.22}$$

which agrees with the fact that $\tilde{\mu}/w < 1$.

By using the solutions to $\tilde{\mu}$ and w, we find the expressions for the entropy and pressure to be

$$\frac{S}{k} = A(\rho_c)\frac{M^3\pi^2}{3\tilde{\beta}}\sqrt{\rho_c-\rho}, \qquad \tilde{P} = B(\rho_c)\frac{1}{\sqrt{\rho_c-\rho}}, \tag{5.23}$$

where $A(\rho_c)$ and $B(\rho_c)$ are complicated, but well defined functions of ρ_c when $l \neq 0$. It is clear that as ρ nears ρ_c, the entropy tends to 0 and the pressure diverges.

It is also of interest to investigate the dependence of the entropy on the volume of the system near critical density. We take the following approach: Assume that at fixed (N, $L_3^{(\mathrm{tot})}$, $\tilde{\beta}$) the initial system volume is at exactly V_c, where V_c is the smallest possible volume into which the N particles may fit. Increasing the system volume up to $V = V_c + \Delta V$, where ΔV is the smallest possible increase in volume at $V = V_c$, would have the entropy scale proportional to some power of V_c. Since N is fixed, one may use the expression $\rho = \frac{\rho_c V_c}{V} = \frac{\rho_c V_c}{V_c+\Delta V}$ and substituting this into the entropy in (5.23) obtains

$$S \sim \sqrt{V_c\,\Delta V}. \tag{5.24}$$

As $V \sim M^3$, one would naively interpret from this that the entropy scales as $M^{3/2}$ near critical density, which scales slower than the surface area (M^2). This, however, ignores the fact that one cannot have ΔV arbitrarily small. Since M quantifies the spherical radius of the system and only assumes positive integer values, it follows that the change in volume at critical density is $\Delta V \sim M_c^2\Delta M$, with $\Delta M = 0, 1, 2, \ldots$. Therefore, rewriting (5.24) as a function of the system radius at critical density M_c yields

$$S \sim \sqrt{M_c^5\,\Delta M} = M_c^2\sqrt{M_c\Delta M}. \tag{5.25}$$

This in turn suggests that the entropy, very close to critical density, scales proportionally faster than the surface area of the system, yet slower than the volume. This result seems reasonable as increasing the volume at critical density increases the amount of previously disallowed states which may now be filled, in addition to the allowed states created. Since all states, in order to preserve angular momentum, are not allowed to be filled, one will never see the entropy scale as fast as the volume. However, the entropy will not scale as slowly as the surface area since particles are allowed to not only occupy new states created, but also some previously-disallowed states.

5.2.2 System with $L = 0$

For the zero-angular momentum case, we will differentiate between the q-potentials of (5.16) and (5.18) as q_I and q_{II} respectively. We will again use the same approach followed in Section 5.2.1, without the dependence on w. The critical density for the $L_3^{(\text{tot})} = 0$ is trivially constant and equal to 1.

Solving now for $\tilde{\mu}$ again up to order $\mathcal{O}(1/\tilde{\beta})$ results in the following for each q-potential:

$$\tilde{\mu}_I = \frac{1}{8}(8 - \pi^2 + 2\pi^2\rho - \pi^2\rho^2), \qquad \tilde{\mu}_{II} = \frac{1}{\tilde{\beta}} \log\left[\frac{2\, I_{(1)}(\tilde{\beta})}{\tilde{\beta}(1-\rho)}\right]. \tag{5.26}$$

Using these results and substituting into eq. (5.4), one finds the expressions for entropy are given as

$$\frac{S_I}{k} = \frac{M^3\pi^2}{36\tilde{\beta}}\left[(1-\rho)\sqrt{16 - \pi^2(1-\rho)^2}\right], \tag{5.27}$$

and

$$\frac{S_{II}}{k} = \frac{M^3(1-\rho)}{3I_{(1)}(\tilde{\beta})}\left[I_{(1)}(\tilde{\beta})\left(3 + \log\left[\frac{2\, I_{(1)}(\tilde{\beta})}{\tilde{\beta}(1-\rho)}\right]\right) - \tilde{\beta}\, I_{(0)}(\tilde{\beta})\right], \tag{5.28}$$

while the scaled pressure for both are given by

$$\tilde{P}_I = \frac{1}{24}\left(8 - \pi^2(1-\rho)^2\right), \qquad \tilde{P}_{II} = \frac{1}{3\tilde{\beta}}\left(1 - \rho + \log\left[\frac{2\, I_{(1)}(\tilde{\beta})}{\tilde{\beta}(1-\rho)}\right]\right). Again, entropy grows \tag{5.29}$$

Here one finds again that, for both cases, the entropy tends to 0 as the particle density reaches the critical density of 1. However, in the case where $\tilde{\mu} \in [-1, 1]$, one finds that the pressure no longer diverges as the one nears the critical density in the expression for P_I, but is indeed seen in for P_{II}. This can, however, be explained by the fact that $\tilde{\mu}$ tends to infinity as one approaches

critical density and therefore the expression for P_I would no longer be applicable in the limit.

Investigating now the behaviour of the entropy expressions near critical density as a function of system size will be approached the same way as in the previous subsection. The dependence of the entropy S_{II} on system size near critical density is then given as

$$S_{II} \sim ({M_c}^2 \Delta M) \log \left[\frac{2\, M_c\, I_{(1)}(\tilde{\beta})}{\tilde{\beta}\, \Delta M} \right]. \tag{5.30}$$

Since $\log[M_c]$ grows much slower than M_c, one can conclude from this that the entropy scales like the surface area of the system. This agrees with the fact that the amount of particle states created by expanding from the critical volume, is proportional to the surface area of the system at the critical volume.

5.2.3 Numeric results

We now investigate the overall behaviour of the systems covered in Sections 5.2.1 and 5.2.2 and compare that to both numerical and commutative results.

In Figure 5.2 find that, in addition to the numerical and analytical results agreeing well, that the entropy plots displays a symmetry around $\rho = 1/2$ with the entropy tending to 0 as the particle density reaches critical values. At very low densities it is seen that (5.3) agrees with commutative results. Furthermore, the dependence of the entropy on system size shows good agreement between analytical and numerical results in Figure 5.3 and also indicates that the entropy of a high density system tends to zero as the system volume is decreased. This effect of the entropy tending to zero as the system volume is decreased, is accompanied by an ever increasing scaled pressure in Figure 5.4. This supports the view that there exists an incompressible limit at which the system volume can no longer be decreased.

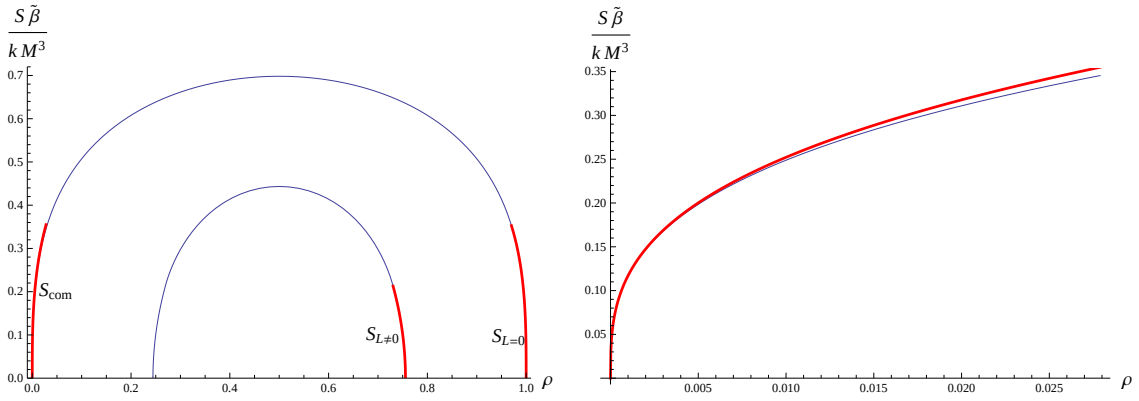

(a) (b)

Figure 5.2: The scaled entropy as a function of particle density. The blue lines are numerical results of (5.3), whilst the red lines are analytic results. (a) The outer blue line has a fixed $L_3^{(\text{tot})}$ value of 0, while the inner blue line has $l = \frac{L_3^{(\text{tot})}}{L_3^{(\text{max})}} = 0.8$. The red lines are classified as follows. The S_{com} line corresponds to a low-density commutative fermi gas, the $S_{L\neq0}$ line to a high-density non-commutative gas with $l = 0.8$ and the $S_{L=0}$ line to a high-density non-commutative gas with $l = 0$. (b) A zoomed view of the low density region with $l = 0$ where the blue line again is the numerical result for (5.3) and the red line is the result for the low-density commutative fermi gas.

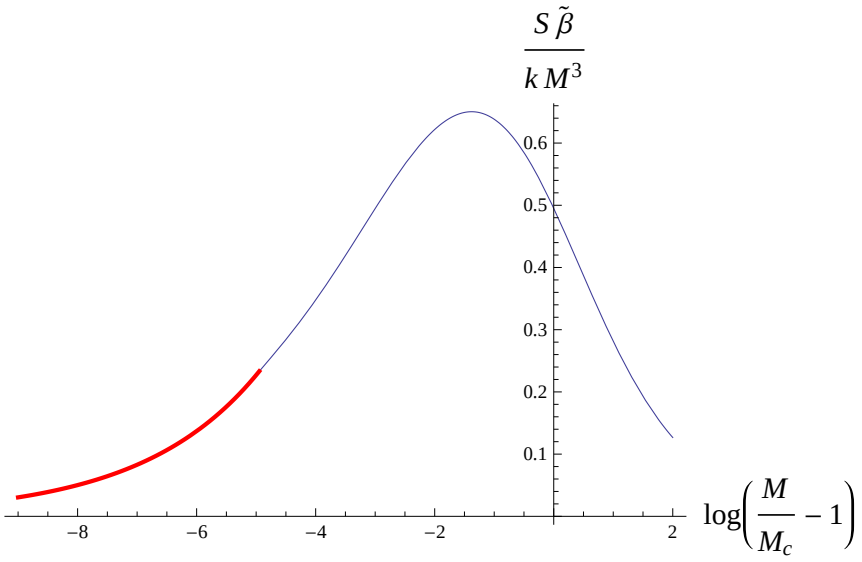

Figure 5.3: The scaled entropy as a function of system size for $l = 0.8$ at high particle densities, with the blue line as the numerical result and the red line being the analytic result.

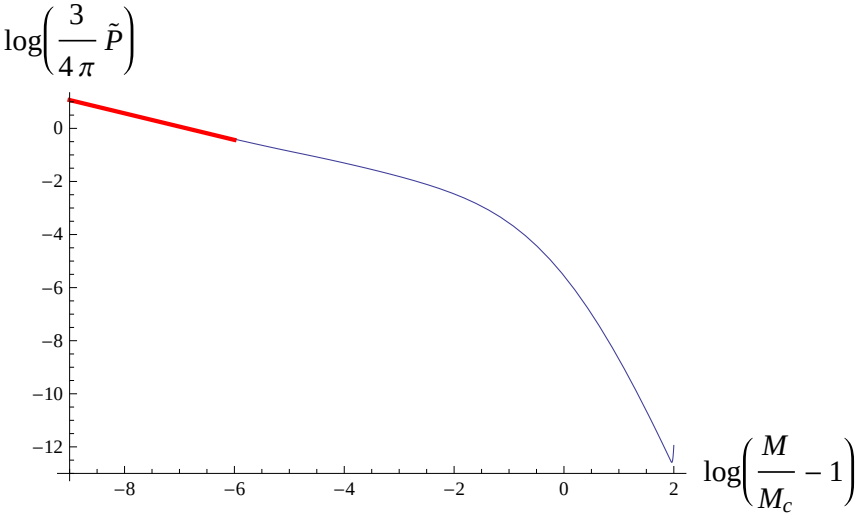

Figure 5.4: The scaled pressure as a function of system size at high particle densities. The blue line being the numerical results for (5.3) and the red line is the analytic result.

5.3 Approaches and results featured in the related published article

We will now briefly discuss the major changes and additions in the published article [17].

The first major difference between this dissertation and the published article is that the article applied a different technique in calculating the q-potential for $L_3^{(\text{tot})} > 0$. This enabled the q-potential to be valid at both low- and high particle densities, in contrast to only near critical density as was presented in this dissertation. This was achieved by mapping the constrained rotating ensemble unto an unconstrained ensemble with an effective density of states at low particle densities, and then inferring the high density behaviour from the low/high density duality. The result of this approach was that the thermodynamic quantities could be calculated for a low temperature ($\beta \gg 1$), but slowly rotating ($|w| \ll 1$) gas for all particle densities. Again, this was in contrast to this dissertation's low temperature ($\beta \gg 1$), fast rotating ($|w| > 1$) gas at critical density.

The case for $L_3^{(\text{tot})} = 0$, however, remained the same and the same approach was used to compute the corresponding q-potential. Similar results were also achieved.

A section containing new work, with novel results, was also contained in the article: Given that possible non-commutative effects can only realistically be observed in systems of very high particle density, it was argued that very dense astro-physical objects, such as neutron stars or white dwarfs, should be considered as candidates for observing non-commutative effects. Therefore, a brief study was done on high particle density system confined by gravity in non-commutative space.

Even though the study did not take relativistic effects into account, some novel results were observed. Firstly, it was found that the hydrostatic equilibrium condition permits solutions for objects with any mass, in contrast to the commutative case where a mass limit (the Chandrasekhar mass) to the solutions was present. This is attributed to the fact that in non-commutative system one finds an minimum volume, or incompressible limit, which prevents the object from collapsing under gravity.

Furthermore, it was found that the object can be thought of as a liquid drop with its particle density rapidly vanishing at the edge. It is also seen that the dilute gas of particles at the edge becomes thinner as the radius of the object increases. This is similar to incompressible quantum Hall liquids which itself is closely related to 2-dimensional non-commutative systems. The system studied in this article, therefore, can be thought of being a generalization to three dimensional

quantum Hall liquids. Agreeing with this, is the fact that it was found that entropic excitations only existed in the thin dilute gas near the edge, where the active degrees of freedom exist, and the entropy in the incompressible bulk vanishes. The entropy at the surface of the object was also found to be non-extensive.

CHAPTER 6

CONCLUSION & OUTLOOK

In conclusion, we briefly summarize the new results obtained in this dissertation, as well as the novel insights it has provided. We will also briefly discuss possible next steps, given this dissertation's work as background.

This dissertation set out to study the generalization of non-commutative coordinates to three-dimensional space, in particular by use of fuzzy coordinate commutation relations, and how such a generalization will affect both the quantum mechanical behaviour, as well as thermodynamic properties, of non-interacting fermionic particles and gases. It proved successful in displaying obvious differences between results for particles in non-commutative systems and the usual commutative systems. These results may aid the pursuit for finding non-commutative effects in real systems.

We take a look at the work of each chapter separately.

6.1 Non-commutative quantum mechanics in three dimensions

Extending the work on research done on non-commutative coordinates in two dimensions that was covered in Chapter 2, we provided a consistent method of describing fermionic particles in three-dimensional space using fuzzy coordinate commutation relations. We have also found exact solutions to the non-commutative Schrödinger equation for both free particles and particles in the presence of a spherical potential well respectively. We have found, in both cases, that there exists a global maximum kinetic energy limit above which no single particle solutions are permitted.

We also obtained matching conditions for the wavefunctions that enabled one to calculate the energy spectrum for both bound and scattering states. Scattering was investigated in detail in the following chapter.

Furthermore, in the spherical well problem, we found that there exists a finite number of bound states. This finite number of bound states is limited due to the fact that the angular momentum j itself was bound by the integer radius of the well $M = \frac{R}{\theta} - 1$. Even extending the spherical well problem to the infinite well, the exact number of bound particle states remained finite.

Given the results above, it was possible to derive expressions for the maximum number of particles

and angular momentum projection as well as an expression for the density of states.

Lastly, we also showed that given the appropriate limit where the non-commutative parameter θ tends to 0, we receive all the usual results as expected from commutative three-dimensional free particle and spherical well problems.

6.2 Scattering states of the finite fuzzy well

Having the matching conditions for scattering states in fuzzy space at our disposal, we continued to investigate particle scattering in this system.

In order for the formulation of scattering in fuzzy space to be detailed, it was first necessary to briefly investigate position representation of states as done by positive operator valued measures (POVMs). This provided us with the ability to interpret spatial probability densities and currents in the finite fuzzy well problem which was integral to the formalism of scattering in fuzzy space. With the formalism for scattering in fuzzy space outlined throughout the chapter, we obtained expressions for the total cross-section, differential cross-section and phase shifts that was necessary to investigate scattering states of the finite fuzzy well in detail.

Further investigation into scattering states of the finite fuzzy well revealed a novel feature that is exclusive to the particles in the fuzzy well problem. This feature was the fact that exotic scattering states exist where the incident energies are larger than the maximum allowed energy within the well, but was sufficiently low outside of the well as to not reach this maximum energy. This caused the exotic scattering states to experience the potential well rather as a repulsive well and making the well infinitely deep provided us with the exact same results as hard sphere scattering.

Again, all of the cross-sectional and phase shift plots displayed commutative behaviour when the non-commutative parameter θ tended to 0, and deviated whenever θ was increased. In addition to this, another interesting result obtained for studying scattering on the finite fuzzy well was the fact that the number of resonance peaks in the phase shifts directly correlates with finite number of bound states present for a given finite well.

6.3 Thermodynamics of a confined fermion gas in fuzzy space

Given the complete results of the energy spectrum and density of states for particles confined in fuzzy space, which we obtained for the infinite spherical fuzzy well problem in Chapter 3, we proceded to investigate the thermodynamics of confined particles in fuzzy space.

Using the grand canonical ensemble as starting point, where we fix the z-component of the total angular momentum $L_3^{(\text{tot})}$, we obtained the expressions for the central thermodynamic quantities for both the cases where $L_3^{(\text{tot})} = 0$ and $L_3^{(\text{tot})} > 0$. In both cases it was found that there exists a critical particle density at which an incompressible limit is reached. At this point the pressure diverges and the entropy of the system tends to 0. This was also supported by the notion that a minimum system volume exists for a given number of particles, beyond which the system cannot be compressed anymore. This effect helped to illustrate that a duality between the low-density and high-density scenarios exists. This effect also arose from the fact that the density of states was symmetric under $E \to -E$ transformations. This duality enabled us to write the high-density problems as a transformation of the low-density problem.

Another effect observed was the entropy scaling as a function of system size. When the system, at critical density, was taken and its number of particles fixed, we increase the system size and observed how the entropy scaled. For the scenario where $L_3^{(\text{tot})} = 0$, we found that the entropy scales directly proportional to the volume of the system. However, in the case where $L_3^{(\text{tot})} > 0$, we found that the entropy scales slower than the volume, but faster than the surface area of the system.

Lastly, as some of the thermodynamic studies conducted in this dissertation were presented in an article [17], new results presented in the article, that are not present in this dissertation, was briefly discussed. One novel approach using our technique was investigating a high particle density system confined by gravity in non-commutative space. This was seen as a possible analog to very large, dense astrophysical objects. Similar results as our particles confined in a spherical fuzzy well were achieved in that an incompressible limit was seen and that the system had a minimum volume for a given mass.

6.4 Outlook

Given that novel results were achieved, a natural next step would be to extend the three-dimensional non-commutative problem to relativistic quantum mechanics. Even though initial

research on interacting particles using a non-commutative Dirac equation [25] has been done, the field on confined relativistic particles in non-commutative space remains bare. Such relativistic studies are vital in searching for non-commutative effects in real macroscopic systems such as dense astrophysical objects.

APPENDIX A

NON-COMMUTATIVE QUANTUM MECHANICS IN THREE DIMENSIONS

Detailed Calculations

A.1 Casimir operator

Given the definitions in (3.2) and (3.3), the Casimir operator is given by:

$$\begin{aligned}
\hat{X}^2 = \hat{X}_1^2 + \hat{X}_2^2 + \hat{X}_3^2 &= \theta^2 \left[\left(\hat{a}_1^\dagger \hat{a}_2 + \hat{a}_2^\dagger \hat{a}_1 \right)^2 + \left(i\hat{a}_2^\dagger \hat{a}_1 - i\hat{a}_1^\dagger \hat{a}_2 \right)^2 + \left(\hat{a}_1^\dagger \hat{a}_1 - \hat{a}_2^\dagger \hat{a}_2 \right)^2 \right] \\
&= \theta^2 \left[2\hat{a}_1^\dagger \hat{a}_1 \hat{a}_2 \hat{a}_2^\dagger + 2\hat{a}_1 \hat{a}_1^\dagger \hat{a}_2^\dagger \hat{a}_2 - 2\hat{a}_1^\dagger \hat{a}_1 \hat{a}_2^\dagger \hat{a}_2 + \hat{a}_1^\dagger \hat{a}_1 \hat{a}_1^\dagger \hat{a}_1 + \hat{a}_2^\dagger \hat{a}_2 \hat{a}_2^\dagger \hat{a}_2 \right] \\
&= \theta^2 \Big[2\hat{a}_1^\dagger \hat{a}_1 \left(\hat{a}_2^\dagger \hat{a}_2 + 1 \right) + 2\hat{a}_2^\dagger \hat{a}_2 \left(\hat{a}_1^\dagger \hat{a}_1 + 1 \right) \\
&\qquad - 2\hat{a}_1^\dagger \hat{a}_1 \hat{a}_2^\dagger \hat{a}_2 + \hat{a}_1^\dagger \hat{a}_1 \hat{a}_1^\dagger \hat{a}_1 + \hat{a}_2^\dagger \hat{a}_2 \hat{a}_2^\dagger \hat{a}_2 \Big] \\
&= \theta^2 \left[2\hat{a}_1^\dagger \hat{a}_1 + 2\hat{a}_2^\dagger \hat{a}_2 + 2\hat{a}_1^\dagger \hat{a}_1 \hat{a}_2^\dagger \hat{a}_2 + \hat{a}_1^\dagger \hat{a}_1 \hat{a}_1^\dagger \hat{a}_1 + \hat{a}_2^\dagger \hat{a}_2 \hat{a}_2^\dagger \hat{a}_2 \right] \\
&= \theta^2 \left[2\hat{N} + \hat{N}^2 \right] \\
&= \theta^2 \hat{N} \left(\hat{N} + 2 \right)
\end{aligned} \tag{A.1}$$

A.2 Normal ordered counting operator of the form $:\hat{N}^k:$

We prove (3.18) using induction in k as follows:

$\underline{k = 1}$:

$$:\hat{N}: |n_1, n_2\rangle = \left(\hat{a}_1^\dagger \hat{a}_1 + \hat{a}_2^\dagger \hat{a}_2 \right) |n_1, n_2\rangle = (n_1 + n_2) |n_1, n_2\rangle = \hat{N} |n_1, n_2\rangle .$$

Suppose now it holds for $k = x$ that

$$:\hat{N}^x: |n_1, n_2\rangle = \frac{\hat{N}!}{(\hat{N} - x)!} |n_1, n_2\rangle = \left[\hat{N}(\hat{N} - 1) \dots (\hat{N} - x + 1) \right] |n_1, n_2\rangle ,$$

then for

$k = x + 1$:

$$
\begin{aligned}
:\hat{N}^{x+1}: |n_1, n_2\rangle &= :\left(\hat{a}_1^\dagger \hat{a}_1 + \hat{a}_2^\dagger \hat{a}_2\right) \hat{N}^x: |n_1, n_2\rangle = \left(\hat{a}_1^\dagger :\hat{N}^x: \hat{a}_1 + \hat{a}_2^\dagger :\hat{N}^x: \hat{a}_2\right) |n_1, n_2\rangle \\
&= \sqrt{n_1}\, \hat{a}_1^\dagger :\hat{N}^x: |n_1 - 1, n_2\rangle + \sqrt{n_2}\, \hat{a}_2^\dagger :\hat{N}^x: |n_1, n_2 - 1\rangle \\
&= \sqrt{n_1}\, \left[n'(n'-1)\dots(n'-x+1)\right] \hat{a}_1^\dagger |n_1 - 1, n_2\rangle \\
&\quad + \sqrt{n_2}\, \left[n'(n'-1)\dots(n'-x+1)\right] \hat{a}_2^\dagger |n_1, n_2 - 1\rangle \\
&= (n_1 + n_2)\left[(n-1)(n-2)\dots(n-x)\right] |n_1, n_2 - 1\rangle \\
&= \left[n(n-1)(n-2)\dots(n-x)\right] |n_1, n_2\rangle = \frac{\hat{N}!}{\left(\hat{N} - (x+1)\right)!} |n_1, n_2\rangle ,
\end{aligned}
$$

with $n' = n_1 + n_2 - 1 = n - 1$ and thus (3.18) is proven by induction.

A.3 Normal ordered counting operator of the form $:e^{-\alpha \hat{N}} \hat{N}^k:$

We also compute a special normal ordered form of the counting operator given by

$$
\begin{aligned}
:e^{-\alpha \hat{N}} \hat{N}^k: &= \sum_{x=0}^{\infty} :\frac{(-\alpha\, \hat{N})^x}{x!} \hat{N}^k: \\
&= \sum_{x=0}^{\infty} \frac{(-\alpha)^x}{x!} :\hat{N}^{x+k}: \\
&= \sum_{x=0}^{\infty} \frac{(-\alpha)^x}{x!} \frac{n!}{(n - (x+k))!} \\
&= (1-\alpha)^{n-k} \frac{n!}{(n-k)!}.
\end{aligned}
\tag{A.2}
$$

A.4 Commutators on the normal ordered radial function

Given the definitions in (3.3), (3.20) and (3.22) we find the actions of the following commutators:

$$\begin{aligned}
\left[\hat{a}_\alpha^\dagger\,,:R(\hat{N}):\right]|n_1,n_2\rangle &= \sum_{k=0}^{\infty} c_k \left[\hat{a}_\alpha^\dagger\,,:\hat{N}^k:\right]|n_1,n_2\rangle \\
&= \sum_{k=0}^{\infty} c_k \left(\hat{a}_\alpha^\dagger\ :\hat{N}^k:\ -\ :\hat{N}^k:\ \hat{a}_\alpha^\dagger\right)|n_1,n_2\rangle \\
&= \sum_{k=0}^{\infty} c_k\sqrt{n_\alpha+1}\left(\frac{n!}{(n-k)!}-\frac{(n+1)!}{(n+1-k)!}\right)|n_1+\delta_{\alpha,1},n_2+\delta_{\alpha,2}\rangle \\
&= \sum_{k=0}^{\infty} c_k\sqrt{n_\alpha+1}\Big(n(n-1)(n-2)\dots(n-k+2)(n-k+1) \\
&\qquad -(n+1)n(n-1)(n-2)\dots(n-k+2)\Big)|n_1+\delta_{\alpha,1},n_2+\delta_{\alpha,2}\rangle \\
&= \sum_{k=0}^{\infty} c_k\sqrt{n_\alpha+1}\frac{n!}{(n-(k-1))!}\Big((n-k+1)-(n+1)\Big)|n_1+\delta_{\alpha,1},n_2+\delta_{\alpha,2}\rangle \\
&= -\sum_{k=0}^{\infty} c_k\,k\sqrt{n_\alpha+1}\,\frac{n!}{(n-(k-1))!}|n_1+\delta_{\alpha,1},n_2+\delta_{\alpha,2}\rangle \\
&= -\hat{a}_\alpha^\dagger\ :R'(\hat{N}):|n_1,n_2\rangle \qquad \text{(A.3)}
\end{aligned}$$

and

$$\begin{aligned}
\left[\hat{a}_\alpha\,,:R(\hat{N}):\right]|n_1,n_2\rangle &= \sum_{k=0}^{\infty} c_k \left[\hat{a}_\alpha\,,:\hat{N^k}:\right]|n_1,n_2\rangle \\
&= \sum_{k=0}^{\infty} c_k \left(\hat{a}_\alpha\ :\hat{N^k}: - :\hat{N^k}:\ \hat{a}_\alpha\right)|n_1,n_2\rangle \\
&= \sum_{k=0}^{\infty} c_k\sqrt{n_\alpha}\left(\frac{n!}{(n-k)!}-\frac{(n-1)!}{(n-1-k)!}\right)|n_1-\delta_{\alpha,1},n_2-\delta_{\alpha,2}\rangle \\
&= \sum_{k=0}^{\infty} c_k\sqrt{n_\alpha}\Big(n(n-1)(n-2)\dots(n-k+1) \\
&\qquad -(n-1)(n-2)\dots(n-k+1)(n-k)\Big)|n_1-\delta_{\alpha,1},n_2-\delta_{\alpha,2}\rangle \\
&= \sum_{k=0}^{\infty} c_k\sqrt{n_\alpha}\frac{(n-1)!}{(n-k)!}\Big(n-(n-k)\Big)|n_1-\delta_{\alpha,1},n_2-\delta_{\alpha,2}\rangle \\
&= \sum_{k=0}^{\infty} c_k\, k\sqrt{n_\alpha}\,\frac{(n-1)!}{((n-1)-(k-1))!}|n_1-\delta_{\alpha,1},n_2-\delta_{\alpha,2}\rangle \\
&= :R'(\hat{N}):\ \hat{a}_\alpha|n_1,n_2\rangle\,, \qquad \text{(A.4)}
\end{aligned}$$

We may, therefore, consider $\left[\hat{a}^\dagger_\alpha\,,:R(\hat{N}):\right] = -\hat{a}^\dagger_\alpha :R'(\hat{N}):$ and $\left[\hat{a}_\alpha\,,:R(\hat{N}):\right] = :R'(\hat{N}):\hat{a}_\alpha$.

A.5 Double commutator on the wavefunction

Simplifying (3.23) yields

$$\begin{aligned}
\left[\hat{a}^\dagger_\alpha,[\hat{a}_\alpha,\hat{\psi}_{jm}]\right] &= \theta^j\sum_{(jm)}\left[\hat{a}_\alpha\,,\frac{(\hat{a}^\dagger_1)^{m_1}(\hat{a}^\dagger_2)^{m_2}}{m_1!\,m_2!}\right]\left[\hat{a}^\dagger_\alpha\,,:R(\hat{N}):\right]\frac{(\hat{a}_1)^{n_1}(-\hat{a}_2)^{n_2}}{n_1!\,n_2!} \\
&+\theta^j\sum_{(jm)}\frac{(\hat{a}^\dagger_1)^{m_1}(\hat{a}^\dagger_2)^{m_2}}{m_1!\,m_2!}\left[\hat{a}_\alpha\,,:R(\hat{N}):\right]\left[\hat{a}^\dagger_\alpha\,,\frac{(\hat{a}_1)^{n_1}(-\hat{a}_2)^{n_2}}{n_1!\,n_2!}\right] \\
&+\theta^j\sum_{(jm)}\left[\hat{a}_\alpha\,,\frac{(\hat{a}^\dagger_1)^{m_1}(\hat{a}^\dagger_2)^{m_2}}{m_1!\,m_2!}\right]:R(\hat{N}):\left[\hat{a}^\dagger_\alpha\,,\frac{(\hat{a}_1)^{n_1}(-\hat{a}_2)^{n_2}}{n_1!\,n_2!}\right] \\
&+\theta^j\sum_{(jm)}\frac{(\hat{a}^\dagger_1)^{m_1}(\hat{a}^\dagger_2)^{m_2}}{m_1!\,m_2!}\left[\hat{a}^\dagger_\alpha\,,\left[\hat{a}_\alpha\,,:R(\hat{N}):\right]\right]\frac{(\hat{a}_1)^{n_1}(-\hat{a}_2)^{n_2}}{n_1!\,n_2!}.
\end{aligned} \qquad \text{(A.5)}$$

By using the results in results in Section A.4, we can further simplify (A.5) to

$$\begin{aligned}\left[\hat{a}_\alpha^\dagger,[\hat{a}_\alpha,\hat{\psi}_{jm}]\right] &= -\theta^j \sum_{(jm)} \left[\hat{a}_\alpha\,,\,\frac{(\hat{a}_1^\dagger)^{m_1}(\hat{a}_2^\dagger)^{m_2}}{m_1!\,m_2!}\right]\hat{a}_\alpha^\dagger :R'(\hat{N}):\frac{(\hat{a}_1)^{n_1}(-\hat{a}_2)^{n_2}}{n_1!\,n_2!}\\ &+\theta^j \sum_{(jm)} \frac{(\hat{a}_1^\dagger)^{m_1}(\hat{a}_2^\dagger)^{m_2}}{m_1!\,m_2!} :R'(\hat{N}):\hat{a}_\alpha\left[\hat{a}_\alpha^\dagger\,,\,\frac{(\hat{a}_1)^{n_1}(-\hat{a}_2)^{n_2}}{n_1!\,n_2!}\right]\\ &+\theta^j \sum_{(jm)} \left[\hat{a}_\alpha\,,\,\frac{(\hat{a}_1^\dagger)^{m_1}(\hat{a}_2^\dagger)^{m_2}}{m_1!\,m_2!}\right] :R(\hat{N}):\left[\hat{a}_\alpha^\dagger\,,\,\frac{(\hat{a}_1)^{n_1}(-\hat{a}_2)^{n_2}}{n_1!\,n_2!}\right]\\ &-\theta^j \sum_{(jm)} \frac{(\hat{a}_1^\dagger)^{m_1}(\hat{a}_2^\dagger)^{m_2}}{m_1!\,m_2!}\left(:\hat{N}\,R''(\hat{N}):+2:R'(\hat{N}):\right)\frac{(\hat{a}_1)^{n_1}(-\hat{a}_2)^{n_2}}{n_1!\,n_2!}.\end{aligned} \tag{A.6}$$

Within (A.6) we see several commutators. However, it is easy to see that those commutators that have not previously been calculated are given by

$$\left[\hat{a}_\alpha\,,\,\frac{(\hat{a}_1^\dagger)^{m_1}(\hat{a}_2^\dagger)^{m_2}}{m_1!\,m_2!}\right] = \left(m_1\delta_{\alpha,1}\hat{a}_2^\dagger + m_2\delta_{\alpha,2}\hat{a}_1^\dagger\right)\frac{(\hat{a}_1^\dagger)^{m_1-1}(\hat{a}_2^\dagger)^{m_2-1}}{m_1!\,m_2!} \tag{A.7}$$

and

$$\left[\hat{a}_\alpha^\dagger\,,\,\frac{(\hat{a}_1)^{n_1}(-\hat{a}_2)^{n_2}}{n_1!\,n_2!}\right] = -\left(n_1\delta_{\alpha,1}(-\hat{a}_2)+n_2\delta_{\alpha,2}\hat{a}_1\right)\frac{(\hat{a}_1)^{n_1-1}(-\hat{a}_2)^{n_2-1}}{n_1!\,n_2!}. \tag{A.8}$$

Using these results we see the first two lines of (A.6) give the same contribution as $m_1+m_2=n_1+n_2=j$ and the third line equates to 0. Therefore, we have the resulting expression of

$$[\hat{a}_\alpha^\dagger,[\hat{a}_\alpha,\hat{\psi}_{jm}]] = -\theta^j \sum_{(jm)} \frac{(\hat{a}_1^\dagger)^{m_1}(\hat{a}_2^\dagger)^{m_2}}{m_1!\,m_2!} :[\hat{N}\,R''(\hat{N})+2(j+1)\,R'(\hat{N})]:\frac{(\hat{a}_1)^{n_1}(-\hat{a}_2)^{n_2}}{n_1!\,n_2!}. \tag{A.9}$$

A.6 Multiplying the radial distance operator and the wavefunction

Given the radial distance operator given in (3.9) and the wavefunction definition set out in (3.17), we find that the multiplication of these two results in

$$\begin{aligned}\hat{r}\,\hat{\psi}_{jm} &= \theta^{j+1}\sum_{(jm)}(\hat{N}+1)\frac{(\hat{a}_1^\dagger)^{m_1}(\hat{a}_2^\dagger)^{m_2}}{m_1!\,m_2!} :R(\hat{N}):\frac{(\hat{a}_1)^{n_1}(-\hat{a}_2)^{n_2}}{n_1!\,n_2!}\\ &= \theta^{j+1}\sum_{(jm)}\frac{(\hat{a}_1^\dagger)^{m_1}(\hat{a}_2^\dagger)^{m_2}}{m_1!\,m_2!}(\hat{N}+1) :R(\hat{N}):\frac{(\hat{a}_1)^{n_1}(-\hat{a}_2)^{n_2}}{n_1!\,n_2!}\\ &+\ \theta^{j+1}\sum_{(jm)}\hat{a}_\alpha^\dagger\left[\hat{a}_\alpha\,,\,\frac{(\hat{a}_1^\dagger)^{m_1}(\hat{a}_2^\dagger)^{m_2}}{m_1!\,m_2!}\right] :R(\hat{N}):\frac{(\hat{a}_1)^{n_1}(-\hat{a}_2)^{n_2}}{n_1!\,n_2!},\end{aligned} \tag{A.10}$$

from which we may use (A.7) and (3.19) to further simplify:

$$\begin{aligned}\hat{r}\,\hat{\psi}_{jm} &= \theta^{j+1}\sum_{(jm)}\frac{(\hat{a}_1^\dagger)^{m_1}(\hat{a}_2^\dagger)^{m_2}}{m_1!\,m_2!}(\hat{N}+m_1+m_2+1):R(\hat{N}):\frac{(\hat{a}_1)^{n_1}(-\hat{a}_2)^{n_2}}{n_1!\,n_2!}\\ &= \theta^{j+1}\sum_{(jm)}\frac{(\hat{a}_1^\dagger)^{m_1}(\hat{a}_2^\dagger)^{m_2}}{m_1!\,m_2!}:\Big[(\hat{N}+j+1)R(\hat{N})+\hat{N}R'(\hat{N})\Big]:\frac{(\hat{a}_1)^{n_1}(-\hat{a}_2)^{n_2}}{n_1!\,n_2!}\end{aligned} \tag{A.11}$$

A.7 Normal ordering the solutions to the radial differential equation

By use of the Taylor expansion for the Bessel function given in (3.40), and by use of the result in (A.2), we are able to normal order the first solution of the radial differential equation given in (3.38):

$$\begin{aligned}\bar{R}_J(n) &= :\hat{N}^{-(j+\frac{1}{2})}e^{-\frac{\kappa^2\hat{N}}{2}}\left(\frac{\kappa}{4}\hat{N}\sqrt{4-\kappa^2}\right)^{j+\frac{1}{2}}\sum_{k=0}^{\infty}\frac{(-\frac{1}{16}\kappa^2\hat{N}^2(4-\kappa^2))^k}{k!\,\Gamma(j+k+\frac{3}{2})}:\\ &= \left(\frac{\kappa}{4}\sqrt{4-\kappa^2}\right)^{j+\frac{1}{2}}\sum_{k=0}^{\infty}\frac{(-\frac{1}{16}\kappa^2(4-\kappa^2))^k}{k!\,\Gamma(j+k+\frac{3}{2})}\;:e^{-\frac{\kappa^2\hat{N}}{2}}\hat{N}^{2k}:\\ &= \left(\frac{\kappa}{4}\sqrt{4-\kappa^2}\right)^{j+\frac{1}{2}}\sum_{k=0}^{\infty}\frac{\left(-\frac{1}{16}\kappa^2(4-\kappa^2)\right)^k}{k!\,\Gamma(j+k+\frac{3}{2})}(1-\frac{\kappa^2}{2})^{n-2k}\frac{n!}{(n-2k)!}\\ &= \frac{2^{-(2j+1)}\left(1-\frac{\kappa^2}{2}\right)^n\left(-\kappa\sqrt{4-\kappa^2}\right)^{j+\frac{1}{2}}}{\Gamma(j+\frac{3}{2})}{}_2F_1(-\frac{n}{2}\,,-\frac{(n-1)}{2}\,;\,j+\frac{3}{2}\,;\,1-\frac{4}{(\kappa^2-2)^2}),\end{aligned} \tag{A.12}$$

Similarly, using the Taylor expansion for the Neumann function given in (3.41), and by use of the result in (A.2), we are able to normal order the first solution of the radial differential equation

given in (3.39):

$$
\begin{aligned}
\bar{R}_Y(n) &= :\hat{N}^{-(j+\frac{1}{2})} e^{-\frac{\kappa^2\hat{N}}{2}} \operatorname{cosec}(\pi(j+\frac{1}{2}))\left(\frac{\kappa}{4}\hat{N}\sqrt{4-\kappa^2}\right)^{-(j+\frac{1}{2})} \sum_{k=0}^{\infty} \frac{(-\frac{1}{16}\kappa^2\hat{N}^2(4-\kappa^2))^k}{k!\,\Gamma(-j+k+\frac{1}{2})} : \\
&= \operatorname{cosec}(\pi(j+\frac{1}{2}))\left(\frac{\kappa}{4}\sqrt{4-\kappa^2}\right)^{-(j+\frac{1}{2})} \sum_{k=0}^{\infty} \frac{(-\frac{1}{16}\kappa^2(4-\kappa^2))^k}{k!\,\Gamma(-j+k+\frac{1}{2})} :e^{-\frac{\kappa^2\hat{N}}{2}}\hat{N}^{2k-2j-1}: \\
&= \operatorname{cosec}(\pi(j+\frac{1}{2}))\left(\frac{\kappa}{4}\sqrt{4-\kappa^2}\right)^{-(j+\frac{1}{2})} \\
&\qquad \times \sum_{k=0}^{\infty} \frac{\left(\frac{1}{16}\kappa^2(\kappa^2-4)\right)^k}{k!\,\Gamma(-j+k+\frac{1}{2})} (1-\frac{\kappa^2}{2})^{n-2k+2j+1} \frac{n!}{(n-2k+2j+1)!} \\
&= (-1)^{j+1}2^{-n}(2-\kappa^2)^{n+2j+1}\left(\kappa\sqrt{4-\kappa^2}\right)^{-(j+\frac{1}{2})} \frac{\Gamma(n+1)}{\Gamma(n+2j+2)\,\Gamma(-j+\frac{1}{2})} \\
&\qquad \times \ {}_2F_1(-\frac{(n+2j+1)}{2}, -\frac{(n+2j)}{2}; -j+\frac{1}{2}; 1-\frac{4}{(\kappa^2-2)^2}).
\end{aligned}
\tag{A.13}
$$

APPENDIX B

THERMODYNAMICS OF A FERMION GAS IN FUZZY SPACE

Detailed Calculations

B.1 Calculating the q-potential for $L_3^{(\mathrm{tot})} \neq 0$

Before computations are done, it is first necessary to establish labeling of the following common recurring integrals in this section:

$$\begin{aligned} I^{(n)}(x,\lambda) &= \int_{x_-}^{x} d\epsilon\, d(\epsilon,\lambda)\, \epsilon^n \\ L(x,\lambda) &= \int_{x_-}^{x} d\epsilon\, I^{(0)}(\epsilon,\lambda) = xI^{(0)}(x,\lambda) - I^{(1)}(x,\lambda) \\ K(x,\lambda) &= \int_{x_-}^{x} d\epsilon\, L(\epsilon,\lambda) = \frac{x^2}{2} I^{(0)}(x,\lambda) - xI^{(1)}(x,\lambda) + \frac{1}{2} I^{(2)}(x,\lambda), \end{aligned} \tag{B.1}$$

where $x_\pm(\lambda) = \pm\sqrt{1-\lambda^2}$.

Useful results for $I^{(n)}(x,\lambda)$ are found in the following special cases:

- $I^{(0)}(x_+,\lambda) = 1-\lambda$.
- $I^{(1)}(x_+,\lambda) = 0$.
- $I^{(2)}(x_+,\lambda) = \frac{1}{2}(1-\lambda)^2$.

Now consider the integral over the energy states x in (5.3)

$$\mathcal{I}(\alpha,\lambda) = \int_{x_-}^{x_+} dx\, d(x,\lambda) \log\left[1 + e^{-\tilde{\beta}(x-f(\alpha))}\right], \tag{B.2}$$

for which it is impossible to compute an analytical solution. However, it is possible to make necessary assumptions to obtain approximate solutions for different domains of x. Recalling that $f(\alpha) = \tilde{\mu} + \alpha w$, we find that in the low temperature limit, i.e. large $\tilde{\beta}$, we can apply the following approximations:

(i) $f(\alpha) < x_-$

Here one finds that $-\tilde{\beta}(x - f(\alpha))$ will be negative over the domain of x and, therefore, the logarithm is exponentially small in $\tilde{\beta}$. The integral over x approximates to

$$\mathcal{I}_1(\alpha, \lambda) \approx 0. \tag{B.3}$$

(ii) $x_- < f(\alpha) < x_+$

This special case requires the use of the Sommerfeld expansion [18]. The expansion results in an approximation of $\mathcal{I}(\alpha, \lambda)$ up to linear order in $\tilde{\beta}^{-1}$, with the result being

$$\mathcal{I}_2(\alpha, \lambda) \approx \tilde{\beta} L(f(a), \lambda) + \frac{\pi^2}{6\tilde{\beta}}\, d(f(\alpha), \lambda). \tag{B.4}$$

(iii) $f(\alpha) > x_+$

In this case $-\tilde{\beta}(x - f(\alpha))$ is strictly positive over the domain of x, resulting in argument of the logarithm being exponentially large in $\tilde{\beta}$. The logarithm can, therefore, be approximated to

$$\log\left[1 + e^{-\tilde{\beta}(x - f(\alpha))}\right] \approx -\tilde{\beta}(x - f(\alpha)),$$

with the integral approximating to

$$\mathcal{I}_3(\alpha, \lambda) \approx \tilde{\beta}(1 - \lambda)\, f(\alpha). \tag{B.5}$$

Given these approximate solutions, it follows that one now solves for the angular momentum projection integral given by

$$\mathcal{J}(\lambda) = \int_{-\lambda}^{+\lambda} d\alpha\, \mathcal{I}(\alpha, \lambda). \tag{B.6}$$

Solving (B.6) requires that one solves an increasing number of different combinations of the integrals in (B.1). The solutions for the angular momentum projection integrals are highly dependent on the values of $\tilde{\mu}$ and w. The results, for different ranges in $\tilde{\mu}$ and w are given by

(i) $x_- < f_- < x_+ < f_+$

$$\mathcal{J}_1(\lambda) = \frac{\tilde{\beta}}{w}\left(\frac{{f_+}^2}{2}(1-\lambda) + \frac{1}{4}(1-\lambda)^2 - K(f_-,\lambda)\right) + \frac{\pi^2}{6\tilde{\beta}w}\left(1-\lambda - I^{(0)}(f_-,\lambda)\right). \quad \text{(B.7)}$$

(ii) $x_- < f_- < f_+ < x_+$

$$\mathcal{J}_2(\lambda) = \frac{\tilde{\beta}}{w}\left(K(f_+,\lambda) - K(f_-,\lambda)\right) + \frac{\pi^2}{6\tilde{\beta}w}\left(I^{(0)}(f_+,\lambda) - I^{(0)}(f_-,\lambda)\right). \quad \text{(B.8)}$$

(iii) $f_- < x_- < x_+ < f_+$

$$\mathcal{J}_3(\lambda) = \frac{\tilde{\beta}(1-\lambda)}{2w}\left({f_+}^2 + \frac{1-\lambda}{2}\right) + \frac{\pi^2(1-\lambda)}{6\tilde{\beta}w}. \quad \text{(B.9)}$$

(iv) $f_- < x_- < f_+ < x_+$

$$\mathcal{J}_4(\lambda) = \frac{\tilde{\beta}}{w}\,K(f_+,\lambda) + \frac{\pi^2}{6\tilde{\beta}w}\,I^{(0)}(f_+,\lambda). \quad \text{(B.10)}$$

(v) $x_+ < f_- < f_+$

$$\mathcal{J}_5(\lambda) = 2\lambda(1-\lambda)\tilde{\beta}\,\tilde{\mu}, \quad \text{(B.11)}$$

with $f_\pm = \tilde{\mu} \pm w\,\lambda$.

All that remains in the solution of the q-potential is that one solves the final integral for total angular momentum given by

$$q(M,\tilde{\beta},\tilde{\mu},w) = M^3\int_0^1 d\lambda\ \mathcal{J}(\lambda,\tilde{\beta},\tilde{\mu},w). \quad \text{(B.12)}$$

It is easy to show that, depending on the values of $\tilde{\mu}$ and w, one has 8 different combination of the integrals in eqs. (B.7-B.11) to solve in order to have a complete solution for the q-potential. This dissertation only focused on specific high-density combinations associated with different scenarios for values of $\tilde{\mu}$ and w, as described in Section 5.1. The case where total angular momentum is non-zero, i.e. $1 < \tilde{\mu} < w$, has the following combination of integrals:

$$q(M,\tilde{\beta},\tilde{\mu},w) = M^3\left(\int_0^{\lambda_-} d\lambda\ \mathcal{J}_5 + \int_{\lambda_-}^{\lambda_+} d\lambda\ \mathcal{J}_1 + \int_{\lambda_+}^1 d\lambda\ \mathcal{J}_3\right), \quad \text{(B.13)}$$

with $\lambda_{\pm} = \frac{\tilde{\mu}w \pm \sqrt{1-\tilde{\mu}^2+w^2}}{1+w^2}$. The resulting expression for the q-potential is then given by

$$q(M,\tilde{\beta},\tilde{\mu},w) = \frac{M^3}{12w^3}\left[\frac{\tilde{\beta}\left((\sqrt{1+w^2}-\tilde{\mu})^4+8w^3\tilde{\mu}\right)}{2} + \frac{\pi^2\left(\sqrt{1+w^2}-\tilde{\mu}\right)^2}{\tilde{\beta}}\right]. \tag{B.14}$$

BIBLIOGRAPHY

[1] H. S. Snyder, *Quantized Space-Time*, Phys. Rev. D **71** (1947) 38.

[2] S. Doplicher, K. Fredenhagen and J. E. Roberts, *The quantum structure of spacetime at the Planck scale and quantum fields*, Commun. Math. Phys. **172** (1995) 187.

[3] N. Seiberg and E. Witten, *String theory and noncommutative geometry*, J. High Energy Phys. **JHEP09** (1999) 032.

[4] A. P. Balachandran, T. R. Govindarajan, C. Molina and P. Teotonio-Sobrinho, *Unitary quantum physics with time-space noncommutativity*, J. High Energy Phys. **JHEP10** (2004) 072.

[5] F. G. Scholtz, L. Gouba, A Hafver and C. M. Rohwer, *Formulation, interpretation and application of non-commutative quantum mechanics*, J. Phys. A: Math. Theor. **42** (2009) 175303.

[6] F. G. Scholtz, B. Chakraborty, J. Govaerts and S Vaidya, *Spectrum of the non-commutative spherical well*, J. Phys. A: Math. Theor. **40** (2007) 14581.

[7] J. D. Thom and F. G. Scholtz, *Bound state energies and phase shifts of a non-commutative well*, J. Phys. A: Math. Theor. **42** (2009) 445301.

[8] M. R. Douglas and N. A. Nekrasov, *Noncommutative field theory*, Rev. Mod. Phys. **73** (2001) 977.

[9] R. J. Szabo, *Quantum field theory on noncommutative spaces*, Phys. Rep. **378** (2003) 207.

[10] J. N. Kriel and F. G. Scholtz, *The entropy of dense non-commutative fermion gases*, J. Phys. A: Math. Theor. **45** (2012) 095301.

[11] D. Sinha, B. Chakraborty and F.G. Scholtz, *Non-commutative quantum mechanics in three dimensions and rotational symmetry*, J. Phys. A: Math. Theor. **45** (2012) 105308.

[12] V. Gáliková and P. Prešnajder, *Coulomb problem in non-commutative quantum mechanics*, J. Math. Phys. **54** (2013) 052102.

[13] N. Chandra, H. W. Groenewald, J. N. Kriel, F. G. Scholtz and S Vaidya, *Spectrum of the three-dimensional fuzzy well*, J. Phys. A: Math. Theor. **47** (2014) 445203.

[14] M. Abromowitz and I. A. Stegun, 2012 *Handbook of Mathematical Functions* (Dover Publications).

[15] J. N. Kriel and F. G. Scholtz, *Eigenvalue distributions from a star product approach*, J. Phys. A: Math. Theor. **45** (2012) 475204.

[16] J. N. Kriel, H. W. Groenewald and F. G. Scholtz, *Scattering in a three-dimensional fuzzy space*, Phys. Rev. D **95** (2017) 025003.

[17] F. G. Scholtz, J. N. Kriel and H. W. Groenewald, *The thermodynamics of Fermi gases in three dimensional fuzzy space*, Phys. Rev. D **92** (2015) 125013.

[18] R. K. Pathria, 1972 *Statistical Mechanics* (Oxford: Pergamon).

[19] G. Szegö, 1939 *Orthogonal Polynomials* (Providence, RI: American Mathematical Society).

[20] A. Perelomov, 1986 *Generalized Coherent States and Their Applications* (New York: Springer).

[21] G. Alexanian, A. Pinzul, and A. Stern, Nucl. Phys. B **600** (2001) 531.

[22] F. Calogero and A. M. Perelomov, 1978 *Lett. Nuovo Cimento* **23** 653.

[23] Gawronski W and Shawyer B, 1991 Strong asymptotics and the limit distributions of the zeros of Jacobi polynomials $P_n^{(an+\alpha,bn+\beta)}$, *Progress in Approximation Theory* ed Nevai P and Pinkus A (New York: Academic Press) pp 379.

[24] I. S. Gradshteyn and I. M. Ryzhik, 2014 *Table of Integrals, Series, and Products* (New Tork: Academic Press).

[25] P. H. Williams and F. G. Scholtz, *A manifestly Lorentz covariant, interacting and non-commutative Dirac equation*, (2015) arXiv:1512.04253